Symbolic Discovery of Optimization Algorithms

Xiangning Chen[1 2 § *] **Chen Liang**[1 §] **Da Huang**[1] **Esteban Real**[1]
Kaiyuan Wang[1] **Yao Liu**[1 †] **Hieu Pham**[1] **Xuanyi Dong**[1] **Thang Luong**[1]
Cho-Jui Hsieh[2] **Yifeng Lu**[1] **Quoc V. Le**[1]

[§]Equal & Core Contribution

[1]Google [2]UCLA

Abstract

We present a method to formulate algorithm discovery as program search, and apply it to discover optimization algorithms for deep neural network training. We leverage efficient search techniques to explore an infinite and sparse program space. To bridge the large generalization gap between proxy and target tasks, we also introduce program selection and simplification strategies. Our method discovers a simple and effective optimization algorithm, **Lion** (*EvoLved Sign Momentum*). It is more memory-efficient than Adam as it only keeps track of the momentum. Different from adaptive optimizers, its update has the same magnitude for each parameter calculated through the sign operation. We compare Lion with widely used optimizers, such as Adam and Adafactor, for training a variety of models on different tasks. On image classification, Lion boosts the accuracy of ViT by up to 2% on ImageNet and saves up to 5x the pre-training compute on JFT. On vision-language contrastive learning, we achieve 88.3% *zero-shot* and 91.1% *fine-tuning* accuracy on ImageNet, surpassing the previous best results by 2% and 0.1%, respectively. On diffusion models, Lion outperforms Adam by achieving a better FID score and reducing the training compute by up to 2.3x. For autoregressive, masked language modeling, and fine-tuning, Lion exhibits a similar or better performance compared to Adam. Our analysis of Lion reveals that its performance gain grows with the training batch size. It also requires a smaller learning rate than Adam due to the larger norm of the update produced by the sign function. Additionally, we examine the limitations of Lion and identify scenarios where its improvements are small or not statistically significant. The implementation of Lion is publicly available.[1]

1 Introduction

Optimization algorithms, i.e., optimizers, play a fundamental role in training neural networks. There are a large number of handcrafted optimizers, mostly adaptive ones, introduced in recent years (Anil et al., 2020; Balles and Hennig, 2018; Bernstein et al., 2018; Dozat, 2016; Liu et al., 2020; Zhuang et al., 2020). However, Adam (Kingma and Ba, 2014) with decoupled weight decay (Loshchilov and Hutter, 2019), also referred to as AdamW, and Adafactor with factorized second moments (Shazeer and Stern, 2018), are still the de facto standard optimizers for training most deep neural networks, especially the recent state-of-the-art language (Brown et al., 2020; Devlin et al., 2019; Vaswani et al., 2017), vision (Dai et al., 2021; Dosovitskiy et al., 2021; Zhai et al., 2021) and multimodal (Radford et al., 2021; Saharia et al., 2022; Yu et al., 2022) models.

[*]Work done as a student researcher at Google Brain.
[†]Work done while at Google.
[1]https://github.com/google/automl/tree/master/lion.
Corresponce: xiangning@cs.ucla.edu, crazydonkey@google.com.

Table 1: Accuracy of BASIC-L (Pham et al., 2021) on ImageNet and several robustness benchmarks. We apply Lion to both vision tower pre-training and vision-language contrastive training stages. The previous SOTA results on *zero-shot* and *fine-tuning* ImageNet accuracy are 86.3% and 91.0% (Yu et al., 2022).

Optimizer	Zero-shot						Fine-tune
	ImageNet	V2	A	R	Sketch	ObjectNet	ImageNet
Adafactor	85.7	80.6	85.6	95.7	76.1	82.3	90.9
Lion	**88.3**	**81.2**	**86.4**	**96.8**	**77.2**	**82.9**	**91.1**

Figure 1: **Left**: ImageNet fine-tuning accuracy vs. pre-training cost of ViT models on JFT-300M. **Right**: FID of the diffusion model on 256^2 image generation. We use DDPM for 1K steps w/o guidance to decode image. As a reference, the FID of ADM is 10.94 (Dhariwal and Nichol, 2021).

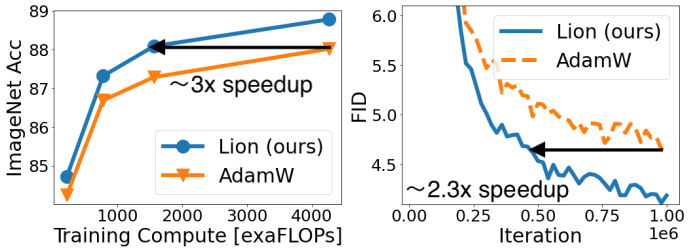

Program 1: Discovered optimizer Lion. $\beta_1 = 0.9$ and $\beta_2 = 0.99$ by default are derived from Program 4. It only tracks momentum and uses the sign operation to compute the update. The two gray lines compute the standard decoupled weight decay, where λ is the strength.

```
def train(weight, gradient, momentum, lr):
  update = interp(gradient, momentum, β1)
  update = sign(update)
  momentum = interp(gradient, momentum, β2)
  weight_decay = weight * λ
  update = update + weight_decay
  update = update * lr
  return update, momentum
```

Another direction is to automatically discover such optimization algorithms. The learning to optimize (L2O) approach proposes to discover optimizers by training parameterized models, e.g., neural networks, to output the updates (Andrychowicz et al., 2016; Li and Malik, 2017; Metz et al., 2019, 2022). However, those black-box optimizers, typically trained on a limited number of small tasks, struggle to generalize to state-of-the-art settings where much larger models are trained with significantly more training steps. Another line of methods (Bello et al., 2017; Wang et al., 2022) apply reinforcement learning or Monte Carlo Sampling to discover new optimizers, where the search space is defined by trees composed from predefined operands (e.g., gradient and momentum) and operators (e.g., unary and binary math operations). However, to make the search manageable, they often restrict the search space by using fixed operands and limiting the size of the tree, thereby limiting the potential for discovery. Consequently, the algorithms discovered have not yet reached the state-of-the-art. AutoML-Zero (Real et al., 2020) is an ambitious effort that attempts to search every component of a machine learning pipeline while evaluating on toy tasks. This work follows the research direction of automatic discovering optimizers and is in particular inspired by AutoML-Zero, but aims at discovering effective optimization algorithms that can improve the state-of-the-art benchmarks.

In this paper, we present a method to formulate algorithm discovery as program search and apply it to discover optimization algorithms. There are two primary challenges. The first one is to find high-quality algorithms in the infinite and sparse program space. The second one is to further select out the algorithms that can generalize from small proxy tasks to much larger, state-of-the-art tasks. To tackle these challenges, we employ a range of techniques including evolutionary search with warm-start and restart, abstract execution, funnel selection, and program simplification.

Our method discovers a simple and effective optimization algorithm: Lion, short for *Evo**L**ved **S**ign **M**omen**t**um*. This algorithm differs from various adaptive algorithms by only tracking momentum and leveraging the sign operation to calculate updates, leading to lower memory overhead and uniform update magnitudes across all dimensions. Despite its simplicity, Lion demonstrates outstanding performance across a range of models (Transformer, MLP, ResNet, U-Net, and Hybrid) and tasks (image classification, vision-language contrastive learning, diffusion, language modeling, and fine-tuning). Notably, we achieve 88.3% *zero-shot* and 91.1% *fine-tuning* accuracy on ImageNet by replacing Adafactor with Lion in BASIC (Pham et al., 2021), surpassing the previous best results by 2% and 0.1%, respectively. Additionally, Lion reduces the pre-training compute

Program 2: An example training loop, where the optimization algorithm that we are searching for is encoded within the `train` function. The main inputs are the weight (`w`), gradient (`g`) and learning rate schedule (`lr`). The main output is the `update` to the weight. `v1` and `v2` are two additional variables for collecting historical information.

```
w = weight_initialize()
v1 = zero_initialize()
v2 = zero_initialize()
for i in range(num_train_steps):
  lr = learning_rate_schedule(i)
  g = compute_gradient(w, get_batch(i))
  update, v1, v2 = train(w, g, v1, v2, lr)
  w = w - update
```

Program 3: Initial program (AdamW). The bias correction and ϵ are omitted for simplicity.

```
def train(w, g, m, v, lr):
  g2 = square(g)
  m = interp(g, m, 0.9)
  v = interp(g2, v, 0.999)
  sqrt_v = sqrt(v)
  update = m / sqrt_v
  wd = w * 0.01
  update = update + wd
  lr = lr * 0.001
  update = update * lr
  return update, m, v
```

Program 4: Discovered program after search, selection and removing redundancies in the raw Program 8. Some variables are renamed for clarity.

```
def train(w, g, m, v, lr):
  g = clip(g, lr)
  g = arcsin(g)
  m = interp(g, v, 0.899)
  m2 = m * m
  v = interp(g, m, 1.109)
  abs_m = sqrt(m2)
  update = m / abs_m
  wd = w * 0.4602
  update = update + wd
  lr = lr * 0.0002
  m = cosh(update)
  update = update * lr
  return update, m, v
```

on JFT by up to 5x, improves training efficiency on diffusion models by 2.3x and achieves a better FID score, and offers similar or better performance on language modeling with up to 2x compute savings.

We analyze the properties and limitations of Lion. Users should be aware that the uniform update calculated using the sign function usually yields a larger norm compared to those generated by SGD and adaptive methods. Therefore, Lion requires a smaller learning rate lr, and a larger decoupled weight decay λ to maintain the effective weight decay strength. For detailed guidance, please refer to Section 5. Additionally, our experiments show that the gain of Lion increases with the batch size and it is more robust to different hyperparameter choices compared to AdamW. For limitations, the difference between Lion and AdamW is not statistical significant on some large-scale language and image-text datasets. The advantage of Lion is smaller if using strong augmentations or a small batch size ($<$64) during training. See Section 6 for details.

2 Symbolic Discovery of Algorithms

We present an approach that formulates algorithm discovery as program search (Brameier et al., 2007; Koza, 1994; Real et al., 2020). We use a symbolic representation in the form of programs for the following advantages: (1) it aligns with the fact that algorithms must be implemented as programs for execution; (2) symbolic representations like programs are easier to analyze, comprehend and transfer to new tasks compared to parameterized models such as neural networks; (3) program length can be used to estimate the complexity of different programs, making it easier to select the simpler, often more generalizable ones. This work focuses on optimizers for deep neural network training, but the method is generally applicable to other tasks.

2.1 Program Search Space

We adhere to the following three criteria while designing the program search space: (1) the search space should be flexible enough to enable the discovery of novel algorithms; (2) the programs should be easy to analyze and incorporate into a machine learning workflow; (3) the programs should focus on the high-level algorithmic design rather than low-level implementation details. We define the programs to contain functions operating over n-dimensional arrays, including structures like lists and dictionaries containing such arrays, in an imperative language. They are similar to Python code using NumPy / JAX (Bradbury et al., 2018; Harris

et al., 2020) as well as pseudo code of optimization algorithms. The details of the design are outlined below, with an example representation of AdamW in Program 3.

Input / output signature The program defines a `train` function, which encodes the optimization algorithm being searched for, where the main inputs are the model weight (`w`), the gradient (`g`) and the learning rate schedule value (`lr`) at the current training step. The main output is the `update` to the weight. The program also incorporates extra variables initialized as zeros to collect historical information during training. For example, AdamW requires two extra variables to estimate first and second moments. Note that those variables can be used arbitrarily, we use the name `m` and `v` in Program 3 just for better readability. This simplified code snippet in Program 2 uses the same signature as AdamW to ensure that the discovered algorithms have smaller or equal memory footprints. As opposed to previous optimizer search attempts (Bello et al., 2017; Wang et al., 2022), our method allows discovering better ways of updating the extra variables.

Building blocks The `train` function consists of a sequence of assignment statements, with no restrictions on the number of statements or local variables. Each statement calls a function using constants or existing variables as inputs, and the resulting value is stored in a new or existing variable. For the program, we select 45 common math functions, most of which corresponds to a function in NumPy or an operation in linear algebra. Some functions are introduced to make the program more compact, such as the linear interpolation function `interp(x, y, a)`, which is made equivalent to `(1 - a) * x + a * y`. Preliminary experiments have investigated the inclusion of more advanced features such as conditional and loop statements, and defining and calling new functions, but these do not yield improved results, so we leave them out. A detailed description of the functions are summarized in Appendix H. When necessary, the types and shapes of the function arguments are automatically cast, e.g., in the case of adding a dictionary of arrays to a scalar.

Mutations and redundant statements The design of mutations utilized in evolutionary search is tightly intertwined with the representation of the program. We include three types of mutations: (1) inserting a new statement at a random location with randomly chosen functions and arguments, (2) deleting a random chosen statement, and (3) modifying a random statement by randomly altering one of its function arguments, which may be either variables or constants. To mutate an argument, we replace it with an existing variable or a newly generated constant obtained by sampling from a normal distribution $X \sim \mathcal{N}(0\ 1)$. Additionally, we can mutate an existing constant by multiplying it by a random factor 2^a, where $a \sim \mathcal{N}(0\ 1)$. These constants serve as tunable hyperparameters in the optimization algorithm, such as the peak learning rate and weight decay in AdamW. Note that we allow a program to include redundant statements during search, i.e., statements that do not impact the final program outputs. This is necessary as mutations are limited to only affecting a single statement. Redundant statements may therefore serve as intermediate steps towards future substantial modifications in the program.

Infinite and sparse search space Given the limitless number of statements and local variables, as well as the presence of mutable constants, the program search space is infinite. Even if we ignore the constants and bound the program length and number of variables, the number of potential programs is still intractably large. A rough estimate of the number of possible programs is $n_p = n_f^l n_v^{n_a * l}$, where n_f is the number of possible functions, n_v is the number of local variables, n_a is the average number of arguments per statement, and l is the program length. More importantly, the challenge comes from the sparsity of high-performing programs in the search space. To illustrate this point, we conduct a random search that evaluates over 2M programs on a low-cost proxy task. The best program among them is still significantly inferior to AdamW.

2.2 Efficient Search Techniques

We employ the following techniques to address the challenges posed by the infinite and sparse search space.

Evolution with warm-start and restart We apply regularized evolution as it is simple, scalable, and has shown success on many AutoML search tasks (Holland, 1992; Real et al., 2019, 2020; So et al., 2019; Ying et al., 2019). It keeps a population of P algorithms that are gradually improved through cycles. Each cycle picks $T < P$ algorithms at random and the best performer is chosen as the *parent*, i.e., *tournament selection* (Goldberg and Deb, 1991). This parent is then copied and *mutated* to produce a *child* algorithm, which is added to

Figure 2: **Left**: We run hyperparameter tuning on AdamW and random search, both with 4x more compute, to get the best results as two baselines (green and red lines). The evolutionary search, with mean and standard error calculated from five runs, significantly outperforms both of them. The use of multiple restarts from the initial program is crucial due to the high variance in the search fitness (blue curves), and restarting from the best program after 300K progress further improves the fitness (orange curves) when the original search plateaus. **Right**: Example curves of search fitness, the cache hit rate, and the percentage of redundant statements. The cache hit rate and the redundant statements percentage increase along with the search progress to ∼90% and ∼70%.

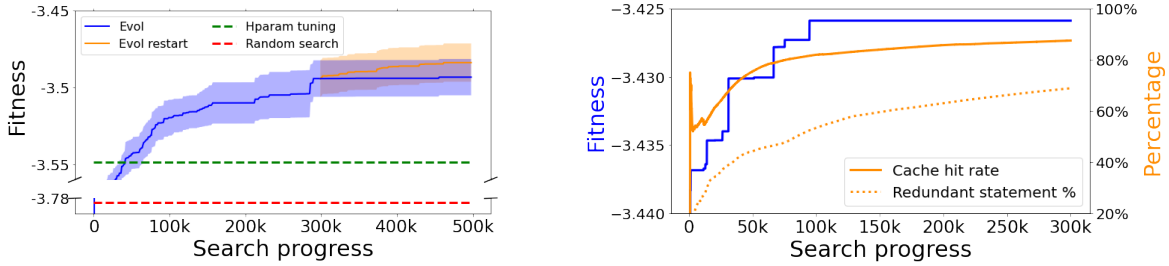

the population, while the oldest algorithm is removed. Normally, evolutionary search starts with random candidates, but we warm-start the initial population as AdamW to accelerate the search. By default, we use a tournament size of two and a population size of 1K. To further improve the search efficiency, we apply two types of restart: (1) restarting from the initial program, which can lead to different local optima due to the randomness in evolution and encourage exploration. This can be done by running multiple searches in parallel. (2) restarting from the best algorithm found thus far to further optimize it, encouraging exploitation. Figure 2 (Left) displays the mean and standard error of five evolutionary search experiments. We run hyperparameter tuning based on AdamW by only allowing mutations of constants in the evolution, and run random search by sampling random programs, both with 4x more compute. Our search significantly outperforms the best results achieved by both baselines, demonstrated as the two dashed lines in the figure. The high variance in the search fitness necessitates running multiple repeats through restarting from the initial program. When the search fitness plateaus after ∼300K progress, restarting from the best program found thus far further improves the fitness shown by the orange curve.

Pruning through abstract execution We propose to prune the redundancies in the program space from three sources: programs with syntax or type / shape errors, functionally equivalent programs, and redundant statements in the programs. Before a program is actually executed, we perform an abstract execution step that (1) infers variable types and shapes to detect programs with errors, and keeps mutating the parent program until a valid child program is generated; (2) produces a hash that uniquely identifies how the outputs are computed from the inputs, allowing us to cache and look up semantically duplicate programs (Gillard et al., 2023); (3) identifies redundant statements that can be ignored during actual execution and analysis. For instance, Program 4 is obtained after removing all redundant statements in Program 8. Abstract execution has negligible cost compared to the actual execution, with each input and function replaced by customized values, e.g., hash. See Appendix I for details of abstract execution. Preliminary experiments have shown that the search process can become overwhelmed with invalid programs and cannot make progress without filtering out invalid programs. As seen in Figure 2 (Right), the percentage of redundant statements and cache hit rate both increase as the search proceeds. Based on five search runs, each covering 300K programs, there are $69.8 \pm 1.9\%$ redundant statements towards the end, implying that redundant statements removal makes the program ∼3x shorter on average, thus easier to analyze. The cache hit rate is $89.1 \pm 0.6\%$, indicating that using the hash table as cache brings ∼10x reduction on the search cost.

Proxy tasks and search cost To reduce search cost, we create low-cost proxies by decreasing the model size, number of training examples, and steps from the target tasks. Evaluation on the proxies can be completed on one TPU V2 chip within 20min. We use the accuracy or perplexity on the validation set as the fitness. Each search experiment utilizes 100 TPU V2 chips and runs for ∼72h. There are a total of 200-300K programs generated during each search experiment. However, the number of programs that are actually evaluated is

Figure 3: **Left**: The meta-validation (defined in Section 2.3) curves of two search runs measured on a ∼500x larger meta-validation task compared to the proxy. The blue one meta-overfits at ∼15% of the search progress, while the orange one meta-overfits at ∼90% and achieves a better metric. **Right**: Histogram of the search progress when meta-overfitting happens based on 50 runs. Half of the runs meta-overfit early but a long tail of runs meta-overfit much later. Blue cross depicts the best meta-validation metric averaged within each bin, indicating that meta-overfitting happening later leads to programs that generalize better.

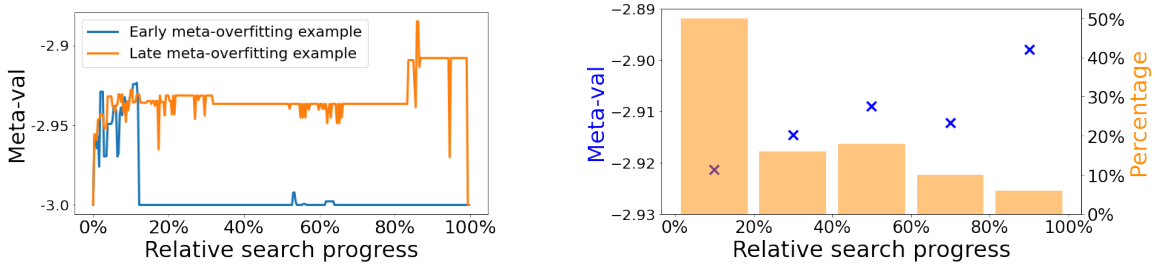

around 20-30K, thanks to the use of the cache through abstract execution. To incorporate restart, we start five repeats of search experiments, followed by another round of search initializing from the best algorithm found thus far. This results in a total cost of ∼3K TPU V2 days. See Appendix F for the details of proxy tasks.

2.3 Generalization: Program Selection and Simplification

The search experiments can discover promising programs on proxy tasks. We use performance on *meta-validation* tasks that are larger than the proxy tasks by increasing the model size and training steps, to select the programs that generalize beyond proxy tasks then further simplify them. The phenomenon of *meta-overfitting* occurs when the search fitness keeps growing, but the meta-validation metric declines, indicating that the discovered algorithms have overfit the proxy tasks. Two examples are shown in Figure 3 (Left), where the blue curve represents early meta-overfitting and the orange curve represents later meta-overfitting.

Large generalization gap The discovered algorithms face a significant challenge due to the substantial gap between the proxy tasks during search and the target tasks. While proxy tasks can typically be completed within 20min on one TPU V2 chip, target tasks can be $> 10^4$x larger and require days of training on 512 TPU V4 chips. Furthermore, we expect the optimizer to perform well on different architectures, datasets and even different domains, so the discovered algorithms need to show strong out-of-distribution generalization. The sparse search space and inherent noise in the evolution process further compound this challenge, leading to inconsistent generalization properties between different runs. Our observation suggests that evolutionary search experiments that meta-overfit later tend to uncover optimization algorithms that generalize better. See more details in Figure 3 (Right).

Funnel selection To mitigate the generalization gap, we collect promising programs based on search fitness and add an extra selection step using a series of meta-validation tasks to select those generalize better. To save compute, we apply a funnel selection process that gradually increases the scale of the meta-validation tasks. For example, starting with proxy task A, we create a 10x larger task B by increasing the model size and the training steps. Only algorithms that surpass the baseline on task B will be evaluated on task C, which is 100x larger. This approach allows us to gradually filter out algorithms that show poor generalization performance, ultimately leading to the selection of algorithms that generalize well to larger tasks.

Simplification Simpler programs are easier to understand and our intuition is that they are more likely to generalize, so we simplify the programs with the following steps. Firstly, we remove redundant statements that do not contribute to the final output as identified through abstract execution. Secondly, we remove statements that are non-redundant but produce minimal differences when removed. This step can also be achieved through evolution by disabling the insertion of new statements in the mutation process. Finally, we rearrange the statements manually, assign clear and descriptive names to variables, and convert the program into its simpler, mathematically equivalent form.

3 Derivation and Analysis of Lion

We arrive at the optimizer Lion due to its simplicity, memory efficiency, and strong performance in search and meta-validation. Note that the search also discovers other existing or novel algorithms shown in Appendix D, e.g., some with better regularization and some resembling AdaBelief (Zhuang et al., 2020) and AdaGrad (Duchi et al., 2011).

3.1 Derivation

The search and funnel selection process lead to Program 4, which is obtained by automatically removing redundant statements from the raw Program 8 (in the Appendix). We further simplify it to get the final algorithm (Lion) in Program 1. Several unnecessary elements are removed from Program 4 during the simplification process. The `cosh` function is removed since `m` would be reassigned in the next iteration (line 3). The statements using `arcsin` and `clip` are also removed as we observe no quality drop without them. The three red statements translate to a single `sign` function. Although both `m` and `v` are utilized in Program 4, `v` only changes how the momentum is updated (two `interp` functions with constants $\sim$0.9 and $\sim$1.1 is equivalent to one with $\sim$0.99) and does not need to be separately tracked. Note that the bias correction is no longer needed, as it does not change the direction. Algorithm 2 shows the pseudocode.

3.2 Analysis

Sign update and regularization The Lion algorithm produces update with uniform magnitude across all dimensions by taking the sign operation, which is in principle different from various adaptive optimizers. Intuitively, the sign operation adds noise to the updates, which acts as a form of regularization and helps with generalization (Chen et al., 2022; Foret et al., 2021; Neelakantan et al., 2017). An evidence is shown in Figure 11 (Right) in the Appendix, where the ViT-B/16 trained by Lion on ImageNet has a higher training error compared to AdamW but a 2% higher accuracy on the validation set (as shown in Table 2). Additionally, the results in Appendix G demonstrate that Lion leads to the convergence in smoother regions, which usually results in better generalization.

Momentum tracking The default EMA factor used to track the momentum in Lion is 0.99 (β_2), compared to the commonly used 0.9 in AdamW and momentum SGD. The current gradient and momentum are interpolated with a factor of 0.9 (β_1) before the sign operation is applied. This choice of EMA factor and interpolation allows Lion to balance between remembering a $\sim$10x longer history of the gradient in momentum and putting more weight on the current gradient in the update. The necessity of both β_1 and β_2 is further discussed in Section 4.6.

Hyperparameter and batch size choices Lion is simpler and has fewer hyperparameters compared to AdamW and Adafactor as it does not require ϵ and factorization-related ones. The update is an element-wise binary ± 1 if we omit the weight decay term, with larger norm than those produced by other optimizers like SGD and adaptive algorithms. As a result, Lion needs a *smaller* learning rate and in turn a *larger* decoupled weight decay to achieve a similar effective weight decay strength (`lr * λ`). Detailed information on tuning Lion can be found in Section 5. Additionally, the advantage of Lion over AdamW enlarges as the batch size increases, which fits the common practice of scaling up model training through data parallelism (Section 4.6).

Memory and runtime benefits Lion only saves the momentum thus has smaller memory footprint than popular adaptive optimizers like AdamW, which is beneficial when training large models and / or using a large batch size. As an example, AdamW needs at least 16 TPU V4 chips to train a ViT-B/16 with image resolution 224 and batch size 4,096, while Lion only needs 8 (both with `bfloat16` momentum). Another practical benefit is that Lion has faster runtime (steps / sec) in our experiments due to its simplicity, usually 2-15% speedup compared to AdamW and Adafactor depending on the task, codebase, and hardware.

Relation to existing optimizers The sign operation has been explored in previous optimizers (Bernstein et al., 2018; Riedmiller and Braun, 1993). The closest to ours is the handcrafted optimizer signSGD (Bernstein et al., 2018) (and its momentum variant) that also utilizes the sign operation to calculate the update but

Table 2: Accuracy on ImageNet, ImageNet ReaL, and ImageNet V2. Numbers in $(\cdot)$ are from Dai et al. (2021); Dosovitskiy et al. (2021). Results are averaged from three runs.

Model	#Params	Optimizer	RandAug + Mixup	ImageNet	ReaL	V2
Train from scratch on ImageNet						
ResNet-50	25.56M	SGD	✗	76.22	82.39	63.93
		AdamW		76.34	**82.72**	**64.24**
		Lion		**76.45**	**82.72**	64.02
Mixer-S/16	18.53M	AdamW	✗	69.26	75.71	55.01
		Lion		**69.92**	**76.19**	**55.75**
Mixer-B/16	59.88M	AdamW	✗	68.12	73.92	53.37
		Lion		**70.11**	**76.60**	**55.94**
ViT-S/16	22.05M	AdamW	✗	76.12	81.94	63.09
		Lion		**76.70**	**82.64**	**64.14**
		AdamW	✓	78.89	84.61	66.73
		Lion		**79.46**	**85.25**	**67.68**
ViT-B/16	86.57M	AdamW	✗	75.48	80.64	61.87
		Lion		**77.44**	**82.57**	**64.81**
		AdamW	✓	80.12	85.46	68.14
		Lion		**80.77**	**86.15**	**69.19**
CoAtNet-1	42.23M	AdamW	✓	83.36 (83.3)	-	-
		Lion		**84.07**	-	-
CoAtNet-3	166.97M	AdamW	✓	84.45 (84.5)	-	-
		Lion		**84.87**	-	-
Pre-train on ImageNet-21K then fine-tune on ImageNet						
ViT-B/16_{384}	86.86M	AdamW	✗	84.12 (83.97)	88.61 (88.35)	73.81
		Lion		**84.45**	**88.84**	**74.06**
ViT-L/16_{384}	304.72M	AdamW	✗	85.07 (85.15)	88.78 (88.40)	75.10
		Lion		**85.59**	**89.35**	**75.84**

has a different momentum update rule from Lion. Their focus is to mitigate communication costs between agents in distributed training, and they observe inferior performance when training ConvNets on image classification tasks. On the other hand, NAdam (Dozat, 2016) combines the updated first moment and the gradient to compute the update, but Lion decouples the momentum tracking and how it is applied to the update through β_2. A comparison of Lion with related optimizers can be found in Section 4.5.

4 Evaluation of Lion

In this section, we present evaluations of Lion, on various benchmarks. We mainly compare it to AdamW (or Adafactor when memory is a bottleneck) as it is exceedingly popular and the de facto standard optimizer on a majority of learning tasks. The result of momentum SGD is only included for ResNet since it performs worse than AdamW elsewhere. We also benchmark other popular optimizers in Section 4.5, whose performance and learning curves are similar to AdamW. We make sure that every optimizer is well-tuned for each task (see Section 5 for tuning details). By default, the learning rate schedule is cosine decay with 10K steps warmup, and the momentum is saved as `bfloat16` to reduce the memory footprint.

4.1 Image Classification

We perform experiments including various datasets and architectures on the image classification task (see Appendix B for dataset details). Apart from training from scratch on ImageNet, we also pre-train on two

Table 3: Model performance when pre-trained on JFT then fine-tuned on ImageNet. Two giant ViT models are pre-trained on JFT-3B while smaller ones are pre-trained on JFT-300M. The ViT-G/14 results are directly from Zhai et al. (2021).

Model	ViT-L/16_{512}		ViT-H/14_{518}		ViT-g/14_{518}		ViT-G/14_{518}	
#Params	305.18M		633.47M		1.04B		1.88B	
Optimizer	AdamW	Lion	AdamW	Lion	Adafactor	Lion	Adafactor	Lion
ImageNet	87.72	**88.50**	88.55	**89.09**	90.25	**90.52**	90.45	**90.71** / **90.71***
ReaL	90.46	**90.91**	90.62	**91.02**	90.84	**91.11**	90.81	**91.06** / **91.25***
V2	79.80	**81.13**	81.12	**82.24**	83.10	**83.39**	83.33	**83.54** / **83.83***
A	52.72	**58.80**	60.64	**63.78**	-	-	-	-
R	66.95	**72.49**	72.30	**75.07**	-	-	-	-

* We observe overfitting in fine-tuning, therefore report both the last and oracle results.

larger well-established datasets, ImageNet-21K and JFT (Sun et al., 2017). The image size is 224^2 by default otherwise specified by the subscript.

Train from scratch on ImageNet Following previous works (Dosovitskiy et al., 2021; He et al., 2016), we train ResNet-50 for 90 epochs with a batch size of 1,024, and other models for 300 epochs with a batch size of 4,096. As shown in Table 2, Lion significantly outperforms AdamW on various architectures. Empirically, the improvement is more substantial on models with larger capacity, with accuracy increases of 1.96% and 0.58% for ViT-B/16 and ViT-S/16, respectively. The performance gaps also tend to enlarger with fewer inductive biases. When strong augmentations are applied, the gain of Lion over AdamW shrinks, but it still outperforms AdamW by 0.42% on CoAtNet-3, despite the strong regularization during training (Dai et al., 2021).

Pre-train on ImageNet-21K We pre-train ViT-B/16 and ViT-L/16 on ImageNet-21K for 90 epochs with a batch size of 4,096. Table 2 shows that Lion still surpasses AdamW even when the training set is enlarged for 10x. The gaps on larger models are consistently bigger, with +0.52% vs. +0.33% (ImageNet), +0.57% vs. +0.23% (ReaL), and +0.74% vs. +0.25% (V2) for ViT-L/16 and ViT-B/16, respectively.

Pre-train on JFT To push the limit, we conduct extensive experiments on JFT. We follow the settings of Dosovitskiy et al. (2021) and Zhai et al. (2021) for both pre-training and fine-tuning. Figure 1 (Left) and 4 present the accuracy of three ViT models (ViT-B/16, ViT-L/16, and ViT-H/14) under different pre-training budgets on JFT-300M. Lion enables the ViT-L/16 to match the performance of ViT-H/14 trained by AdamW on ImageNet and ImageNet V2 but with 3x less pre-training cost. On ImageNet ReaL, the compute saving further becomes 5x. Another evidence is that even when a ViT-L/16 is trained by AdamW for 4M steps by Zhai et al. (2021), its performance still lags behind the same model trained by Lion for 1M steps.

Table 3 shows the fine-tuning results, with higher resolution and Polyak averaging. Our ViT-L/16 matches the previous ViT-H/14 results trained by AdamW, while being 2x smaller. The advantage is larger on more challenging benchmarks, such as +1.33% (V2), +6.08% (A), +5.54% (R) for ViT-L/16. After we scale up the pre-training dataset to JFT-3B, the ViT-g/14 trained by Lion outperforms the previous ViT-G/14 results (Zhai et al., 2021), with 1.8x fewer parameters. Our ViT-G/14 further achieves a 90.71% accuracy on ImageNet.

4.2 Vision-Language Contrastive Learning

This section focuses on the CLIP style vision-language contrastive training (Radford et al., 2021). Instead of learning all the parameters from scratch, we initialize the image encoder with a strong pre-trained model as it is suggested to be more efficient (Zhai et al., 2022).

Locked-image text Tuning (LiT) We perform a comparison between Lion and AdamW on LiT (Zhai et al., 2022) by training the text encoder (Zhai et al., 2022) in a contrastive manner using the same frozen pre-trained ViT. All models are trained for 1B image-text pairs with a batch size of 16,384. Table 4 shows the zero-shot image classification results on three model scales, with the name specifies the size, e.g., LiT-B/16-B denotes

Figure 4: ImageNet ReaL (**Left**) and ImageNet V2 (**Right**) accuracy after we pre-train ViT models on JFT-300M then fine-tune on ImageNet. See Table 8 (in the Appendix) for the detailed numbers.

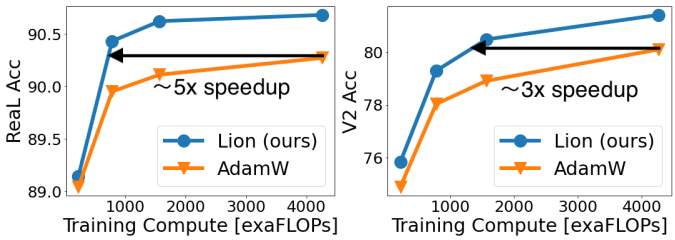

Table 4: Zero-shot accuracy of LiTs on ImageNet, CIFAR-100, and Oxford-IIIT Pet. As a reference, the zero-shot accuracy of CLIP (Radford et al., 2021) on ImageNet is 76.2%.

Model	Optimizer	ImageNet	C100	Pet
LiT-B/32-B	AdamW	68.78	71.41	86.62
	Lion	**69.88**	**71.78**	**87.36**
LiT-B/16-B	AdamW	74.26	72.25	89.83
	Lion	**75.39**	**72.49**	**91.20**
LiT-g/14_{288}-L	AdamW	83.43	80.93	94.88
	Lion	**84.09**	**81.43**	**95.86**

Figure 5: The zero-shot ImageNet accuracy curve of LiT-B/16-B (**Left**). FID comparison on 64×64 (**Middle**) and 128×128 (**Right**) image generation when training diffusion models. We decode image w/o guidance.

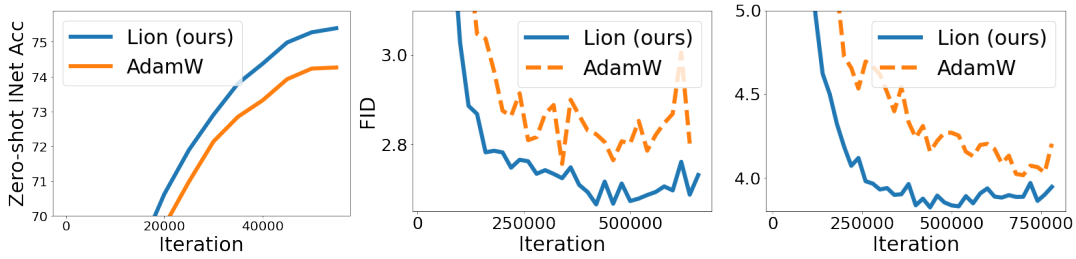

a ViT-B/16 and a base size Transformer as the text encoder. Our method, Lion, demonstrates consistent improvement over AdamW with gains of +1.10%, +1.13%, and +0.66% on zero-shot ImageNet accuracy for LiT-B/32-B, LiT-B/16-B, and LiT-g/14_{288}-L, respectively. Figure 5 (Left) depicts an example zero-shot learning curve of LiT-B/16-B. Similar results are obtained on the other two datasets. The zero-shot image-text retrieval results on MSCOCO (Lin et al., 2014) and Flickr30K (Plummer et al., 2015) can be found in Figure 9 (in the Appendix). The evaluation metric is Recall@K, calculated based on if the ground truth label of the query appears in the top-K retrieved examples. Lion outperforms AdamW on both datasets, with a larger gain in Recall@1 than Recall@10 on Flicker30K, implying more accurate retrieval results: +1.70% vs. +0.60% for image $\rightarrow$ text and +2.14% vs. +0.20% for text $\rightarrow$ image.

BASIC Pham et al. (2021) propose to scale up batch size, dataset, and model size simultaneously, achieving drastic improvements over CLIP. It uses a sophisticated CoAtNet (Dai et al., 2021) pre-trained on JFT-5B as the image encoder. Furthermore, the contrastive training is performed on 6.6B image-text pairs with a larger 65,536 batch size. To push the limit, we only experiment on the largest BASIC-L, and use Lion on *both* image encoder pre-training and contrastive learning stages. As illustrated in Table 1, we achieve a significant 2.6% gain over the baseline, striking a 88.3% accuracy on zero-shot ImageNet classification. Note that this result is 2.0% higher than the previous best result (Yu et al., 2022). The performance gain is consistent on five other robustness benchmarks. After fine-tuning the image encoder (CoAtNet-7) in BASIC-L obtained by Lion, we further achieve a 91.1% top-1 accuracy on ImageNet, which is 0.1% better than the previous SOTA.

4.3 Diffusion Model

Recently, diffusion models achieve a huge success on image generation (Dhariwal and Nichol, 2021; Ho and Salimans, 2022; Ho et al., 2020; Saharia et al., 2022; Song et al., 2021). Given its enormous potential, we test the performance of Lion on unconditional image synthesis and multimodal text-to-image generation.

Image synthesis on ImageNet We utilize the improved U-Net architecture introduced in Dhariwal and

Figure 6: Evaluation of the Imagen text-to-image 64^2 (**Left**) and the $64^2 \rightarrow 256^2$ diffusion models (**Right**).

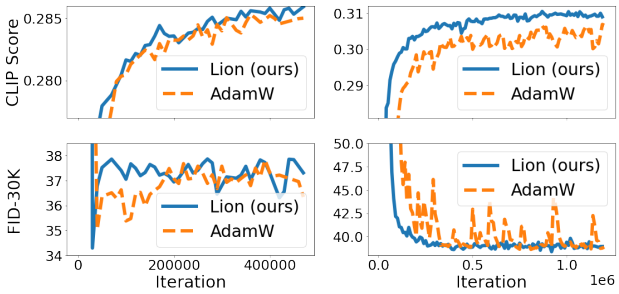

Figure 7: Log perplexity on Wiki-40B (**Left**) and PG-19 (**Right**). The speedup brought by Lion tends to increase with the model scale. The largest model on Wiki-40B is omitted as we observe severe overfitting.

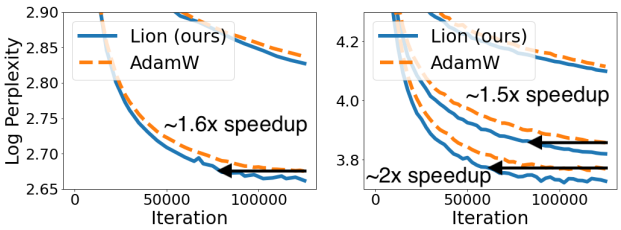

Nichol (2021) and perform 64×64, 128×128, and 256×256 image generation on ImageNet. The batch size is set as 2,048 and the learning rate remains constant throughout training. For decoding, we apply DDPM (Ho et al., 2020) for 1K sampling steps *without* classifier-free guidance.The evaluation metric is the standard FID score. Illustrated by Figure 1 (Right) and 5 (Middle and Right), Lion enables both better quality and faster convergence on the FID score. Note that the gap between Lion and AdamW tends to increase with the image resolution, where the generation task becomes more challenging. When generating 256×256 images, Lion achieves the final performance of AdamW at 440K steps, reducing 2.3x iterations. The final FID scores are 4.1 (Lion) vs. 4.7 (AdamW), and for reference, the FID of ADM (Dhariwal and Nichol, 2021) is 10.94.

Text-to-image generation We follow the Imagen (Saharia et al., 2022) setup to train a base 64×64 text-to-image model and a $64 \times 64 \rightarrow 256 \times 256$ super-resolution model. All models are trained on a high-quality internal image-text dataset with a batch size of 2,048 and a constant learning rate. Due to computational constraints, our base U-Net has a width of 192 compared to 512 in the original 2B model, while the 600M super-resolution model is identical to the original Imagen setup. Along with the training, 2K images are sampled from the MSCOCO (Lin et al., 2014) validation set for real-time evaluation. We use the CLIP score to measure image-text alignment and the zero-shot FID-30K to measure image fidelity. Classifier-free guidance (Ho and Salimans, 2022) with a weight of 5.0 is applied as it has been shown to improve image-text alignment. Figure 6 depicts the learning curve. While there is no clear improvement on the base 64×64 model, Lion outperforms AdamW on the text-conditional super-resolution model. It achieves a higher CLIP score and has a less noisy FID metric compared to AdamW.

4.4 Language Modeling and Fine-tuning

This section focuses on language modeling and fine-tuning. On language-only tasks, we find that tuning β_1 and β_2 can improve the quality for both AdamW and Lion. See Section 5 for tuning details.

Autoregressive language modeling We first experiment on two smaller-scale academic datasets Wiki-40B (Guo et al., 2020) and PG-19 (Rae et al., 2020) following Hua et al. (2022). The employed Transformer spans three scales: small (110M), medium (336M), and large (731M). The architecture details can be found in Appendix E. All models are trained with 2^{18} tokens per batch for 125K steps, with a learning rate schedule of 10K steps warmup followed by linear decay. The context length is set to 512 for Wiki-40B and 1,024 for PG-19. Figure 7 illustrates the token-level perplexity for Wiki-40B and word-level perplexity for PG-19. Lion consistently achieves lower validation perplexity than AdamW. It achieves 1.6x and 1.5x speedup when training the medium size model on Wiki-40B and PG-19, respectively. When the model is increased to the large size, the speedup on PG-19 further increases to 2x.

Scaling up the scale of language models and pre-training datasets has revolutionized the field of NLP. So we further perform larger-scale experiments. Our pre-training dataset, similar to that used in GLaM (Du et al., 2022), consists of 1.6 trillion tokens spanning a wide range of natural language use cases. Following GPT-3 (Brown et al., 2020), we train three models, ranging from 1.1B to 7.5B parameters, for 300B tokens with

Table 5: One-shot evaluation averaged over three NLG and 21 NLU tasks. The results of GPT-3 (Brown et al., 2020) and PaLM (Chowdhery et al., 2022) are included for reference. The LLMs trained by Lion have better in-context learning ability. See Table 11 (in the Appendix) for detailed results on all tasks.

Task	1.1B		2.1B		7.5B		6.7B	8B
	Adafactor	Lion	Adafactor	Lion	Adafactor	Lion	GPT-3	PaLM
#Tokens	300B						300B	780B
Avg NLG	11.1	**12.1**	15.6	**16.5**	24.1	**24.7**	23.1	23.9
Avg NLU	53.2	**53.9**	56.8	**57.4**	61.3	**61.7**	58.5	59.4

Table 6: Fine-tuning performance of the T5 Base, Large, and 11B on the GLUE dev set. Results reported are the peak validation scores per task.

Model	Optimizer	CoLA	SST-2	MRPC	STS-B	QQP	MNLI -m	MNLI -mm	QNLI	RTE	Avg
Base	AdamW	60.87	95.18	92.39 / 89.22	**90.70** / **90.51**	89.23 / 92.00	86.77	86.91	93.70	81.59	87.42
	Lion	**61.07**	**95.18**	**92.52** / **89.46**	90.61 / 90.40	**89.52** / **92.20**	**87.27**	**87.25**	**93.85**	**85.56**	**87.91**
Large	AdamW	63.89	96.10	93.50 / 90.93	91.69 / 91.56	90.08 / 92.57	89.69	89.92	94.45	89.17	89.46
	Lion	**65.12**	**96.22**	**94.06** / **91.67**	**91.79** / **91.60**	**90.23** / **92.67**	**89.85**	**89.94**	**94.89**	**90.25**	**89.86**
11B	AdamW	69.50	97.02	93.75 / 91.18	92.57 / 92.61	90.45 / 92.85	**92.17**	**91.99**	96.41	92.42	91.08
	Lion	**71.31**	**97.13**	**94.58** / **92.65**	**93.04** / **93.04**	**90.57** / **92.95**	91.88	91.65	**96.56**	**93.86**	**91.60**

a batch size of 3M tokens and a context length of 1K. We evaluate them on three natural language generative (NLG) and 21 natural language understanding (NLU) tasks (see Appendix C for task details). On this massive dataset, we observe no perplexity difference throughout training. Nevertheless, Lion outperforms Adafactor on the average in-context learning ability, as shown in Table 5. Our 7.5B baseline model, trained for 300B tokens, outperforms the 8B PaLM, trained for 780B tokens, demonstrating the strength of our setup. Lion outperforms Adafactor on both NLG and NLU tasks, particularly on the NLG tasks, with an exact match improvement of +1.0, +0.9, and +0.6 for the 1.1B, 2.1B, and 7.5B models, respectively.

Masked language modeling We also perform BERT training on the C4 dataset (Raffel et al., 2020). It requires the language models to reconstruct randomly masked out tokens in the input sequence. We use the same architectures and training setups as the smaller-scale autoregressive experiments. Lion performs slightly better than AdamW regarding the validation perplexity: 4.18 vs. 4.25 (small), 3.42 vs. 3.54 (medium), and 3.18 vs. 3.25 (large). See Figure 11 (Left) in the Appendix for the learning curves.

Fine-tuning We fine-tune Base (220M), Large (770M), and the largest 11B T5 (Raffel et al., 2020) models on the GLUE benchmark (Wang et al., 2019a). Every model is fine-tuned for 500K steps with a batch size of 128 and a constant learning rate. Table 6 shows the results on the GLUE dev set. For MRPC and QQP, we report the F1 / Accuracy scores, for STS-B, we report the Pearson / Spearman correlation, and for the other datasets, we report their default metric. On average, Lion beats AdamW across all three model scales. It achieves 10, 12, and 10 wins out of 12 scores for T5 Base, Large, and 11B models, respectively.

4.5 Comparison with Other Popular Optimizers

We also employ four popular optimizers RAdam (Liu et al., 2020), NAdam (Dozat, 2016), AdaBelief (Zhuang et al., 2020) and AMSGrad (Reddi et al., 2018) to train ViT-S/16 and ViT-B/16 on ImageNet (with RandAug and Mixup). We thoroughly tune the peak learning rate lr and decoupled weight decay λ (Loshchilov and Hutter, 2019) of every optimizer, while other hyperparameters are set as the default values in Optax[2] - a gradient processing and optimization library for JAX. As shown in Table 7, Lion is still the best performing one. We notice that there is no clear winner amongst the baselines. AMSGrad performs the best on ViT-S/16

[2] https://github.com/deepmind/optax

Table 7: The performance of various optimizers to train ViT-S/16 and ViT-B/16 on ImageNet (with RandAug and Mixup). Lion is still the best performing one, and there is no clear winner amongst the baselines.

Model	Task	AdamW	RAdam	NAdam	AdaBelief	AMSGrad	Ablation$_{0.9}$	Ablation$_{0.99}$	Lion
ViT-S/16	ImageNet	78.89	78.59	78.91	78.71	79.01	78.23	78.19	**79.46**
	ReaL	84.61	84.47	84.62	84.56	85.01	84.28	84.17	**85.25**
	V2	66.73	66.39	66.02	66.35	66.82	66.13	65.96	**67.68**
ViT-B/16	ImageNet	80.12	80.26	80.32	80.29	79.85	79.54	79.90	**80.77**
	ReaL	85.46	85.45	85.44	85.48	85.16	85.10	85.36	**86.15**
	V2	68.14	67.76	68.46	68.19	68.48	68.07	68.20	**69.19**

Figure 8: **Left**: Ablation for the effect of batch size. Lion prefers a larger batch than AdamW. ImageNet accuracy of ViT-B/16 trained from scratch when we vary lr and λ for AdamW (**Middle**) and Lion (**Right**). Lion is more robust to different hyperparameter choices.

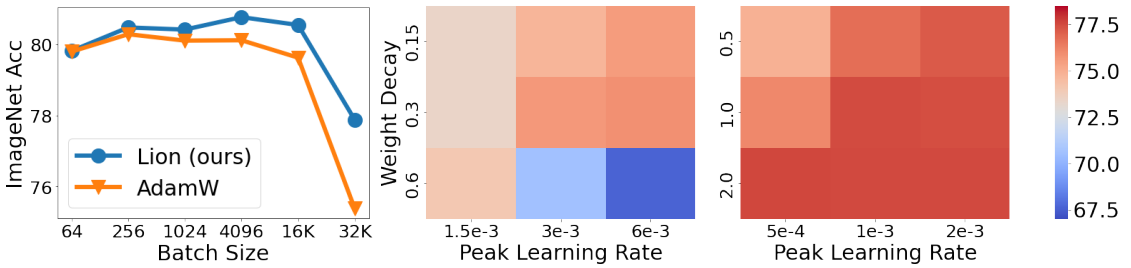

but the worst on ViT-B/16. Figure 10 (in the Appendix) further shows that the learning curves of the five adaptive optimizers are pretty similar, whereas Lion has a unique one that learns faster.

4.6 Ablations

Momentum tracking To ablate the effects of both β_1 and β_2, we compare to a simple update rule: `m = interp(g, m, β); update = sign(m)`. Two optimizers, Ablation$_{0.9}$ and Ablation$_{0.99}$, are created with β values of 0.9 and 0.99 respectively. Illustrated by Table 7, the two ablated optimization algorithms perform worse than all five compared baselines, let alone our Lion. Further ablation studies on the language modeling task (as depicted in Figure 12 in the Appendix) yield similar conclusions. Those results validate the effectiveness and necessity of using two linear interpolation functions, letting Lion to remember longer gradient history meanwhile assign a higher weight to the current gradient.

Effect of batch size Some may question whether Lion requires a large batch size to accurately determine the direction due to the added noise from the sign operation. To address this concern, we train a ViT-B/16 model on ImageNet using various batch sizes while maintaining the total training epoch as 300, and incorporating RandAug and Mixup techniques. As shown in Figure 8 (Left), the optimal batch size for AdamW is 256, while for Lion is 4,096. This indicates that Lion indeed prefers a larger batch size, but its performance remains robust even with a small 64 batch size. Furthermore, when the batch size enlarges to 32K, leading to only 11K training steps, Lion achieves a significant 2.5% accuracy gain over AdamW (77.9% vs. 75.4%), demonstrating its effectiveness in the large batch training setting.

5 Hyperparameter Tuning

To ensure a fair comparison, we tune the peak learning rate lr and decoupled weight decay λ for both AdamW (Adafactor) and our Lion using a logarithmic scale. The default values for β_1 and β_2 in AdamW are set as 0.9 and 0.999, respectively, with an ϵ of $1e-8$, while in Lion, the default values for β_1 and β_2 are discovered

through the program search process and set as 0.9 and 0.99, respectively. We only tune those hyperparameters in language tasks (Section 4.4), where $\beta_1 = 0.9$, $\beta_2 = 0.99$ in AdamW, and $\beta_1 = 0.95$, $\beta_2 = 0.98$ in Lion. Additionally, the ϵ in AdamW is set as $1e-6$ instead of the default $1e-8$ as it improves stability in our experiments, similar to the observations in RoBERTa (Liu et al., 2019b).

The update generated by Lion is an element-wise binary ± 1, as a result of the sign operation, therefore it has a larger norm than those generated by other optimizers. Based on our experience, a suitable learning rate for Lion is typically 3-10x smaller than that for AdamW. Since the effective weight decay is `lr * λ`: `update += w * λ`; `update *= lr`, the value of λ used for Lion is 3-10x larger than that for AdamW in order to maintain a similar strength. For instance, (1) $lr = 1e-4$, $\lambda = 10.0$ in Lion and $lr = 1e-3$, $\lambda = 1.0$ in AdamW when training ViT-B/16 on ImageNet with strong augmentations; (2) $lr = 3e-5$, $\lambda = 0.1$ in Lion and $lr = 3e-4$, $\lambda = 0.01$ in AdamW for diffusion models; (3) $lr = 1e-4$, $\lambda = 0.01$ in Lion and $lr = 1e-3$, $\lambda = 0.001$ in Adafactor for the 7.5B language modeling. Please see Table 12 (in the Appendix) for all hyperparameters.

Apart from the peak performance, the sensitivity to hyperparameters and the difficulty in tuning them are also critical for the adoption of an optimizer in practice. In Figure 8 (Middle and Right), we alter both lr and λ when training ViT-B/16 from scratch on ImageNet. Suggested by the heatmaps, Lion is more robust to different hyperparameter choices compared to AdamW.

6 Limitations

Limitations of search Despite the efforts to make the search space less restrictive, it remains inspired by the popular first-order optimization algorithms, leading to a bias towards similar algorithms. It also lacks the functions required to construct advanced second-order algorithms (Anil et al., 2020; Gupta et al., 2018; Martens and Grosse, 2015). The search cost is still quite large and the algorithm simplification requires manual intervention. Further reducing the bias in the search space to discover more novel algorithms and improving the search efficiency are important future directions. The current program structure is quite simplistic, as we do not find a good usage of more advanced program constructs such as conditional, loop statements, and defining new functions. Exploring how to incorporate these elements has the potential to unlock new possibilities.

Limitations of Lion While we endeavour to evaluate Lion on as many tasks as possible, the assessment is limited to the chosen tasks. On vision tasks, the performance gap between Lion and AdamW narrows when strong augmentations are utilized. There are also several tasks where Lion performs similarly to AdamW, including: (1) the Imagen text-to-image base model, (2) the perplexity of autoregressive language model trained on the large-scale internal dataset, which is arguably a more reliable metric the in-context learning benchmarks, and (3) masked language modeling on C4. These tasks have a common characteristic in that the datasets are massive and of high quality, which results in a reduced difference between optimizers. Another potential limitation is the batch size. Though people often scale up the batch size to enable more parallelism, it is likely that Lion performs no better than AdamW if the batch size is small ($<$64). Additional, Lion still requires momentum tracking in `bfloat16`, which can be expensive for training giant models. One potential solution is to factorize the momentum to save memory.

7 Related Work

Our work lies in the area of AutoML and meta-learning that includes learning to learn (Andrychowicz et al., 2016; Bello et al., 2017; Metz et al., 2019, 2022; Ravi and Larochelle, 2017; Wichrowska et al., 2017; Xiong et al., 2022), neural architecture search (Chen and Hsieh, 2020; Chen et al., 2021; Liu et al., 2019a; Pham et al., 2018; Real et al., 2019; So et al., 2019; Wang et al., 2021; Yang et al., 2022; Zoph and Le, 2017) and hyperparameter optimization (Dong et al., 2021; Hutter et al., 2011; Jamieson and Talwalkar, 2016; Li et al., 2017), etc. There is also a long history of using evolutionary methods to search for programs, i.e., genetic programming (Brameier et al., 2007; Holland, 1992; Koza, 1994). Our approach builds upon a symbolic

search space similar to AutoML-Zero (Peng et al., 2020; Real et al., 2020). However, instead of discovering programs with fixed dimensional matrices, vector, and scalars for toy tasks, our goal is to develop programs that operate on n-dimensional arrays and can generalize to state-of-the-art tasks. Other related works include numerous handcrafted optimizers (Anil et al., 2020; Bernstein et al., 2018; Dozat, 2016; Duchi et al., 2011; Gupta et al., 2018; Kingma and Ba, 2014; Liu et al., 2020; Reddi et al., 2018; Riedmiller and Braun, 1993; Shazeer and Stern, 2018; Zhuang et al., 2020), which we discuss in Section 3.2.

8 Conclusion

This paper proposes to discover optimization algorithms via program search. We propose techniques to address the challenges in searching an infinite and sparse search space, and large generalization gap between the proxy and target tasks. Our method discovers a simple and effective optimizer, Lion, that is memory-efficient and achieves strong generalization across architectures, datasets and tasks.

Acknowledgements

We would like to thank (in alphabetical order) Angel Yu, Boqing Gong, Chen Cheng, Chitwan Saharia, Daiyi Peng, David So, Hanxiao Liu, Hanzhao Lin, Jeff Lund, Jiahui Yu, Jingru Xu, Julian Grady, Junyang Shen, Kevin Regan, Li Sheng, Liu Yang, Martin Wicke, Mingxing Tan, Mohammad Norouzi, Qiqi Yan, Rakesh Shivanna, Rohan Anil, Ruiqi Gao, Steve Li, Vlad Feinberg, Wenbo Zhang, William Chan, Xiao Wang, Xiaohua Zhai, Yaguang Li, Yang Li, Zhuoshu Li, Zihang Dai, Zirui Wang for helpful discussions, and the Google Brain team at large for providing a supportive research environment.

References

Marcin Andrychowicz, Misha Denil, Sergio Gómez, Matthew W Hoffman, David Pfau, Tom Schaul, Brendan Shillingford, and Nando de Freitas. Learning to learn by gradient descent by gradient descent. In D. Lee, M. Sugiyama, U. Luxburg, I. Guyon, and R. Garnett, editors, *Advances in Neural Information Processing Systems*, volume 29. Curran Associates, Inc., 2016.

Rohan Anil, Vineet Gupta, Tomer Koren, Kevin Regan, and Yoram Singer. Scalable second order optimization for deep learning, 2020.

Lukas Balles and Philipp Hennig. Dissecting adam: The sign, magnitude and variance of stochastic gradients. In Jennifer Dy and Andreas Krause, editors, *Proceedings of the 35th International Conference on Machine Learning*, volume 80 of *Proceedings of Machine Learning Research*, pages 404–413. PMLR, 10–15 Jul 2018.

Andrei Barbu, David Mayo, Julian Alverio, William Luo, Christopher Wang, Dan Gutfreund, Josh Tenenbaum, and Boris Katz. Objectnet: A large-scale bias-controlled dataset for pushing the limits of object recognition models. In H. Wallach, H. Larochelle, A. Beygelzimer, F. d'Alché-Buc, E. Fox, and R. Garnett, editors, *Advances in Neural Information Processing Systems*, volume 32. Curran Associates, Inc., 2019.

Irwan Bello, Barret Zoph, Vijay Vasudevan, and Quoc V. Le. Neural optimizer search with reinforcement learning. In *Proceedings of the 34th International Conference on Machine Learning - Volume 70*, ICML'17, page 459–468. JMLR.org, 2017.

Jonathan Berant, Andrew Chou, Roy Frostig, and Percy Liang. Semantic parsing on Freebase from question-answer pairs. In *Proceedings of the 2013 Conference on Empirical Methods in Natural Language Processing*, pages 1533–1544, Seattle, Washington, USA, October 2013. Association for Computational Linguistics.

Jeremy Bernstein, Yu-Xiang Wang, Kamyar Azizzadenesheli, and Animashree Anandkumar. signSGD: Compressed optimisation for non-convex problems. In Jennifer Dy and Andreas Krause, editors, *Proceedings of the 35th International Conference on Machine Learning*, volume 80 of *Proceedings of Machine Learning Research*, pages 560–569. PMLR, 10–15 Jul 2018.

Lucas Beyer, Olivier J. Hénaff, Alexander Kolesnikov, Xiaohua Zhai, and Aäron van den Oord. Are we done with imagenet?, 2020.

Yonatan Bisk, Rowan Zellers, Ronan Le bras, Jianfeng Gao, and Yejin Choi. Piqa: Reasoning about physical commonsense in natural language. *Proceedings of the AAAI Conference on Artificial Intelligence*, 34(05): 7432–7439, Apr. 2020. doi: 10.1609/aaai.v34i05.6239.

James Bradbury, Roy Frostig, Peter Hawkins, Matthew James Johnson, Chris Leary, Dougal Maclaurin, George Necula, Adam Paszke, Jake VanderPlas, Skye Wanderman-Milne, and Qiao Zhang. JAX: composable transformations of Python+NumPy programs, 2018. URL http://github.com/google/jax.

Markus Brameier, Wolfgang Banzhaf, and Wolfgang Banzhaf. *Linear genetic programming*, volume 1. Springer, 2007.

Tom B. Brown, Benjamin Mann, Nick Ryder, Melanie Subbiah, Jared Kaplan, Prafulla Dhariwal, Arvind Neelakantan, Pranav Shyam, Girish Sastry, Amanda Askell, Sandhini Agarwal, Ariel Herbert-Voss, Gretchen Krueger, Tom Henighan, Rewon Child, Aditya Ramesh, Daniel M. Ziegler, Jeffrey Wu, Clemens Winter, Christopher Hesse, Mark Chen, Eric Sigler, Mateusz Litwin, Scott Gray, Benjamin Chess, Jack Clark, Christopher Berner, Sam McCandlish, Alec Radford, Ilya Sutskever, and Dario Amodei. Language models are few-shot learners, 2020.

Ciprian Chelba, Tomas Mikolov, Mike Schuster, Qi Ge, Thorsten Brants, and Phillipp Koehn. One billion word benchmark for measuring progress in statistical language modeling. *CoRR*, abs/1312.3005, 2013.

Xiangning Chen and Cho-Jui Hsieh. Stabilizing differentiable architecture search via perturbation-based regularization. In Hal Daumé III and Aarti Singh, editors, *Proceedings of the 37th International Conference on Machine Learning*, volume 119 of *Proceedings of Machine Learning Research*, pages 1554–1565. PMLR, 13–18 Jul 2020.

Xiangning Chen, Ruochen Wang, Minhao Cheng, Xiaocheng Tang, and Cho-Jui Hsieh. DrNAS: Dirichlet neural architecture search. In *International Conference on Learning Representations*, 2021.

Xiangning Chen, Cho-Jui Hsieh, and Boqing Gong. When vision transformers outperform resnets without pre-training or strong data augmentations. In *International Conference on Learning Representations*, 2022.

Aakanksha Chowdhery, Sharan Narang, Jacob Devlin, Maarten Bosma, Gaurav Mishra, Adam Roberts, Paul Barham, Hyung Won Chung, Charles Sutton, Sebastian Gehrmann, Parker Schuh, Kensen Shi, Sasha Tsvyashchenko, Joshua Maynez, Abhishek Rao, Parker Barnes, Yi Tay, Noam Shazeer, Vinodkumar Prabhakaran, Emily Reif, Nan Du, Ben Hutchinson, Reiner Pope, James Bradbury, Jacob Austin, Michael Isard, Guy Gur-Ari, Pengcheng Yin, Toju Duke, Anselm Levskaya, Sanjay Ghemawat, Sunipa Dev, Henryk Michalewski, Xavier Garcia, Vedant Misra, Kevin Robinson, Liam Fedus, Denny Zhou, Daphne Ippolito, David Luan, Hyeontaek Lim, Barret Zoph, Alexander Spiridonov, Ryan Sepassi, David Dohan, Shivani Agrawal, Mark Omernick, Andrew M. Dai, Thanumalayan Sankaranarayana Pillai, Marie Pellat, Aitor Lewkowycz, Erica Moreira, Rewon Child, Oleksandr Polozov, Katherine Lee, Zongwei Zhou, Xuezhi Wang, Brennan Saeta, Mark Diaz, Orhan Firat, Michele Catasta, Jason Wei, Kathy Meier-Hellstern, Douglas Eck, Jeff Dean, Slav Petrov, and Noah Fiedel. Palm: Scaling language modeling with pathways, 2022.

Christopher Clark, Kenton Lee, Ming-Wei Chang, Tom Kwiatkowski, Michael Collins, and Kristina Toutanova. BoolQ: Exploring the surprising difficulty of natural yes/no questions. In *Proceedings of the 2019 Conference of the North American Chapter of the Association for Computational Linguistics: Human Language Technologies, Volume 1* (*Long and Short Papers*), pages 2924–2936, Minneapolis, Minnesota, June 2019. Association for Computational Linguistics. doi: 10.18653/v1/N19-1300.

Peter Clark, Isaac Cowhey, Oren Etzioni, Tushar Khot, Ashish Sabharwal, Carissa Schoenick, and Oyvind Tafjord. Think you have solved question answering? try arc, the ai2 reasoning challenge, 2018.

Ido Dagan, Oren Glickman, and Bernardo Magnini. The pascal recognising textual entailment challenge. In Joaquin Quiñonero-Candela, Ido Dagan, Bernardo Magnini, and Florence d'Alché Buc, editors, *Machine Learning Challenges. Evaluating Predictive Uncertainty, Visual Object Classification, and Recognising Tectual Entailment*, pages 177–190, Berlin, Heidelberg, 2006. Springer Berlin Heidelberg.

Zihang Dai, Hanxiao Liu, Quoc V Le, and Mingxing Tan. Coatnet: Marrying convolution and attention for all data sizes. In M. Ranzato, A. Beygelzimer, Y. Dauphin, P.S. Liang, and J. Wortman Vaughan, editors, *Advances in Neural Information Processing Systems*, volume 34, pages 3965–3977. Curran Associates, Inc., 2021.

Marie-Catherine de Marneffe, Mandy Simons, and Judith Tonhauser. The commitmentbank: Investigating projection in naturally occurring discourse. *Proceedings of Sinn und Bedeutung*, 23(2):107–124, Jul. 2019. doi: 10.18148/sub/2019.v23i2.601.

Jacob Devlin, Ming-Wei Chang, Kenton Lee, and Kristina Toutanova. BERT: Pre-training of deep bidirectional transformers for language understanding. In *Proceedings of the 2019 Conference of the North American Chapter of the Association for Computational Linguistics: Human Language Technologies, Volume 1 (Long and Short Papers)*, pages 4171–4186, Minneapolis, Minnesota, June 2019. Association for Computational Linguistics. doi: 10.18653/v1/N19-1423.

Prafulla Dhariwal and Alexander Nichol. Diffusion models beat gans on image synthesis. In M. Ranzato, A. Beygelzimer, Y. Dauphin, P.S. Liang, and J. Wortman Vaughan, editors, *Advances in Neural Information Processing Systems*, volume 34, pages 8780–8794. Curran Associates, Inc., 2021.

Xuanyi Dong, Mingxing Tan, Adams Wei Yu, Daiyi Peng, Bogdan Gabrys, and Quoc V Le. AutoHAS: Efficient hyperparameter and architecture search. In *2nd Workshop on Neural Architecture Search at ICLR*, 2021.

Alexey Dosovitskiy, Lucas Beyer, Alexander Kolesnikov, Dirk Weissenborn, Xiaohua Zhai, Thomas Unterthiner, Mostafa Dehghani, Matthias Minderer, Georg Heigold, Sylvain Gelly, Jakob Uszkoreit, and Neil Houlsby. An image is worth 16x16 words: Transformers for image recognition at scale. In *International Conference on Learning Representations*, 2021.

Timothy Dozat. Incorporating Nesterov Momentum into Adam. In *Proceedings of the 4th International Conference on Learning Representations*, pages 1–4, 2016.

Nan Du, Yanping Huang, Andrew M Dai, Simon Tong, Dmitry Lepikhin, Yuanzhong Xu, Maxim Krikun, Yanqi Zhou, Adams Wei Yu, Orhan Firat, Barret Zoph, Liam Fedus, Maarten P Bosma, Zongwei Zhou, Tao Wang, Emma Wang, Kellie Webster, Marie Pellat, Kevin Robinson, Kathleen Meier-Hellstern, Toju Duke, Lucas Dixon, Kun Zhang, Quoc Le, Yonghui Wu, Zhifeng Chen, and Claire Cui. GLaM: Efficient scaling of language models with mixture-of-experts. In Kamalika Chaudhuri, Stefanie Jegelka, Le Song, Csaba Szepesvari, Gang Niu, and Sivan Sabato, editors, *Proceedings of the 39th International Conference on Machine Learning*, volume 162 of *Proceedings of Machine Learning Research*, pages 5547–5569. PMLR, 17–23 Jul 2022.

John Duchi, Elad Hazan, and Yoram Singer. Adaptive subgradient methods for online learning and stochastic optimization. *Journal of Machine Learning Research*, 12(61):2121–2159, 2011.

Pierre Foret, Ariel Kleiner, Hossein Mobahi, and Behnam Neyshabur. Sharpness-aware minimization for efficiently improving generalization. In *International Conference on Learning Representations*, 2021.

Ryan Gillard, Stephen Jonany, Yingjie Miao, Michael Munn, Connal de Souza, Jonathan Dungay, Chen Liang, David R. So, Quoc V. Le, and Esteban Real. Unified functional hashing in automatic machine learning, 2023.

David E Goldberg and Kalyanmoy Deb. A comparative analysis of selection schemes used in genetic algorithms. *FOGA*, 1991.

Andrew Gordon, Zornitsa Kozareva, and Melissa Roemmele. SemEval-2012 task 7: Choice of plausible alternatives: An evaluation of commonsense causal reasoning. In **SEM 2012: The First Joint Conference on Lexical and Computational Semantics – Volume 1: Proceedings of the main conference and the shared task, and Volume 2: Proceedings of the Sixth International Workshop on Semantic Evaluation (SemEval 2012)*, pages 394–398, Montréal, Canada, 7-8 June 2012. Association for Computational Linguistics.

Mandy Guo, Zihang Dai, Denny Vrandečić, and Rami Al-Rfou. Wiki-40B: Multilingual language model dataset. In *Proceedings of the Twelfth Language Resources and Evaluation Conference*, pages 2440–2452, Marseille, France, May 2020. European Language Resources Association. ISBN 979-10-95546-34-4.

Vineet Gupta, Tomer Koren, and Yoram Singer. Shampoo: Preconditioned stochastic tensor optimization. In Jennifer Dy and Andreas Krause, editors, *Proceedings of the 35th International Conference on Machine Learning*, volume 80 of *Proceedings of Machine Learning Research*, pages 1842–1850. PMLR, 10–15 Jul 2018.

Charles R. Harris, K. Jarrod Millman, Stéfan J. van der Walt, Ralf Gommers, Pauli Virtanen, David Cournapeau, Eric Wieser, Julian Taylor, Sebastian Berg, Nathaniel J. Smith, Robert Kern, Matti Picus, Stephan Hoyer, Marten H. van Kerkwijk, Matthew Brett, Allan Haldane, Jaime Fernández del Río, Mark Wiebe, Pearu Peterson, Pierre Gérard-Marchant, Kevin Sheppard, Tyler Reddy, Warren Weckesser, Hameer Abbasi, Christoph Gohlke, and Travis E. Oliphant. Array programming with NumPy. *Nature*, 585(7825):357–362, September 2020. doi: 10.1038/s41586-020-2649-2.

Kaiming He, Xiangyu Zhang, Shaoqing Ren, and Jian Sun. Deep residual learning for image recognition. In *2016 IEEE Conference on Computer Vision and Pattern Recognition (CVPR)*, pages 770–778, 2016. doi: 10.1109/CVPR.2016.90.

Dan Hendrycks, Steven Basart, Norman Mu, Saurav Kadavath, Frank Wang, Evan Dorundo, Rahul Desai, Tyler Zhu, Samyak Parajuli, Mike Guo, Dawn Song, Jacob Steinhardt, and Justin Gilmer. The many faces of robustness: A critical analysis of out-of-distribution generalization. In *Proceedings of the IEEE/CVF International Conference on Computer Vision (ICCV)*, pages 8340–8349, October 2021a.

Dan Hendrycks, Kevin Zhao, Steven Basart, Jacob Steinhardt, and Dawn Song. Natural adversarial examples. In *Proceedings of the IEEE/CVF Conference on Computer Vision and Pattern Recognition (CVPR)*, pages 15262–15271, June 2021b.

Jonathan Ho and Tim Salimans. Classifier-free diffusion guidance, 2022.

Jonathan Ho, Ajay Jain, and Pieter Abbeel. Denoising diffusion probabilistic models. In H. Larochelle, M. Ranzato, R. Hadsell, M.F. Balcan, and H. Lin, editors, *Advances in Neural Information Processing Systems*, volume 33, pages 6840–6851. Curran Associates, Inc., 2020.

John H Holland. *Adaptation in natural and artificial systems: an introductory analysis with applications to biology, control, and artificial intelligence*. MIT press, 1992.

Weizhe Hua, Zihang Dai, Hanxiao Liu, and Quoc Le. Transformer quality in linear time. In Kamalika Chaudhuri, Stefanie Jegelka, Le Song, Csaba Szepesvari, Gang Niu, and Sivan Sabato, editors, *Proceedings of the 39th International Conference on Machine Learning*, volume 162 of *Proceedings of Machine Learning Research*, pages 9099–9117. PMLR, 17–23 Jul 2022.

Frank Hutter, Holger H. Hoos, and Kevin Leyton-Brown. Sequential model-based optimization for general algorithm configuration. In Carlos A. Coello Coello, editor, *Learning and Intelligent Optimization*, pages 507–523, Berlin, Heidelberg, 2011. Springer Berlin Heidelberg.

Kevin Jamieson and Ameet Talwalkar. Non-stochastic best arm identification and hyperparameter optimization. In Arthur Gretton and Christian C. Robert, editors, *Proceedings of the 19th International Conference on Artificial Intelligence and Statistics*, volume 51 of *Proceedings of Machine Learning Research*, pages 240–248, Cadiz, Spain, 09–11 May 2016. PMLR.

Mandar Joshi, Eunsol Choi, Daniel Weld, and Luke Zettlemoyer. TriviaQA: A large scale distantly supervised challenge dataset for reading comprehension. In *Proceedings of the 55th Annual Meeting of the Association for Computational Linguistics* (*Volume 1: Long Papers*), pages 1601–1611, Vancouver, Canada, July 2017. Association for Computational Linguistics. doi: 10.18653/v1/P17-1147.

Nitish Shirish Keskar, Dheevatsa Mudigere, Jorge Nocedal, Mikhail Smelyanskiy, and Ping Tak Peter Tang. On large-batch training for deep learning: Generalization gap and sharp minima. In *International Conference on Learning Representations*, 2017.

Daniel Khashabi, Snigdha Chaturvedi, Michael Roth, Shyam Upadhyay, and Dan Roth. Looking beyond the surface: A challenge set for reading comprehension over multiple sentences. In *Proceedings of the 2018 Conference of the North American Chapter of the Association for Computational Linguistics: Human Language Technologies, Volume 1* (*Long Papers*), pages 252–262, New Orleans, Louisiana, June 2018. Association for Computational Linguistics. doi: 10.18653/v1/N18-1023.

Diederik P. Kingma and Jimmy Ba. Adam: A method for stochastic optimization, 2014.

John R Koza. Genetic programming as a means for programming computers by natural selection. *Statistics and computing*, 4:87–112, 1994.

Alex Krizhevsky. Learning multiple layers of features from tiny images. Technical report, 2009.

Tom Kwiatkowski, Jennimaria Palomaki, Olivia Redfield, Michael Collins, Ankur Parikh, Chris Alberti, Danielle Epstein, Illia Polosukhin, Jacob Devlin, Kenton Lee, Kristina Toutanova, Llion Jones, Matthew Kelcey, Ming-Wei Chang, Andrew M. Dai, Jakob Uszkoreit, Quoc Le, and Slav Petrov. Natural questions: A benchmark for question answering research. *Transactions of the Association for Computational Linguistics*, 7: 452–466, 2019.

Guokun Lai, Qizhe Xie, Hanxiao Liu, Yiming Yang, and Eduard Hovy. RACE: Large-scale ReAding comprehension dataset from examinations. In *Proceedings of the 2017 Conference on Empirical Methods in Natural Language Processing*, pages 785–794, Copenhagen, Denmark, September 2017. Association for Computational Linguistics. doi: 10.18653/v1/D17-1082.

Hector J. Levesque, Ernest Davis, and Leora Morgenstern. The winograd schema challenge. In *Proceedings of the Thirteenth International Conference on Principles of Knowledge Representation and Reasoning*, KR'12, page 552–561. AAAI Press, 2012. ISBN 9781577355601.

Ke Li and Jitendra Malik. Learning to optimize. In *International Conference on Learning Representations*, 2017.

Lisha Li, Kevin Jamieson, Giulia DeSalvo, Afshin Rostamizadeh, and Ameet Talwalkar. Hyperband: A novel bandit-based approach to hyperparameter optimization. *J. Mach. Learn. Res.*, 18(1):6765–6816, jan 2017. ISSN 1532-4435.

Tsung-Yi Lin, Michael Maire, Serge Belongie, James Hays, Pietro Perona, Deva Ramanan, Piotr Dollár, and C. Lawrence Zitnick. Microsoft coco: Common objects in context. In David Fleet, Tomas Pajdla, Bernt Schiele, and Tinne Tuytelaars, editors, *Computer Vision – ECCV 2014*, pages 740–755, Cham, 2014. Springer International Publishing.

Hanxiao Liu, Karen Simonyan, and Yiming Yang. DARTS: Differentiable architecture search. In *International Conference on Learning Representations*, 2019a.

Liyuan Liu, Haoming Jiang, Pengcheng He, Weizhu Chen, Xiaodong Liu, Jianfeng Gao, and Jiawei Han. On the variance of the adaptive learning rate and beyond. In *International Conference on Learning Representations*, 2020.

Yinhan Liu, Myle Ott, Naman Goyal, Jingfei Du, Mandar Joshi, Danqi Chen, Omer Levy, Mike Lewis, Luke Zettlemoyer, and Veselin Stoyanov. Roberta: A robustly optimized bert pretraining approach, 2019b.

Ilya Loshchilov and Frank Hutter. Decoupled weight decay regularization. In *International Conference on Learning Representations*, 2019.

James Martens and Roger Grosse. Optimizing neural networks with kronecker-factored approximate curvature. In *International conference on machine learning*, pages 2408–2417. PMLR, 2015.

Luke Metz, Niru Maheswaranathan, Jeremy Nixon, Daniel Freeman, and Jascha Sohl-Dickstein. Understanding and correcting pathologies in the training of learned optimizers. In Kamalika Chaudhuri and Ruslan Salakhutdinov, editors, *Proceedings of the 36th International Conference on Machine Learning*, volume 97 of *Proceedings of Machine Learning Research*, pages 4556–4565. PMLR, 09–15 Jun 2019.

Luke Metz, James Harrison, C. Daniel Freeman, Amil Merchant, Lucas Beyer, James Bradbury, Naman Agrawal, Ben Poole, Igor Mordatch, Adam Roberts, and Jascha Sohl-Dickstein. Velo: Training versatile learned optimizers by scaling up, 2022.

Todor Mihaylov, Peter Clark, Tushar Khot, and Ashish Sabharwal. Can a suit of armor conduct electricity? a new dataset for open book question answering. In *Proceedings of the 2018 Conference on Empirical Methods in Natural Language Processing*, pages 2381–2391, Brussels, Belgium, October-November 2018. Association for Computational Linguistics. doi: 10.18653/v1/D18-1260.

Nasrin Mostafazadeh, Nathanael Chambers, Xiaodong He, Devi Parikh, Dhruv Batra, Lucy Vanderwende, Pushmeet Kohli, and James Allen. A corpus and cloze evaluation for deeper understanding of commonsense stories. In *Proceedings of the 2016 Conference of the North American Chapter of the Association for Computational Linguistics: Human Language Technologies*, pages 839–849, San Diego, California, June 2016. Association for Computational Linguistics. doi: 10.18653/v1/N16-1098.

Arvind Neelakantan, Luke Vilnis, Quoc V. Le, Lukasz Kaiser, Karol Kurach, Ilya Sutskever, and James Martens. Adding gradient noise improves learning for very deep networks, 2017.

Yixin Nie, Adina Williams, Emily Dinan, Mohit Bansal, Jason Weston, and Douwe Kiela. Adversarial NLI: A new benchmark for natural language understanding. In *Proceedings of the 58th Annual Meeting of the Association for Computational Linguistics*, pages 4885–4901, Online, July 2020. Association for Computational Linguistics. doi: 10.18653/v1/2020.acl-main.441.

O. M. Parkhi, A. Vedaldi, A. Zisserman, and C. V. Jawahar. Cats and dogs. In *IEEE Conference on Computer Vision and Pattern Recognition*, 2012.

Daiyi Peng, Xuanyi Dong, Esteban Real, Mingxing Tan, Yifeng Lu, Gabriel Bender, Hanxiao Liu, Adam Kraft, Chen Liang, and Quoc Le. Pyglove: Symbolic programming for automated machine learning. In H. Larochelle, M. Ranzato, R. Hadsell, M.F. Balcan, and H. Lin, editors, *Advances in Neural Information Processing Systems*, volume 33, pages 96–108. Curran Associates, Inc., 2020.

Hieu Pham, Melody Guan, Barret Zoph, Quoc Le, and Jeff Dean. Efficient neural architecture search via parameters sharing. In Jennifer Dy and Andreas Krause, editors, *Proceedings of the 35th International Conference on Machine Learning*, volume 80 of *Proceedings of Machine Learning Research*, pages 4095–4104. PMLR, 10–15 Jul 2018.

Hieu Pham, Zihang Dai, Golnaz Ghiasi, Kenji Kawaguchi, Hanxiao Liu, Adams Wei Yu, Jiahui Yu, Yi-Ting Chen, Minh-Thang Luong, Yonghui Wu, Mingxing Tan, and Quoc V. Le. Combined scaling for open-vocabulary image classification, 2021.

Mohammad Taher Pilehvar and Jose Camacho-Collados. WiC: the word-in-context dataset for evaluating context-sensitive meaning representations. In *Proceedings of the 2019 Conference of the North American Chapter of the Association for Computational Linguistics: Human Language Technologies, Volume 1 (Long and Short Papers)*, pages 1267–1273, Minneapolis, Minnesota, June 2019. Association for Computational Linguistics. doi: 10.18653/v1/N19-1128.

Bryan A. Plummer, Liwei Wang, Chris M. Cervantes, Juan C. Caicedo, Julia Hockenmaier, and Svetlana Lazebnik. Flickr30k entities: Collecting region-to-phrase correspondences for richer image-to-sentence models. In *2015 IEEE International Conference on Computer Vision (ICCV)*, pages 2641–2649, 2015. doi: 10.1109/ICCV.2015.303.

Alec Radford, Jong Wook Kim, Chris Hallacy, Aditya Ramesh, Gabriel Goh, Sandhini Agarwal, Girish Sastry, Amanda Askell, Pamela Mishkin, Jack Clark, Gretchen Krueger, and Ilya Sutskever. Learning transferable visual models from natural language supervision. In Marina Meila and Tong Zhang, editors, *Proceedings of the 38th International Conference on Machine Learning*, volume 139 of *Proceedings of Machine Learning Research*, pages 8748–8763. PMLR, 18–24 Jul 2021.

Jack W. Rae, Anna Potapenko, Siddhant M. Jayakumar, Chloe Hillier, and Timothy P. Lillicrap. Compressive transformers for long-range sequence modelling. In *International Conference on Learning Representations*, 2020.

Colin Raffel, Noam Shazeer, Adam Roberts, Katherine Lee, Sharan Narang, Michael Matena, Yanqi Zhou, Wei Li, and Peter J. Liu. Exploring the limits of transfer learning with a unified text-to-text transformer. *Journal of Machine Learning Research*, 21(140):1–67, 2020.

Sachin Ravi and Hugo Larochelle. Optimization as a model for few-shot learning. In *International Conference on Learning Representations*, 2017.

Esteban Real, Alok Aggarwal, Yanping Huang, and Quoc V. Le. Regularized evolution for image classifier architecture search. *Proceedings of the AAAI Conference on Artificial Intelligence*, 33(01):4780–4789, Jul. 2019. doi: 10.1609/aaai.v33i01.33014780.

Esteban Real, Chen Liang, David So, and Quoc Le. Automl-zero: Evolving machine learning algorithms from scratch. In *International Conference on Machine Learning*, pages 8007–8019. PMLR, 2020.

Benjamin Recht, Rebecca Roelofs, Ludwig Schmidt, and Vaishaal Shankar. Do ImageNet classifiers generalize to ImageNet? In Kamalika Chaudhuri and Ruslan Salakhutdinov, editors, *Proceedings of the 36th International Conference on Machine Learning*, volume 97 of *Proceedings of Machine Learning Research*, pages 5389–5400. PMLR, 09–15 Jun 2019.

Sashank J. Reddi, Satyen Kale, and Sanjiv Kumar. On the convergence of adam and beyond. In *International Conference on Learning Representations*, 2018.

M. Riedmiller and H. Braun. A direct adaptive method for faster backpropagation learning: the rprop algorithm. In *IEEE International Conference on Neural Networks*, pages 586–591 vol.1, 1993. doi: 10.1109/ICNN.1993.298623.

Chitwan Saharia, William Chan, Saurabh Saxena, Lala Li, Jay Whang, Emily Denton, Seyed Kamyar Seyed Ghasemipour, Raphael Gontijo-Lopes, Burcu Karagol Ayan, Tim Salimans, Jonathan Ho, David J. Fleet, and Mohammad Norouzi. Photorealistic text-to-image diffusion models with deep language understanding. In Alice H. Oh, Alekh Agarwal, Danielle Belgrave, and Kyunghyun Cho, editors, *Advances in Neural Information Processing Systems*, 2022.

Keisuke Sakaguchi, Ronan Le Bras, Chandra Bhagavatula, and Yejin Choi. Winogrande: An adversarial winograd schema challenge at scale. *Proceedings of the AAAI Conference on Artificial Intelligence*, 34(05): 8732–8740, Apr. 2020. doi: 10.1609/aaai.v34i05.6399.

Noam Shazeer and Mitchell Stern. Adafactor: Adaptive learning rates with sublinear memory cost. In Jennifer Dy and Andreas Krause, editors, *Proceedings of the 35th International Conference on Machine Learning*, volume 80 of *Proceedings of Machine Learning Research*, pages 4596–4604. PMLR, 10–15 Jul 2018.

David So, Quoc Le, and Chen Liang. The evolved transformer. In *International Conference on Machine Learning*, pages 5877–5886. PMLR, 2019.

Jiaming Song, Chenlin Meng, and Stefano Ermon. Denoising diffusion implicit models. In *International Conference on Learning Representations*, 2021.

Chen Sun, Abhinav Shrivastava, Saurabh Singh, and Abhinav Gupta. Revisiting unreasonable effectiveness of data in deep learning era. In *Proceedings of the IEEE International Conference on Computer Vision (ICCV)*, Oct 2017.

Ashish Vaswani, Noam Shazeer, Niki Parmar, Jakob Uszkoreit, Llion Jones, Aidan N Gomez, Łukasz Kaiser, and Illia Polosukhin. Attention is all you need. *Advances in neural information processing systems*, 30, 2017.

Alex Wang, Amanpreet Singh, Julian Michael, Felix Hill, Omer Levy, and Samuel R. Bowman. GLUE: A multi-task benchmark and analysis platform for natural language understanding. In *International Conference on Learning Representations*, 2019a.

Haohan Wang, Songwei Ge, Zachary Lipton, and Eric P Xing. Learning robust global representations by penalizing local predictive power. In H. Wallach, H. Larochelle, A. Beygelzimer, F. d'Alché-Buc, E. Fox, and R. Garnett, editors, *Advances in Neural Information Processing Systems*, volume 32. Curran Associates, Inc., 2019b.

Ruochen Wang, Minhao Cheng, Xiangning Chen, Xiaocheng Tang, and Cho-Jui Hsieh. Rethinking architecture selection in differentiable NAS. In *International Conference on Learning Representations*, 2021.

Ruochen Wang, Yuanhao Xiong, Minhao Cheng, and Cho-Jui Hsieh. Efficient non-parametric optimizer search for diverse tasks. *arXiv preprint arXiv:2209.13575*, 2022.

Olga Wichrowska, Niru Maheswaranathan, Matthew W. Hoffman, Sergio Gómez Colmenarejo, Misha Denil, Nando de Freitas, and Jascha Sohl-Dickstein. Learned optimizers that scale and generalize. In *Proceedings of the 34th International Conference on Machine Learning - Volume 70*, ICML'17, page 3751–3760. JMLR.org, 2017.

Yuanhao Xiong, Li-Cheng Lan, Xiangning Chen, Ruochen Wang, and Cho-Jui Hsieh. Learning to schedule learning rate with graph neural networks. In *International Conference on Learning Representations*, 2022.

Chengrun Yang, Gabriel Bender, Hanxiao Liu, Pieter-Jan Kindermans, Madeleine Udell, Yifeng Lu, Quoc V Le, and Da Huang. TabNAS: Rejection sampling for neural architecture search on tabular datasets. In Alice H. Oh, Alekh Agarwal, Danielle Belgrave, and Kyunghyun Cho, editors, *Advances in Neural Information Processing Systems*, 2022.

Chris Ying, Aaron Klein, Esteban Real, Eric Christiansen, Kevin Murphy, and Frank Hutter. Nas-bench-101: Towards reproducible neural architecture search. *ICML*, 2019.

Jiahui Yu, Zirui Wang, Vijay Vasudevan, Legg Yeung, Mojtaba Seyedhosseini, and Yonghui Wu. Coca: Contrastive captioners are image-text foundation models. *Transactions on Machine Learning Research*, 2022.

Rowan Zellers, Ari Holtzman, Yonatan Bisk, Ali Farhadi, and Yejin Choi. HellaSwag: Can a machine really finish your sentence? In *Proceedings of the 57th Annual Meeting of the Association for Computational Linguistics*, pages 4791–4800, Florence, Italy, July 2019. Association for Computational Linguistics. doi: 10.18653/v1/P19-1472.

Xiaohua Zhai, Alexander Kolesnikov, Neil Houlsby, and Lucas Beyer. Scaling vision transformers, 2021.

Xiaohua Zhai, Xiao Wang, Basil Mustafa, Andreas Steiner, Daniel Keysers, Alexander Kolesnikov, and Lucas Beyer. Lit: Zero-shot transfer with locked-image text tuning. In *Proceedings of the IEEE/CVF Conference on Computer Vision and Pattern Recognition (CVPR)*, pages 18123–18133, June 2022.

Sheng Zhang, Xiaodong Liu, Jingjing Liu, Jianfeng Gao, Kevin Duh, and Benjamin Van Durme. Record: Bridging the gap between human and machine commonsense reading comprehension, 2018.

Juntang Zhuang, Tommy Tang, Yifan Ding, Sekhar C Tatikonda, Nicha Dvornek, Xenophon Papademetris, and James Duncan. Adabelief optimizer: Adapting stepsizes by the belief in observed gradients. In H. Larochelle, M. Ranzato, R. Hadsell, M.F. Balcan, and H. Lin, editors, *Advances in Neural Information Processing Systems*, volume 33, pages 18795–18806. Curran Associates, Inc., 2020.

Barret Zoph and Quoc V. Le. Neural architecture search with reinforcement learning. In *International Conference on Learning Representations (ICLR)*, 2017.

Table 8: Model performance when pre-trained on JFT-300M then fine-tuned on ImageNet. Those numbers correspond to Figure 1 (Left) and Figure 4. The fine-tuning resolution is 384^2 for ViT-B/16 and ViT-L/16, and 392^2 for ViT-H/14. Following Dosovitskiy et al. (2021), Polyak averaging is not applied here.

Model	#Params	Epochs / Steps	Optimizer	ImageNet	ReaL	V2	A	R
ViT-B/16_{384}	86.86M	7 / 517,791	AdamW	84.24	89.04	74.89	27.39	53.71
			Lion	**84.72**	**89.14**	**75.83**	**29.65**	**55.86**
ViT-L/16_{384}	304.72M	7 / 517,791	AdamW	86.69	89.95	78.03	40.55	64.47
			Lion	**87.32**	**90.43**	**79.29**	**47.13**	**68.49**
		14 / 1,035,583	AdamW	87.29	90.11	78.91	42.56	64.34
			Lion	**88.09**	**90.62**	**80.48**	**51.55**	**70.72**
ViT-H/14_{392}	632.72M	14 / 1,035,583	AdamW	88.02	90.27	80.10	53.14	69.48
			Lion	**88.78**	**90.68**	**81.41**	**58.21**	**73.09**

A Pseudocode for AdamW and Lion

Algorithm 1 AdamW Optimizer

given β_1, β_2, ϵ, λ, η, f
initialize θ_0, $m_0 \leftarrow 0$, $v_0 \leftarrow 0$, $t \leftarrow 0$
while θ_t not converged **do**
  $t \leftarrow t + 1$
  $g_t \leftarrow \nabla_\theta f(\theta_{t-1})$
  update EMA of g_t **and** g_t^2
  $m_t \leftarrow \beta_1 m_{t-1} + (1 - \beta_1) g_t$
  $v_t \leftarrow \beta_2 v_{t-1} + (1 - \beta_2) g_t^2$
  bias correction
  $\hat{m}_t \leftarrow m_t / (1 - \beta_1^t)$
  $\hat{v}_t \leftarrow v_t / (1 - \beta_2^t)$
  update model parameters
  $\theta_t \leftarrow \theta_{t-1} - \eta_t (\hat{m}_t / (\sqrt{\hat{v}_t} + \epsilon) + \lambda \theta_{t-1})$
end while
return θ_t

Algorithm 2 Lion Optimizer (ours)

given β_1, β_2, λ, η, f
initialize θ_0, $m_0 \leftarrow 0$
while θ_t not converged **do**
  $g_t \leftarrow \nabla_\theta f(\theta_{t-1})$
  update model parameters
  $c_t \leftarrow \beta_1 m_{t-1} + (1 - \beta_1) g_t$
  $\theta_t \leftarrow \theta_{t-1} - \eta_t (\text{sign}(c_t) + \lambda \theta_{t-1})$
  update EMA of g_t
  $m_t \leftarrow \beta_2 m_{t-1} + (1 - \beta_2) g_t$
end while
return θ_t

B Image Classification Tasks

Our evaluation covers various benchmarks: ImageNet, ImageNet ReaL (Beyer et al., 2020), ImageNet V2 (Recht et al., 2019), ImageNet A (Hendrycks et al., 2021b), ImageNet R (Hendrycks et al., 2021a), ImageNet Sketch (Wang et al., 2019b), ObjectNet (Barbu et al., 2019), CIFAR-100 (Krizhevsky, 2009), and Oxford-IIIT Pet (Parkhi et al., 2012).

C NLP Tasks

This section shows all the natural language generation (NLG) and natural language understanding (NLU) tasks where we evaluate the large-scale language models in Section 4.4. Those tasks include *Open-Domain Question Answering*, *Cloze and Completion Tasks*, *Winograd-Style Tasks*, *Common Sense Reasoning*, *In-Context Reading Comprehension*, *SuperGLUE*, and *Natural Language Inference*.

SIGNSGD: Compressed Optimisation for Non-Convex Problems

Jeremy Bernstein [1 2] **Yu-Xiang Wang** [2 3] **Kamyar Azizzadenesheli** [4] **Anima Anandkumar** [1 2]

Abstract

Training large neural networks requires distributing learning across multiple workers, where the cost of communicating gradients can be a significant bottleneck. SIGNSGD alleviates this problem by transmitting just the sign of each minibatch stochastic gradient. We prove that it can get the best of both worlds: compressed gradients *and* SGD-level convergence rate. The relative ℓ_1/ℓ_2 geometry of gradients, noise and curvature informs whether SIGNSGD or SGD is theoretically better suited to a particular problem. On the practical side we find that the momentum counterpart of SIGNSGD is able to match the accuracy and convergence speed of ADAM on deep Imagenet models. We extend our theory to the distributed setting, where the parameter server uses majority vote to aggregate gradient signs from each worker enabling 1-bit compression of worker-server communication *in both directions*. Using a theorem by Gauss (1823) we prove that majority vote can achieve the same reduction in variance as full precision distributed SGD. Thus, there is great promise for sign-based optimisation schemes to achieve fast communication *and* fast convergence. Code to reproduce experiments is to be found at `https://github.com/jxbz/signSGD`.

1. Introduction

Deep neural networks have learnt to solve numerous natural human tasks (LeCun et al., 2015; Schmidhuber, 2015). Training these large-scale models can take days or even weeks. The learning process can be accelerated by distributing training over multiple processors—either GPUs linked within a single machine, or even multiple machines linked together. Communication between workers is typically handled using a parameter-server framework (Li et al., 2014), which involves repeatedly communicating the gradients of every parameter in the model. This can still be time-intensive for large-scale neural networks. The communication cost can be reduced if gradients are compressed before being transmitted. In this paper, we analyse the theory of robust schemes for gradient compression.

An elegant form of gradient compression is just to take the sign of each coordinate of the stochastic gradient vector, which we call SIGNSGD. The algorithm is as simple as throwing away the exponent and mantissa of a 32-bit floating point number. Sign-based methods have been studied at least since the days of RPROP (Riedmiller & Braun, 1993). This algorithm inspired many popular optimisers—like RMSPROP (Tieleman & Hinton, 2012) and ADAM (Kingma & Ba, 2015). But researchers were interested in RPROP and variants because of their robust and fast convergence, and not their potential for gradient compression.

Until now there has been no rigorous theoretical explanation for the empirical success of sign-based stochastic gradient

Algorithm 1 SIGNSGD

Input: learning rate δ, current point x_k
$\tilde{g}_k \leftarrow \text{stochasticGradient}(x_k)$
$x_{k+1} \leftarrow x_k - \delta \,\text{sign}(\tilde{g}_k)$

Algorithm 2 SIGNUM

Input: learning rate δ, momentum constant $\beta \in (0,1)$, current point x_k, current momentum m_k
$\tilde{g}_k \leftarrow \text{stochasticGradient}(x_k)$
$m_{k+1} \leftarrow \beta m_k + (1-\beta)\tilde{g}_k$
$x_{k+1} \leftarrow x_k - \delta \,\text{sign}(m_{k+1})$

Algorithm 3 Distributed training by majority vote

Input: learning rate δ, current point x_k, # workers M each with an independent gradient estimate $\tilde{g}_m(x_k)$
on server
  pull $\text{sign}(\tilde{g}_m)$ **from** each worker
  push $\text{sign}\left[\sum_{m=1}^{M} \text{sign}(\tilde{g}_m)\right]$ **to** each worker
on each worker
  $x_{k+1} \leftarrow x_k - \delta \,\text{sign}\left[\sum_{m=1}^{M} \text{sign}(\tilde{g}_m)\right]$

[1]Caltech [2]Amazon AI [3]UC Santa Barbara [4]UC Irvine. Correspondence to: Jeremy Bernstein <bernstein@caltech.edu>, Yu-Xiang Wang <yuxiangw@amazon.edu>.

Proceedings of the 35^{th} International Conference on Machine Learning, Stockholm, Sweden, PMLR 80, 2018.

methods. The sign of the stochastic gradient is a biased approximation to the true gradient, making it more challenging to analyse compared to standard SGD. In this paper, we provide extensive theoretical analysis of sign-based methods for non-convex optimisation under transparent assumptions. We show that SIGNSGD is especially efficient in problems with a particular ℓ_1 geometry: when gradients are as dense or denser than stochasticity and curvature, then SIGNSGD can converge with a theoretical rate that has similar or even better dimension dependence than SGD. We find empirically that *both gradients and noise are dense* in deep learning problems, consistent with the observation that SIGNSGD converges at a similar rate to SGD in practice.

We then analyse SIGNSGD in the distributed setting where the parameter server aggregates gradient signs of the workers by a majority vote. Thus we allow worker-server communication to be 1-bit compressed in both directions. We prove that the theoretical speedup matches that of distributed SGD, under natural assumptions that are validated by experiments.

We also extend our theoretical framework to the SIGNUM optimiser—which takes the sign of the momentum. Our theory suggests that momentum may be useful for controlling a tradeoff between bias and variance in the estimate of the stochastic gradient. On the practical side, we show that SIGNUM easily scales to large Imagenet models, and provided the learning rate and weight decay are tuned, all other hyperparameter settings—such as momentum, weight initisialiser, learning rate schedules and data augmentation—may be lifted from an SGD implementation.

2. Related Work

Distributed machine learning: From the information theoretic angle, Suresh et al. (2017) study the communication limits of estimating the mean of a general quantity known about only through samples collected from M workers. In contrast, we focus exclusively on communication of gradients for optimisation, which allows us to exploit the fact that we do not care about incorrectly communicating small gradients in our theory. Still our work has connections with information theory. When the parameter server aggregates gradients by majority vote, it is effectively performing maximum likelihood decoding of a repetition encoding of the true gradient sign that is supplied by the M workers.

As for existing gradient compression schemes, Seide et al. (2014) and Strom (2015) demonstrated empirically that 1-bit quantisation can still give good performance whilst dramatically reducing gradient communication costs in distributed systems. Alistarh et al. (2017) and Wen et al. (2017) provide schemes with theoretical guarantees by using random number generators to ensure that the compressed gradient is still an unbiased approximation to the true gradient. Whilst unbiasedness allows these schemes to bootstrap SGD theory, it unfortunately comes at the cost of hugely inflated variance, and this variance explosion[1] basically renders the SGD-style bounds vacuous in the face of the empirical success of these algorithms. The situation only gets worse when the parameter server must aggregate and send back the received gradients, since merely summing up quantised updates reduces the quantisation efficiency. We compare the schemes in Table 1—notice how the existing schemes pick up log factors in the transmission from parameter-server back to workers. Our proposed approach is different, in that we directly employ the sign gradient which is *biased*. This avoids the randomisation needed for constructing an unbiased quantised estimate, avoids the problem of variance exploding in the theoretical bounds, and even enables 1-bit compression in both directions between parameter-server and workers, at no theoretical loss compared to distributed SGD.

Table 1. The communication cost of different gradient compression schemes, when training a d-dimensional model with M workers.

ALGORITHM	# BITS PER ITERATION
SGD (Robbins & Monro, 1951)	$64Md$
QSGD (Alistarh et al., 2017)	$(2+\log(2M+1))Md$
TERNGRAD (Wen et al., 2017)	$(2+\log(2M+1))Md$
SIGNSGD with majority vote	$2Md$

Deep learning: stochastic gradient descent (Robbins & Monro, 1951) is a simple and extremely effective optimiser for training neural networks. Still Riedmiller & Braun (1993) noted the good practical performance of sign-based methods like RPROP for training deep nets, and since then variants such as RMSPROP (Tieleman & Hinton, 2012) and ADAM (Kingma & Ba, 2015) have become increasingly popular. ADAM updates the weights according to the mean divided by the root mean square of recent gradients. Let $\langle . \rangle_\beta$ denote an exponential moving average with timescale β, and $\tilde{g}$ the stochastic gradient. Then

$$\text{ADAM step} \sim \frac{\langle \tilde{g} \rangle_{\beta_1}}{\sqrt{\langle \tilde{g}^2 \rangle_{\beta_2}}}$$

Therefore taking the time scale of the exponential moving averages to zero, $\beta_1, \beta_2 \to 0$, yields SIGNSGD

$$\text{SIGNSGD step} = \text{sign}(\tilde{g}) = \frac{\tilde{g}}{\sqrt{\tilde{g}^2}}.$$

To date there has been no convincing theory of the {RPROP, RMSPROP, ADAM} family of algorithms, known as 'adaptive gradient methods'. Indeed Reddi et al. (2018) point out

[1] For the version of QSGD with 1-bit compression, the variance explosion is by a factor of $\sqrt{d}$, where d is the number of weights. It is common to have $d > 10^8$ in modern deep networks.

problems in the original convergence proof of ADAM, even in the convex setting. Since SIGNSGD belongs to this same family of algorithms, we expect that our theoretical analysis should be relevant for all algorithms in the family. In a parallel work, Balles & Hennig (2017) explore the connection between SIGNSGD and ADAM in greater detail, though their theory is more restricted and lives in the convex world, and they do not analyse SIGNUM as we do but employ it on heuristic grounds.

Optimisation: much of classic optimisation theory focuses on convex problems, where *local information* in the gradient tells you *global information* about the direction to the minimum. Whilst elegant, this theory is less relevant for modern problems in deep learning which are non-convex. In non-convex optimisation, finding the global minimum is generally intractable. Theorists usually settle for measuring some restricted notion of success, such as rate of convergence to stationary points (Ghadimi & Lan, 2013; Allen-Zhu, 2017a) or local minima (Nesterov & Polyak, 2006). Though Dauphin et al. (2014) suggest saddle points should abound in neural network error landscapes, practitioners report not finding this a problem in practice (Goodfellow et al., 2015) and therefore a theory of convergence to stationary points is useful and informative.

On the algorithmic level, the *non-stochastic* version of SIGNSGD can be viewed as the classical steepest descent algorithm with ℓ_∞-norm (see, e.g., Boyd & Vandenberghe, 2004, Section 9.4). The convergence of steepest descent is well-known (see Karimi et al., 2016, Appendix C, for an analysis of signed gradient updates under the Polyak-Łojasiewicz condition). Carlson et al. (2016) study a stochastic version of the algorithm, but again under an ℓ_∞ majorisation. To the best of our knowledge, we are the first to study the convergence of signed gradient updates under an (often more natural) ℓ_2 majorisation (Assumption 2).

Experimental benchmarks: throughout the paper we will make use of the CIFAR-10 (Krizhevsky, 2009) and Imagenet (Russakovsky et al., 2015) datasets. As for neural network architectures, we train Resnet-20 (He et al., 2016a) on CIFAR-10, and Resnet-50 v2 (He et al., 2016b) on Imagenet.

3. Convergence Analysis of SIGNSGD

We begin our analysis of sign stochastic gradient descent in the non-convex setting. The standard assumptions of the stochastic optimisation literature are nicely summarised by Allen-Zhu (2017b). We will use more fine-grained assumptions. SIGNSGD can exploit this additional structure, much as ADAGRAD (Duchi et al., 2011) exploits sparsity. We emphasise that these fine-grained assumptions do not lose anything over typical SGD assumptions, since *our assumptions can be obtained from SGD assumptions and vice versa*.

Assumption 1 (Lower bound)**.** *For all x and some constant f^*, we have objective value $f(x) \geq f^*$.*

This assumption is standard and necessary for guaranteed convergence to a stationary point.

The next two assumptions will naturally encode notions of heterogeneous curvature and gradient noise.

Assumption 2 (Smooth)**.** *Let $g(x)$ denote the gradient of the objective $f(.)$ evaluated at point x. Then $\forall x, y$ we require that for some non-negative constant $\vec{L} := [L_1, ..., L_d]$*

$$\Big| f(y) - \big[f(x) + g(x)^T(y-x)\big] \Big| \leq \frac{1}{2}\sum_i L_i (y_i - x_i)^2.$$

For twice differentiable f, this implies that $-\text{diag}(\vec{L}) \prec H \prec \text{diag}(\vec{L})$. This is related to the slightly weaker coordinate-wise Lipschitz condition used in the block coordinate descent literature (Richtárik & Takáč, 2014).

Lastly, we assume that we have access to the following stochastic gradient oracle:

Assumption 3 (Variance bound)**.** *Upon receiving query $x \in \mathbb{R}^d$, the stochastic gradient oracle gives us an* independent *unbiased estimate $\tilde{g}$ that has coordinate bounded variance:*

$$\mathbb{E}[\tilde{g}(x)] = g(x), \qquad \mathbb{E}\left[(\tilde{g}(x)_i - g(x)_i)^2\right] \leq \sigma_i^2$$

for a vector of non-negative constants $\vec{\sigma} := [\sigma_1, .., \sigma_d]$.

Bounded variance may be unrealistic in practice, since as $x \to \infty$ the variance might well diverge. Still this assumption is useful for understanding key properties of stochastic optimisation algorithms. In our theorem, we will be working with a mini-batch of size n_k in the k^{th} iteration, and the corresponding mini-batch stochastic gradient is modeled as the average of n_k calls to the above oracle at x_k. This squashes the variance bound on $\tilde{g}(x)_i$ to σ_i^2/n_k.

Assumptions 2 and 3 are different from the assumptions typically used for analysing the convergence properties of SGD (Nesterov, 2013; Ghadimi & Lan, 2013), but they are natural to the geometry induced by algorithms with signed updates such as SIGNSGD and SIGNUM.

Assumption 2 is more fine-grained than the standard assumption, which is recovered by defining ℓ_2 Lipschitz constant $L := \|\vec{L}\|_\infty = \max_i L_i$. Then Assumption 2 implies that

$$\Big| f(y) - \big[f(x) + g(x)^T(y-x)\big] \Big| \leq \frac{L}{2}\|y_i - x_i\|_2^2.$$

which is the standard assumption of Lipschitz smoothness.

Assumption 3 is more fined-grained than the standard stochastic gradient oracle assumption used for SGD analysis. But again, the standard variance bound is recovered by defining $\sigma^2 := ||\vec{\sigma}||_2^2$. Then Assumption 3 implies that

$$\mathbb{E}\|\tilde{g}(x) - g(x)\|^2 \leq \sigma^2$$

which is the standard assumption of bounded total variance.

Under these assumptions, we have the following result:

Theorem 1 (Non-convex convergence rate of SIGNSGD)**.** *Run algorithm 1 for K iterations under Assumptions 1 to 3. Set the learning rate and mini-batch size (independently of step k) as*

$$\delta_k = \frac{1}{\sqrt{\|\vec{L}\|_1 K}}, \qquad n_k = K$$

Let N be the cumulative number of stochastic gradient calls up to step K, i.e. $N = O(K^2)$. Then we have

$$\mathbb{E}\left[\frac{1}{K}\sum_{k=0}^{K-1}\|g_k\|_1\right]^2 \leq \frac{1}{\sqrt{N}}\left[\sqrt{\|\vec{L}\|_1}\left(f_0 - f_* + \frac{1}{2}\right) + 2\|\vec{\sigma}\|_1\right]^2$$

The proof is given in Section B of the supplementary material. It follows the well known strategy of relating the norm of the gradient to the expected improvement made in a single algorithmic step, and comparing this with the total possible improvement under Assumption 1. A key technical challenge we overcome is in showing how to directly deal with a biased approximation to the true gradient. Here we will provide some intuition about the proof.

To pass the stochasticity through the non-linear sign operation in a controlled fashion, we need to prove the key statement that at the k^{th} step for the i^{th} gradient component

$$\mathbb{P}[\text{sign}(\tilde{g}_{k,i}) \neq \text{sign}(g_{k,i})] \leq \frac{\sigma_{k,i}}{|g_{k,i}|}$$

This formalises the intuition that the probability of the sign of a component of the stochastic gradient being incorrect should be controlled by the signal-to-noise ratio of that component. When a component's gradient is large, the probability of making a mistake is low, and one expects to make good progress. When the gradient is small compared to the noise, the probability of making mistakes can be high, but due to the large batch size this only happens when we are already close to a stationary point.

The large batch size in the theorem may seem unusual, but large batch training actually presents a systems advantage (Goyal et al., 2017) since it can be parallelised. The number of gradient calls N is the important quantity to measure convergence, but large batch training achieves N gradient calls in only $O(\sqrt{N})$ iterations whereas small batch training needs $O(N)$ iterations. Fewer iterations also means fewer rounds of communication in the distributed setting. Convergence guarantees *can* be extended to the small batch case under the additional assumption of unimodal symmetric gradient noise using Lemma D.1 in the supplementary, but we leave this for future work. Experiments in this paper were indeed conducted in the small batch regime.

Another unusual feature requiring discussion is the ℓ_1 geometry of SIGNSGD. The convergence rate strikingly depends on the ℓ_1-norm of the gradient, the stochasticity and the curvature. To understand this better, let's define a notion of density of a high-dimensional vector $\vec{v} \in \mathbb{R}^d$ as follows:

$$\phi(\vec{v}) := \frac{\|\vec{v}\|_1^2}{d\|\vec{v}\|_2^2} \tag{1}$$

To see that this is a natural definition of density, notice that for a fully dense vector, $\phi(\vec{v}) = 1$ and for a fully sparse vector, $\phi(\vec{v}) = 1/d \approx 0$. We trivially have that $\|\vec{v}\|_1^2 \leq \phi(\vec{v})d^2\|\vec{v}\|_\infty^2$ so this notion of density provides an easy way to translate from norms in ℓ_1 to both ℓ_2 and ℓ_∞.

Remember that under our assumptions, SGD-style assumptions hold with Lipschitz constant $L := \|\vec{L}\|_\infty$ and total variance bound $\sigma^2 := \|\vec{\sigma}\|_2^2$. Using our notion of density we can translate our constants into the language of SGD:

$$\begin{aligned}
\|g_k\|_1^2 &= \phi(g_k)d\|g_k\|_2^2 &&\geq \phi(g)d\|g_k\|_2^2 \\
\|\vec{L}\|_1^2 &\leq \phi(\vec{L})d^2\|\vec{L}\|_\infty^2 &&= \phi(\vec{L})d^2L^2 \\
\|\vec{\sigma}\|_1^2 &= \phi(\vec{\sigma})d\|\vec{\sigma}\|_2^2 &&= \phi(\vec{\sigma})d\sigma^2
\end{aligned}$$

where we have assumed $\phi(g)$ to be a lower bound on the gradient density over the entire space. Using that $(x+y)^2 \leq 2(x^2+y^2)$ and changing variables in the bound, we reach the following result for SIGNSGD

$$\mathbb{E}\left[\frac{1}{K}\sum_{k=0}^{K-1}\|g_k\|_2\right]^2 \leq \frac{2}{\sqrt{N}}\left[\frac{\sqrt{\phi(\vec{L})}}{\phi(g)}L\left(f_0 - f_* + \frac{1}{2}\right)^2 + 4\frac{\phi(\vec{\sigma})}{\phi(g)}\sigma^2\right]$$

whereas, for comparison, a typical SGD bound (proved in Supplementary C) is

$$\mathbb{E}\left[\frac{1}{K}\sum_{k=0}^{K-1}\|g_k\|_2^2\right] \leq \frac{1}{\sqrt{N}}\left[2L(f_0 - f_*) + \sigma^2\right].$$

The bounds are very similar, except for most notably the appearance of ratios of densities R_1 and R_2, defined as

$$R_1 := \frac{\sqrt{\phi(\vec{L})}}{\phi(g)} \qquad R_2 := \frac{\phi(\vec{\sigma})}{\phi(g)}$$

Naïvely comparing the bounds suggests breaking into cases:

(I) $R_1 \gg 1$ and $R_2 \gg 1$. This means that both the curvature and the stochasticity are much denser than the typical gradient and the comparison suggests SGD is better suited than SIGNSGD.

(II) NOT$[R_1 \gg 1]$ and NOT$[R_2 \gg 1]$. This means that neither curvature nor stochasticity are much denser than the gradient, and the comparison suggests that SIGNSGD may converge as fast or faster than SGD, and also get the benefits of gradient compression.

(III) neither of the above holds, for example $R_1 \ll 1$ and $R_2 \gg 1$. Then the comparison is indeterminate about whether SIGNSGD or SGD is more suitable.

Let's briefly provide some intuition to understand how it's possible that SIGNSGD could outperform SGD. Imagine a scenario where the gradients are dense but there is a sparse set of extremely noisy components. Then the dynamics of SGD will be dominated by this noise, and (unless the learning rate is reduced a lot) SGD will effectively perform a random walk along these noisy components, paying less attention to the gradient signal. SIGNSGD however will treat all components equally, so it will scale down the sparse noise and scale up the dense gradients comparatively, and thus make good progress. See Figure A.1 in the supplementary for a simple example of this.

Still we must be careful when comparing upper bounds, and interpreting the dependence on curvature density is more subtle than noise density. This is because the SGD bound proved in Supplementary C is slacker under situations of sparse curvature than dense curvature. That is to say that SGD, like SIGNSGD, benefits under situations of sparse curvature but this is not reflected in the SGD bound. The potentially slack step in SGD's analysis is in switching from L_i to $\|\vec{L}\|_\infty$. Because of this it is safer to interpret the curvature comparison as telling us a regime where SIGNSGD is expected to lose out to SGD (rather than vice versa). This happens when $R_1 \gg 1$ and gradients are sparser than curvature. Intuitively, in this case SIGNSGD will push many components in highly curved directions even though these components had small gradient, and this can be undesirable.

To summarise, our theory suggests that when gradients are dense, SIGNSGD should be more robust to large stochasticity on a sparse set of coordinates. When gradients are sparse, SGD should be more robust to dense curvature and noise. In practice for deep networks, we find that SIGNSGD converges about as fast as SGD. That would suggest that we are either in regime (II) or (III) above. But what is the real situation for the error landscape of deep neural networks?

To measure gradient and noise densities in practice, we use Welford's algorithm (Welford, 1962; Knuth, 1997) to compute the true gradient g and its stochasticity vector $\vec{\sigma}$ at every epoch of training for a Resnet-20 model on CIFAR-10. Welford's algorithm is numerically stable and only takes a single pass through the data to compute the vectorial mean and variance. Therefore if we train a network for 160 epochs, we make an additional 160 passes through the data to evaluate these gradient statistics. Results are plotted in Figure 1. Notice that the gradient density and noise density are of the same order throughout training, and this indeed puts us in regime (II) or (III) as predicted by our theory.

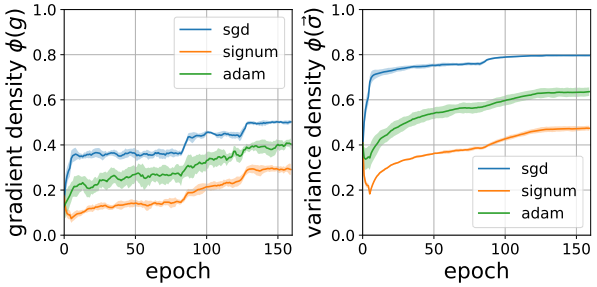

Figure 1. Gradient and noise density during an entire training run of a Resnet-20 model on the CIFAR-10 dataset. Results are averaged over 3 repeats for each of 3 different training algorithms, and corresponding error bars are plotted. At the beginning of every epoch, at that fixed point in parameter space, we do a full pass over the data to compute the exact mean of the stochastic gradient, g, and its exact standard deviation vector $\vec{\sigma}$ (square root of diagonal of covariance matrix). The density measure $\phi(\vec{v}) := \frac{\|v\|_1^2}{d\|v\|_2^2}$ is 1 for a fully dense vector and ≈ 0 for a fully sparse vector. Notice that both gradient and noise are dense, and moreover the densities appear to be coupled during training. Noticable jumps occur at epoch 80 and 120 when the learning rate is decimated. Our stochastic gradient oracle (Assumption 3) is fine-grained enough to encode such dense geometries of noise.

In Figure A.2 of the supplementary, we present preliminary evidence that this finding generalises, by showing that gradients are dense across a range of datasets and network architectures. We have not devised an efficient means to measure curvature densities, which we leave for future work.

4. Majority Rule: the Power of Democracy in the Multi-Worker Setting

In the most common form of distributed training, workers (such as GPUs) each evaluate gradients on their own split of the data, and send the results up to a parameter-server. The parameter server aggregates the results and transmits them back to each worker (Li et al., 2014).

Up until this point in the paper, we have only analysed

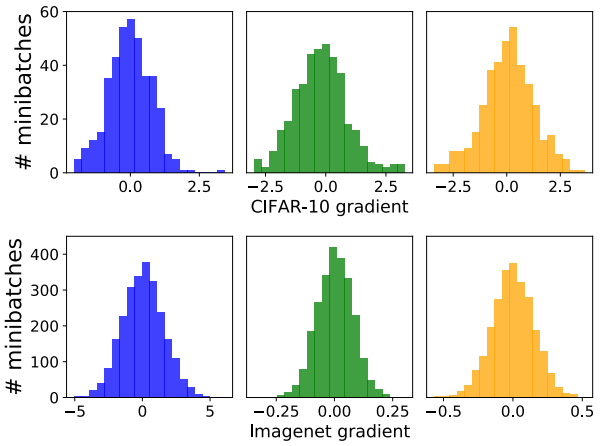

Figure 2. Histograms of the noise in the stochastic gradient, each plot for a different randomly chosen parameter (not cherry-picked). Top row: Resnet-20 architecture trained to epoch 50 on CIFAR-10 with a batch size of 128. Bottom row: Resnet-50 architecture trained to epoch 50 on Imagenet with a batch size of 256. From left to right: model trained with SGD, SIGNUM, ADAM. All noise distributions appear to be unimodal and approximately symmetric. For a batch size of 256 Imagenet images, the central limit theorem has visibly kicked in and the distributions look Gaussian.

SIGNSGD where the update is of the form

$$x_{k+1} = x_k - \delta\,\mathrm{sign}(\tilde{g})$$

To get the benefits of compression we want the m^{th} worker to send the sign of the gradient evaluated only on its portion of the data. This suggests an update of the form

$$x_{k+1} = x_k - \delta \sum_{m=1}^{M} \mathrm{sign}(\tilde{g}_m) \qquad \text{(good)}$$

This scheme is good since what gets sent *to* the parameter will be 1-bit compressed. But what gets sent back almost certainly will not. Could we hope for a scheme where all communication is 1-bit compressed?

What about the following scheme:

$$x_{k+1} = x_k - \delta\,\mathrm{sign}\left[\sum_{m=1}^{M} \mathrm{sign}(\tilde{g}_m)\right] \qquad \text{(best)}$$

This is called majority vote, since each worker is essentially voting with its belief about the sign of the true gradient. The parameter server counts the votes, and sends its 1-bit decision back to every worker.

The machinery of Theorem 1 is enough to establish convergence for the (good) scheme, but majority vote is more elegant *and* more communication efficient, therefore we focus on this scheme from here on.

In Theorem 2 we first establish the general convergence rate of majority vote, followed by a regime where majority vote enjoys a variance reduction from $\|\vec{\sigma}\|_1$ to $\|\vec{\sigma}\|_1/\sqrt{M}$.

Theorem 2 (Non-convex convergence rate of distributed SIGNSGD with majority vote)**.** *Run algorithm 3 for K iterations under Assumptions 1 to 3. Set the learning rate and mini-batch size for each worker (independently of step k) as*

$$\delta_k = \frac{1}{\sqrt{\|\vec{L}\|_1 K}} \qquad n_k = K$$

*Then **(a)** majority vote with M workers converges at least as fast as* SIGNSGD *in Theorem 1.*

*And **(b)** further assuming that the noise in each component of the stochastic gradient is unimodal and symmetric about the mean (e.g. Gaussian), majority vote converges at improved rate:*

$$\mathbb{E}\left[\frac{1}{K}\sum_{k=0}^{K-1}\|g_k\|_1\right]^2 \leq \frac{1}{\sqrt{N}}\left[\sqrt{\|\vec{L}\|_1}\left(f_0 - f_* + \frac{1}{2}\right) + \frac{2}{\sqrt{M}}\|\vec{\sigma}\|_1\right]^2$$

where N is the cumulative number of stochastic gradient calls per worker up to step K.

The proof is given in the supplementary material, but here we sketch some details. Consider the signal-to-noise ratio of a single component of the stochastic gradient, defined as $S := \frac{|g_i|}{\sigma_i}$. For $S < 1$ the gradient is small and it doesn't matter if we get the sign wrong. For $S > 1$, we can show using a one-sided version of Chebyshev's inequality (Cantelli, 1928) that the failure probability, q, of that sign bit on an individual worker satisfies $q < \frac{1}{2}$. This means that the parameter server is essentially receiving a repetition code R_M and the majority vote decoder is known to drive down the failure probability of a repetition code exponentially in the number of repeats (MacKay, 2002).

Remark: Part (a) of the theorem does not describe a speedup over just using a single machine, and that might hint that all those extra $M-1$ workers are a waste in this setting. **This is not the case**. From the proof sketch above, it should be clear that part (a) is an extremely conservative statement. In particular, we expect all regions of training where the signal-to-noise ratio of the stochastic gradient satisfies $S > 1$ to enjoy a significant speedup due to variance reduction. It's just that since we don't get the speedup when

$S < 1$, it's hard to express this in a compact bound.

To sketch a proof for part (b), note that a sign bit from each worker is a Bernoulli trial—call its failure probability q. We can get a tight control of q by a convenient tail bound owing to Gauss (1823) that holds under conditions of unimodal symmetry. Then the sum of bits received by the parameter server is a binomial random variable, and we can use Cantelli's inequality to bound its tail. This turns out to be enough to get tight enough control on the error probability of the majority vote decoder to prove the theorem.

Remark 1: assuming that the stochastic gradient of each worker is approximately symmetric and unimodal is very reasonable. In particular for increasing mini-batch size it will be an ever-better approximation by the central limit theorem. Figure 2 plots histograms of real stochastic gradients for neural networks. Even at batch-size 256 the stochastic gradient for an Imagenet model already looks Gaussian.

Remark 2: if you delve into the proof of Theorem 2 and graph all of the inequalities, you will notice that some of them are uniformly slack. This suggests that the assumptions of symmetry and unimodality can actually be relaxed to only hold approximately. This raises the possibility of proving a relaxed form of Gauss' inequality and using a third moment bound in the Berry-Esseen theorem to derive a minimal batch size for which the majority vote scheme is guaranteed to work by the central limit theorem. We leave this for future work.

Remark 3: why does this theorem have anything to do with unimodality or symmetry at all? It's because there exist very skewed or bimodal random variables X with mean μ such that $\mathbb{P}[\text{sign}(X) = \text{sign}(\mu)]$ is arbitrarily small. This can either be seen by applying Cantelli's inequality which is known to be tight, or by playing with distributions like

$$\mathbb{P}[X = x] = \begin{cases} 0.1 & \text{if } x = 50 \\ 0.9 & \text{if } x = -1 \end{cases}$$

Distributions like these are a problem because it means that adding more workers will actually drive up the error probability rather than driving it down. The beauty of the central limit theorem is that even for such a skewed and bimodal distribution, the mean of just a few tens of samples will already start to look Gaussian.

5. Extending the Theory to SIGNUM

Momentum is a popular trick used by neural network practitioners that can, in our experience, speed up the training of deep neural networks and improve the robustness of algorithms to other hyperparameter settings. Instead of taking steps according to the gradient, momentum algorithms take steps according to a running average of recent gradients.

Existing theoretical analyses of momentum often rely on the absence of gradient stochasticity (e.g. Jin et al. (2017)) or convexity (e.g. Goh (2017)) to show that momentum's asymptotic convergence rate can beat gradient descent.

It is easy to incorporate momentum into SIGNSGD, merely by taking the sign of the momentum We call the resulting algorithm SIGNUM and present the algorithmic step formally in Algorithm 2. SIGNUM fits into our theoretical framework, and we prove its convergence rate in Theorem 3.

Theorem 3 (Convergence rate of SIGNUM)**.** *In Algorithm 2, set the learning rate, mini-batch size and momentum parameter respectively as*

$$\delta_k = \frac{\delta}{\sqrt{k+1}} \qquad n_k = k+1 \qquad \beta$$

Our analysis also requires a warmup period to let the bias in the momentum settle down. The warmup should last for $C(\beta)$ iterations, where C is a constant that depends on the momentum parameter β as follows:

$$C(\beta) = \min_{C \in \mathbb{Z}^+} C \quad \text{s.t.} \quad \frac{C}{2}\beta^C \leq \frac{1}{1-\beta^2}\frac{1}{C+1} \quad \& \quad \beta^{C+1} \leq \frac{1}{2}$$

Note that for $\beta = 0.9$, we have $C = 54$ which is negligible. For the first $C(\beta)$ iterations, accumulate the momentum as normal, but use the sign of the stochastic gradient to make updates instead of the sign of the momentum.

Let N be the cumulative number of stochastic gradient calls up to step K, i.e. $N = O(K^2)$. Then for $K \gg C$ we have

$$\mathbb{E}\left[\frac{1}{K-C}\sum_{k=C}^{K-1}\|g_k\|_1\right]^2 = O\left(\frac{1}{\sqrt{N}}\left[\frac{f_C - f_*}{\delta} + (1+\log N)\left(\frac{\delta\|\vec{L}\|_1}{1-\beta} + \|\vec{\sigma}\|_1\sqrt{1-\beta}\right)\right]^2\right)$$

where we have used $O(.)$ to hide numerical constants and the β-dependent constant C.

The proof is the greatest technical challenge of the paper, and is given in the supplementary material. We focus on presenting the proof in a modular form, anticipating that parts may be useful in future theoretical work. It involves a very general master lemma, Lemma E.1, which can be used to help prove all the theorems in this paper.

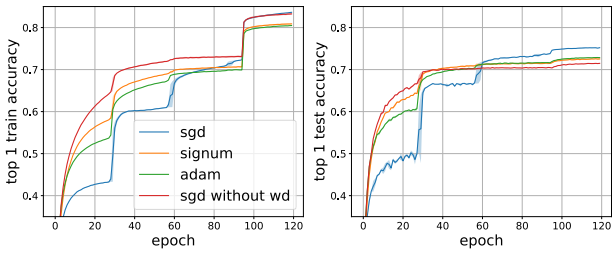

Figure 3. Imagenet train and test accuracies using the momentum version of SIGNSGD, called SIGNUM, to train Resnet-50 v2. We based our implementation on an open source implementation by `github.com/tornadomeet`. Initial learning rate and weight decay were tuned on a separate validation set split off from the training set and all other hyperparameters were chosen to be those found favourable for SGD by the community. There is a big jump at epoch 95 when we switch off data augmentation. SIGNUM gets test set performance approximately the same as ADAM, better than SGD with out weight decay, but about 2% worse than SGD with a well-tuned weight decay.

Remark 1: switching optimisers after a warmup period is in fact commonly done by practitioners (Akiba et al., 2017).

Remark 2: the theory suggests that momentum can be used to control a bias-variance tradeoff in the quality of stochastic gradient estimates. Sending $\beta \to 1$ kills the variance term in $\|\vec{\sigma}\|_1$ due to averaging gradients over a longer time horizon. But averaging in stale gradients induces bias due to curvature of $f(x)$, and this blows up the $\delta\|\vec{L}\|_1$ term.

Remark 3: for generality, we state this theorem with a tunable learning rate δ. For variety, we give this theorem in any-time form with a growing batch size and decaying learning rate. This comes at the cost of $\log$ factors appearing.

We benchmark SIGNUM on Imagenet (Figure 3) and CIFAR-10 (Figure A.3 of supplementary). The full results of a giant hyperparameter grid search for the CIFAR-10 experiments are also given in the supplementary. SIGNUM's performance rivals ADAM's in all experiments.

6. Discussion

Gradient compression schemes like TERNGRAD (Wen et al., 2017) quantise gradients into three levels $\{0, \pm 1\}$. This is desirable when the ternary quantisation is sparse, since it can allow further compression. Our scheme of majority vote should easily be compatible with a ternary quantisation—in both directions of communication. This can be cast as "majority vote with abstention". The scheme is as follows: workers send their vote to the parameter server, unless they are very unsure about the sign of the true gradient in which case they send zero. The parameter-server counts the votes, and if quorum is not reached (i.e. too many workers disagreed or abstained) the parameter-server sends back zero. This extended algorithm should readily fit into our theory.

In Section 2 we pointed out that SIGNSGD and SIGNUM are closely related to ADAM. In all our experiments we find that SIGNUM and ADAM have very similar performance, although both lose out to SGD by about 2% test accuracy on Imagenet. Wilson et al. (2017) observed that ADAM tends to generalise slightly worse than SGD. Though it is still unclear why this is the case, perhaps it could be because we don't know how to properly regularise such methods. Whilst we found that neither standard weight decay nor the suggestion of Loshchilov & Hutter (2017) completely closed our Imagenet test set gap with SGD, it is possible that some other regularisation scheme might. One idea, suggested by our theory, is that SIGNSGD could be squashing down noise levels. There is some evidence (Smith & Le, 2018) that a certain level of noise can be good for generalisation, biasing the optimiser towards wider valleys in the objective function. Perhaps, then, adding Gaussian noise to the SIGNUM update might help it generalise better. This can be achieved in a communication efficient manner in the distributed setting by sharing a random seed with each worker, and then generating the same noise on each worker.

Finally, in Section 3 we discuss some geometric implications of our theory, and provide an efficient and robust experimental means of measuring one aspect—the ratio between noise and gradient density—through the Welford algorithm. We believe that since this density ratio is easy to measure, it may be useful to help guide those doing architecture search, to find network architectures which are amenable to fast training through gradient compression schemes.

7. Conclusion

We have presented a general framework for studying sign-based methods in stochastic non-convex optimisation. We present non-vacuous bounds for gradient compression schemes, and elucidate the special ℓ_1 geometries under which these schemes can be expected to succeed. Our theoretical framework is broad enough to handle signed-momentum schemes—like SIGNUM—and also multi-worker distributed schemes—like majority vote.

Our work touches upon interesting aspects of the geometry of high-dimensional error surfaces, which we wish to explore in future work. But the next step for us will be to reach out to members of the distributed systems community to help benchmark the majority vote algorithm which shows such great theoretical promise for 1-bit compression in both directions between parameter-server and workers.

Acknowledgments

The authors are grateful to the anonymous reviewers for their helpful comments, as well as Jiawei Zhao, Michael Tschannen, Julian Salazar, Tan Nguyen, Fanny Yang, Mu Li, Aston Zhang and Zack Lipton for useful discussions. Thanks to Ryan Tibshirani for pointing out the connection to steepest descent.

KA is supported in part by NSF Career Award CCF-1254106 and Air Force FA9550-15-1-0221. AA is supported in part by Microsoft Faculty Fellowship, Google Faculty Research Award, Adobe Grant, NSF Career Award CCF-1254106, and AFOSR YIP FA9550-15-1-0221.

References

Akiba, T., Suzuki, S., and Fukuda, K. Extremely Large Minibatch SGD: Training ResNet-50 on ImageNet in 15 Minutes. *arXiv:1711.04325*, 2017.

Alistarh, D., Grubic, D., Li, J., Tomioka, R., and Vojnovic, M. QSGD: Communication-Efficient SGD via Gradient Quantization and Encoding. In *Advances in neural information processing systems (NIPS-17)*, 2017.

Allen-Zhu, Z. Natasha: Faster Non-Convex Stochastic Optimization via Strongly Non-Convex Parameter. In *International Conference on Machine Learning (ICML-17)*, 2017a.

Allen-Zhu, Z. Natasha 2: Faster Non-Convex Optimization Than SGD. *arXiv:1708.08694*, 2017b.

Balles, L. and Hennig, P. Dissecting Adam: The Sign, Magnitude and Variance of Stochastic Gradients. *arXiv:1705.07774*, 2017.

Boyd, S. and Vandenberghe, L. *Convex Optimization*. Cambridge University Press, 2004.

Cantelli, F. P. Sui confini della probabilit. *Atti del Congresso Internazionale dei Matematici*, 1928.

Carlson, D., Hsieh, Y., Collins, E., Carin, L., and Cevher, V. Stochastic spectral descent for discrete graphical models. *IEEE Journal of Selected Topics in Signal Processing*, 10 (2):296–311, 2016.

Dauphin, Y. N., Pascanu, R., Gulcehre, C., Cho, K., Ganguli, S., and Bengio, Y. Identifying and Attacking the Saddle Point Problem in High-Dimensional Non-Convex Optimization. In *Advances in neural information processing systems (NIPS-14)*, 2014.

Duchi, J., Hazan, E., and Singer, Y. Adaptive subgradient methods for online learning and stochastic optimization. *Journal of Machine Learning Research*, 12:2121–2159, 2011.

Gauss, C. F. Theoria combinationis observationum erroribus minimis obnoxiae, pars prior. *Commentationes Societatis Regiae Scientiarum Gottingensis Recentiores*, 1823.

Ghadimi, S. and Lan, G. Stochastic first-and zeroth-order methods for nonconvex stochastic programming. *SIAM Journal on Optimization*, 23(4):2341–2368, 2013.

Glorot, X. and Bengio, Y. Understanding the Difficulty of Training Deep Feedforward Neural Networks. In *Artificial intelligence and statistics (AISTATS-10)*, 2010.

Goh, G. Why Momentum Really Works. *Distill*, 2017.

Goodfellow, I. J., Vinyals, O., and Saxe, A. M. Qualitatively Characterizing Neural Network Optimization Problems. In *International Conference on Learning Representations (ICLR-15)*, 2015.

Goyal, P., Dollár, P., Girshick, R. B., Noordhuis, P., Wesolowski, L., Kyrola, A., Tulloch, A., Jia, Y., and He, K. Accurate, Large Minibatch SGD: Training ImageNet in 1 Hour. *arXiv:1706.02677*, 2017.

He, K., Zhang, X., Ren, S., and Sun, J. Deep residual learning for image recognition. In *IEEE Conference on Computer Vision and Pattern Recognition (CVPR-16)*, pp. 770–778, 2016a.

He, K., Zhang, X., Ren, S., and Sun, J. Identity mappings in deep residual networks. In *European Conference on Computer Vision (ECCV-16)*, pp. 630–645. Springer, 2016b.

Jin, C., Netrapalli, P., and Jordan, M. I. Accelerated Gradient Descent Escapes Saddle Points Faster than Gradient Descent. *arXiv:1711.10456*, 2017.

Karimi, H., Nutini, J., and Schmidt, M. Linear convergence of gradient and proximal-gradient methods under the Polyak-łojasiewicz condition. In *European Conference on Machine Learning and Principles and Practice of Knowledge Discovery in Databases (ECML-PKDD-16)*, pp. 795–811. Springer, 2016.

Kingma, D. P. and Ba, J. Adam: A Method for Stochastic Optimization. In *International Conference on Learning Representations (ICLR-15)*, 2015.

Knuth, D. E. *The Art of Computer Programming, Volume 2 (3rd Ed.): Seminumerical Algorithms*. Addison-Wesley Longman Publishing Co., Inc., 1997.

Krizhevsky, A. Learning Multiple Layers of Features from Tiny Images. Technical report, University of Toronto, 2009.

LeCun, Y., Bengio, Y., and Hinton, G. Deep learning. *Nature*, 521(7553):436, 2015.

Li, M., Andersen, D. G., Park, J. W., Smola, A. J., Ahmed, A., Josifovski, V., Long, J., Shekita, E. J., and Su, B.-Y. Scaling Distributed Machine Learning with the Parameter Server. In *Symposium on Operating Systems Design and Implementation (OSDI-14)*, pp. 583–598, 2014.

Loshchilov, I. and Hutter, F. Fixing Weight Decay Regularization in Adam. *arXiv:1711.05101*, 2017.

MacKay, D. J. C. *Information Theory, Inference & Learning Algorithms*. Cambridge University Press, 2002.

Nesterov, Y. *Introductory Lectures on Convex Optimization: A Basic Course*. Springer, 2013.

Nesterov, Y. and Polyak, B. Cubic Regularization of Newton Method and its Global Performance. *Mathematical Programming*, 2006.

Pukelsheim, F. The Three Sigma Rule. *The American Statistician*, 1994.

Reddi, S. J., Kale, S., and Kumar, S. On the Convergence of Adam and Beyond. In *International Conference on Learning Representations (ICLR-18)*, 2018.

Richtárik, P. and Takáč, M. Iteration complexity of randomized block-coordinate descent methods for minimizing a composite function. *Mathematical Programming*, 144 (1-2):1–38, 2014.

Riedmiller, M. and Braun, H. A Direct Adaptive Method for Faster Backpropagation Learning: the RPROP Algorithm. In *International Conference on Neural Networks (ICNN-93)*, pp. 586–591. IEEE, 1993.

Robbins, H. and Monro, S. A Stochastic Approximation Method. *The Annals of Mathematical Statistics*, 1951.

Russakovsky, O., Deng, J., Su, H., Krause, J., Satheesh, S., Ma, S., Huang, Z., Karpathy, A., Khosla, A., Bernstein, M., et al. Imagenet large scale visual recognition challenge. *International Journal of Computer Vision*, 115(3): 211–252, 2015.

Schmidhuber, J. Deep Learning in Neural Networks: an Overview. *Neural Networks*, 2015.

Seide, F., Fu, H., Droppo, J., Li, G., and Yu, D. 1-Bit Stochastic Gradient Descent and Application to Data-Parallel Distributed Training of Speech DNNs. In *Conference of the International Speech Communication Association (INTERSPEECH-14)*, 2014.

Smith, S. L. and Le, Q. V. A Bayesian Perspective on Generalization and Stochastic Gradient Descent. In *International Conference on Learning Representations (ICLR-18)*, 2018.

Strom, N. Scalable distributed DNN training using commodity GPU cloud computing. In *Conference of the International Speech Communication Association (INTERSPEECH-15)*, 2015.

Suresh, A. T., Yu, F. X., Kumar, S., and McMahan, H. B. Distributed Mean Estimation with Limited Communication. In *International Conference on Machine Learning (ICML-17)*, 2017.

Tieleman, T. and Hinton, G. RMSprop. *Coursera: Neural Networks for Machine Learning*, Lecture 6.5, 2012.

Welford, B. P. Note on a Method for Calculating Corrected Sums of Squares and Products. *Technometrics*, 1962.

Wen, W., Xu, C., Yan, F., Wu, C., Wang, Y., Chen, Y., and Li, H. TernGrad: Ternary Gradients to Reduce Communication in Distributed Deep Learning. In *Advances in neural information processing systems (NIPS-17)*, 2017.

Wilson, A. C., Roelofs, R., Stern, M., Srebro, N., and Recht, B. The Marginal Value of Adaptive Gradient Methods in Machine Learning. In *Advances in neural information processing systems (NIPS-17)*, 2017.

A. Further experimental results

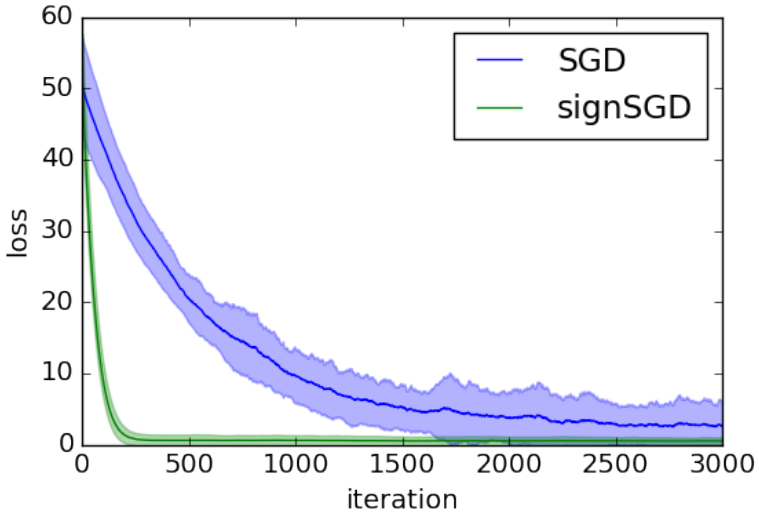

Figure A.1. A simple toy problem where SIGNSGD converges faster than SGD. The objective function is just a quadratic $f(x) = \frac{1}{2}x^2$ for $x \in \mathbb{R}^{100}$. The gradient of this function is just $g(x) = x$. We construct an artificial stochastic gradient by adding Gaussian noise $\mathcal{N}(0, 100^2)$ to only the first component of the gradient. Therefore the noise is extremely sparse. The initial point is sampled from a unit variance spherical Gaussian. For each algorithm we tune a separate, constant learning rate finding 0.001 best for SGD and 0.01 best for SIGNSGD. SIGNSGD appears more robust to the sparse noise in this problem. Results are averaged over 50 repeats with ± 1 standard deviation shaded.

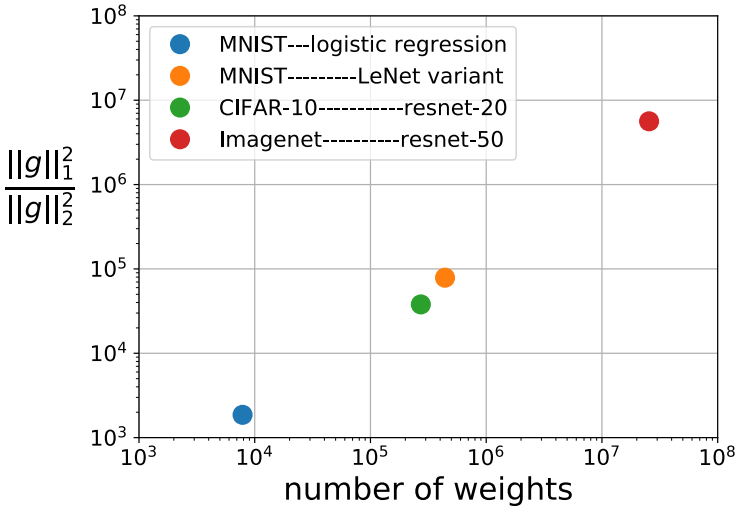

Figure A.2. Measuring gradient density via ratio of norms, over a range of datasets and architectures. For each network, we take a point in parameter space provided by the Xavier initialiser (Glorot & Bengio, 2010). We do a full pass over the data to compute the full gradient at this point. It is remarkably dense in all cases.

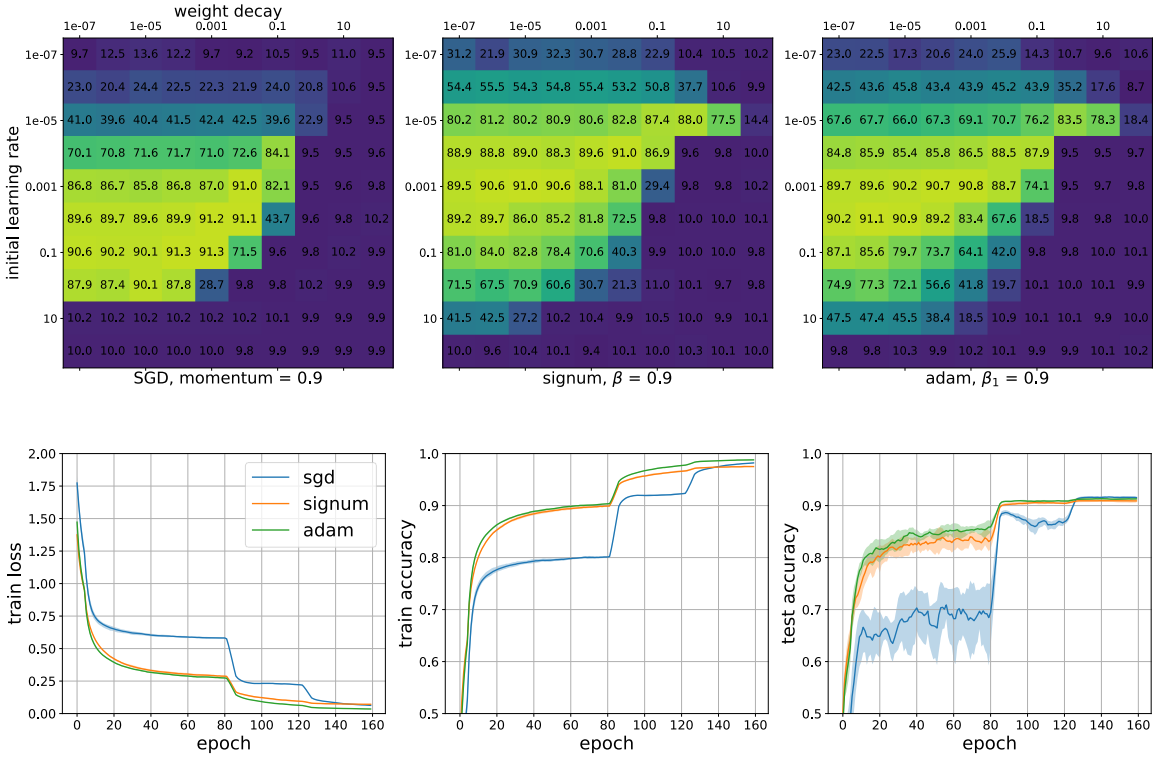

Figure A.3. CIFAR-10 results using SIGNUM to train a Resnet-20 model. Top: validation accuracies from a hyperparameter sweep on a separate validation set carved out from the training set. We used this to tune initial learning rate, weight decay and momentum for all algorithms. All other hyperparameter settings were chosen as in (He et al., 2016a) as found favourable for SGD. The hyperparameter sweep for other values of momentum is plotted in Figure A.4 of the supplementary. Bottom: there is little difference between the final test set performance of the algorithms. SIGNUM closely resembles ADAM in all of these plots.

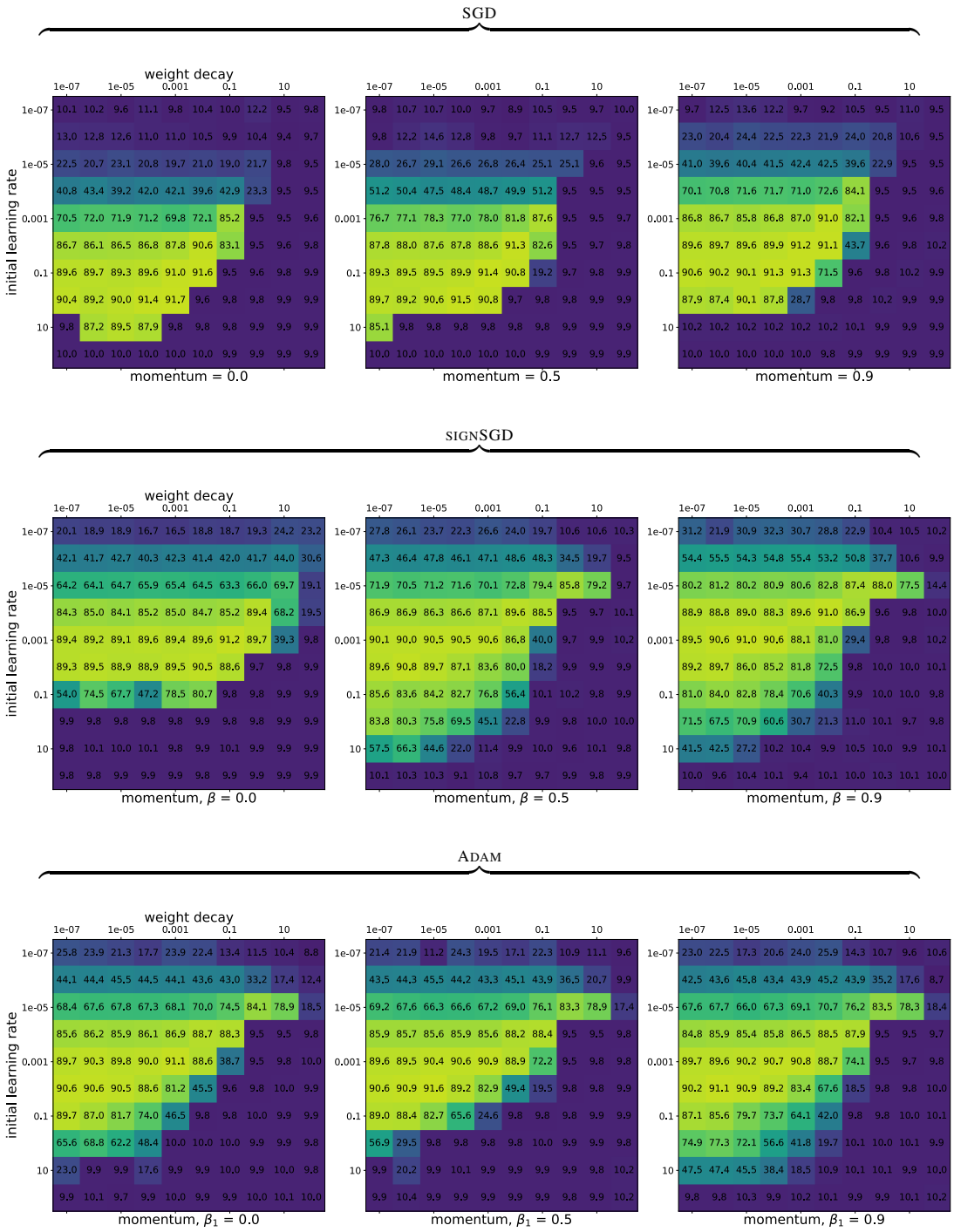

Figure A.4. Results of a massive grid search over hyperparameters for training Resnet-20 (He et al., 2016a) on CIFAR-10 (Krizhevsky, 2009). All non-algorithm specific hyperparameters (such as learning rate schedules) were set as in (He et al., 2016a). In ADAM, β_2 and ϵ were chosen as recommended in (Kingma & Ba, 2015). Data was divided according to a $\{45k/5k/10k\}$ $\{$train/val/test$\}$ split. Validation accuracies are plotted above, and the best performer on the validation set was chosen for the final test run (shown in Figure A.3). All algorithms at the least get close to the baseline reported in (He et al., 2016a) of 91.25%. Note the broad similarity in general shape of the heatmap between ADAM and SIGNSGD, supporting a notion of algorithmic similarity. Also note that whilst SGD has a larger region of very high-scoring hyperparameter configurations, SIGNSGD and ADAM appear stable over a larger range of learning rates. Notice that the SGD heat map shifts up for increasing momentum, since the implementation of SGD in the mxnet deep learning framework actually couples the momentum and learning rate parameters.

B. Proving the convergence rate of SIGNSGD

Theorem 1 (Non-convex convergence rate of SIGNSGD)**.** *Run algorithm 1 for K iterations under Assumptions 1 to 3. Set the learning rate and mini-batch size (independently of step k) as*

$$\delta_k = \frac{1}{\sqrt{\|\vec{L}\|_1 K}}, \qquad n_k = K$$

Let N be the cumulative number of stochastic gradient calls up to step K, i.e. $N = O(K^2)$. Then we have

$$\mathbb{E}\left[\frac{1}{K}\sum_{k=0}^{K-1}\|g_k\|_1\right]^2 \leq \frac{1}{\sqrt{N}}\left[\sqrt{\|\vec{L}\|_1}\left(f_0 - f_* + \frac{1}{2}\right) + 2\|\vec{\sigma}\|_1\right]^2$$

Proof. First let's bound the improvement of the objective during a single step of the algorithm for one instantiation of the noise. $\mathbb{I}[.]$ is the indicator function, $g_{k,i}$ denotes the i^{th} component of the true gradient $g(x_k)$ and $\tilde{g}_k$ is a stochastic sample obeying Assumption 3.

First take Assumption 2, plug in the step from Algorithm 1, and decompose the improvement to expose the stochasticity-induced error:

$$\begin{aligned} f_{k+1} - f_k &\leq g_k^T(x_{k+1} - x_k) + \sum_{i=1}^{d}\frac{L_i}{2}(x_{k+1} - x_k)_i^2 \\ &= -\delta_k g_k^T \text{sign}(\tilde{g}_k) + \delta_k^2 \sum_{i=1}^{d}\frac{L_i}{2} \\ &= -\delta_k\|g_k\|_1 + \frac{\delta_k^2}{2}\|\vec{L}\|_1 \\ &\quad + 2\delta_k\sum_{i=1}^{d}|g_{k,i}|\,\mathbb{I}[\text{sign}(\tilde{g}_{k,i}) \neq \text{sign}(g_{k,i})] \end{aligned}$$

Next we find the expected improvement at time $k+1$ conditioned on the previous iterate.

$$\begin{aligned} \mathbb{E}[f_{k+1} - f_k | x_k] &\leq -\delta_k\|g_k\|_1 + \frac{\delta_k^2}{2}\|\vec{L}\|_1 \\ &\quad + 2\delta_k\sum_{i=1}^{d}|g_{k,i}|\,\mathbb{P}[\text{sign}(\tilde{g}_{k,i}) \neq \text{sign}(g_{k,i})] \end{aligned}$$

So the expected improvement crucially depends on the probability that each component of the sign vector is correct, which is intuitively controlled by the relative scale of the gradient to the noise. To make this rigorous, first relax the probability, then use Markov's inequality followed by Jensen's inequality:

$$\begin{aligned} \mathbb{P}[\text{sign}(\tilde{g}_{k,i}) \neq \text{sign}(g_{k,i})] &\leq \mathbb{P}[|\tilde{g}_{k,i} - g_{k,i}| \geq |g_{k,i}|] \\ &\leq \frac{\mathbb{E}[|\tilde{g}_{k,i} - g_{k,i}|]}{|g_{k,i}|} \\ &\leq \frac{\sqrt{\mathbb{E}[(\tilde{g}_{k,i} - g_{k,i})^2]}}{|g_{k,i}|} \\ &= \frac{\sigma_{k,i}}{|g_{k,i}|} \end{aligned}$$

$\sigma_{k,i}$ refers to the variance of the k^{th} stochastic gradient estimate, computed over a mini-batch of size n_k. Therefore, by Assumption 3, we have that $\sigma_{k,i} \leq \sigma_i/\sqrt{n_k}$.

We now substitute these results and our learning rate and mini-batch settings into the expected improvement:

$$\begin{aligned}\mathbb{E}[f_{k+1} - f_k | x_k] &\leq -\delta_k \|g_k\|_1 + 2\frac{\delta_k}{\sqrt{n_k}}\|\vec{\sigma}\|_1 + \frac{\delta_k^2}{2}\|\vec{L}\|_1 \\ &= -\frac{1}{\sqrt{\|\vec{L}\|_1 K}}\|g_k\|_1 + \frac{2}{\sqrt{\|\vec{L}\|_1 K}}\|\vec{\sigma}\|_1 + \frac{1}{2K}\end{aligned}$$

Now extend the expectation over randomness in the trajectory, and perform a telescoping sum over the iterations:

$$\begin{aligned}f_0 - f^* &\geq f_0 - \mathbb{E}[f_K] \\ &= \mathbb{E}\left[\sum_{k=0}^{K-1} f_k - f_{k+1}\right] \\ &\geq \mathbb{E}\sum_{k=0}^{K-1}\left[\frac{1}{\sqrt{\|\vec{L}\|_1 K}}\|g_k\|_1 - \frac{1}{2\sqrt{\|\vec{L}\|_1 K}}\left(4\|\sigma\|_1 + \sqrt{\|\vec{L}\|_1}\right)\right] \\ &= \sqrt{\frac{K}{\|\vec{L}\|_1}}\mathbb{E}\left[\frac{1}{K}\sum_{k=0}^{K-1}\|g_k\|_1\right] - \frac{1}{2\sqrt{\|\vec{L}\|_1}}\left(4\|\vec{\sigma}\|_1 + \sqrt{\|\vec{L}\|_1}\right)\end{aligned}$$

We can rearrange this inequality to yield the rate:

$$\mathbb{E}\left[\frac{1}{K}\sum_{k=0}^{K-1}\|g_k\|_1\right] \leq \frac{1}{\sqrt{K}}\left[\sqrt{\|\vec{L}\|_1}\left(f_0 - f_* + \frac{1}{2}\right) + 2\|\vec{\sigma}\|_1\right]$$

Since we are growing our mini-batch size, it will take $N = O(K^2)$ gradient calls to reach step K. Substitute this in, square the result, and we are done. □

C. Large and small batch SGD

Algorithm C.1 SGD

Input: learning rate δ, current point x_k
$\tilde{g}_k \leftarrow \text{stochasticGradient}(x_k)$
$x_{k+1} \leftarrow x_k - \delta\,\tilde{g}_k$

For comparison with SIGNSGD theory, here we present non-convex convergence rates for SGD. These are classical results and we are not sure of the earliest reference.

We noticeably get exactly the same rate for large and small batch SGD when measuring convergence in terms of number of stochastic gradient calls. Although the rates are the same for a given number of gradient calls N, the large batch setting is preferred (in theory) since it achieves these N gradient calls in only $\sqrt{N}$ iterations, whereas the small batch setting requires N iterations. Fewer iterations in the large batch case implies a smaller wall-clock time to reach a given accuracy (assuming the large batch can be parallelised) as well as fewer rounds of communication in the distributed setting. These systems benefits of large batch learning have been observed by practitioners (Goyal et al., 2017).

Theorem C.1 (Non-convex convergence rate of SGD)**.** *Run algorithm C.1 for K iterations under Assumptions 1 to 3. Define $L := \|L\|_\infty$ and $\sigma^2 := \|\vec{\sigma}\|_2^2$. Set the learning rate and mini-batch size (independently of step k) as either*

$$\textit{(large batch)} \qquad \delta_k = \frac{1}{L} \qquad\qquad n_k = K$$

$$\textit{(small batch)} \qquad \delta_k = \frac{1}{L\sqrt{K}} \qquad\qquad n_k = 1$$

Let N be the cumulative number of stochastic gradient calls up to step K, i.e. $N = O(K^2)$ for large batch and $N = O(K)$ for small batch. Then, in either case, we have

$$\mathbb{E}\left[\frac{1}{K}\sum_{k=0}^{K-1}\|g_k\|_2^2\right] \leq \frac{1}{\sqrt{N}}\left[2L(f_0 - f_*) + \sigma^2\right]$$

Proof. The proof begins the same for the large and small batch case.

First we bound the improvement of the objective during a single step of the algorithm for one instantiation of the noise. g_k denotes the true gradient at step k and $\tilde{g}_k$ is a stochastic sample obeying Assumption 3.

Take Assumption 2 and plug in the algorithmic step.

$$\begin{aligned} f_{k+1} - f_k &\leq g_k^T(x_{k+1} - x_k) + \sum_{i=1}^{d}\frac{L_i}{2}(x_{k+1} - x_k)_i^2 \\ &\leq g_k^T(x_{k+1} - x_k) + \frac{\|L\|_\infty}{2}\|x_{k+1} - x_k\|_2^2 \\ &= -\delta_k g_k^T\tilde{g}_k + \delta_k^2\frac{L}{2}\|\tilde{g}_k\|_2^2 \end{aligned}$$

Next we find the expected improvement at time $k+1$ conditioned on the previous iterate.

$$\mathbb{E}[f_{k+1} - f_k | x_k] \leq -\delta_k\|g_k\|_2^2 + \delta_k^2\frac{L}{2}\left(\sigma_k^2 + \|g_k\|_2^2\right).$$

σ_k^2 refers to the variance of the k^{th} stochastic gradient estimate, computed over a mini-batch of size n_k. Therefore, by Assumption 3, we have that $\sigma_k^2 \leq \sigma^2/n_k$.

First let's substitute in the **(large batch)** hyperparameters.

$$\begin{aligned} \mathbb{E}[f_{k+1} - f_k | x_k] &\leq -\frac{1}{L}\|g_k\|_2^2 + \frac{1}{2L}\left(\frac{\sigma^2}{K} + \|g_k\|_2^2\right) \\ &= -\frac{1}{2L}\|g_k\|_2^2 + \frac{1}{2L}\frac{\sigma^2}{K}. \end{aligned}$$

Now extend the expectation over randomness in the trajectory, and perform a telescoping sum over the iterations:

$$\begin{aligned} f_0 - f^* &\geq f_0 - \mathbb{E}[f_K] \\ &= \mathbb{E}\left[\sum_{k=0}^{K-1} f_k - f_{k+1}\right] \\ &\geq \frac{1}{2L}\mathbb{E}\sum_{k=0}^{K-1}\left[\|g_k\|_2^2 - \sigma^2\right] \end{aligned}$$

We can rearrange this inequality to yield the rate:

$$\mathbb{E}\left[\frac{1}{K}\sum_{k=0}^{K-1}\|g_k\|_2^2\right] \leq \frac{1}{K}\left[2L(f_0 - f_*) + \sigma^2\right].$$

Since we are growing our mini-batch size, it will take $N = O(K^2)$ gradient calls to reach step K. Substitute this in and we are done for the **(large batch)** case.

Now we need to show that the same result holds for the **(small batch)** case. Following the initial steps of the large batch proof, we get

$$\mathbb{E}[f_{k+1} - f_k | x_k] \leq -\delta_k \|g_k\|_2^2 + \delta_k^2 \frac{L}{2}\left(\sigma_k^2 + \|g_k\|_2^2\right).$$

This time $\sigma_k^2 = \sigma^2$. Substituting this and our learning rate and mini-batch settings into the expected improvement:

$$\begin{aligned}\mathbb{E}[f_{k+1} - f_k | x_k] &\leq -\frac{1}{L\sqrt{K}}\|g_k\|_2^2 + \frac{1}{2LK}\left(\sigma^2 + \|g_k\|_2^2\right) \\ &\leq -\frac{1}{2L\sqrt{K}}\|g_k\|_2^2 + \frac{1}{2L}\frac{\sigma^2}{K}.\end{aligned}$$

Now extend the expectation over randomness in the trajectory, and perform a telescoping sum over the iterations:

$$\begin{aligned}f_0 - f^* &\geq f_0 - \mathbb{E}[f_K] \\ &= \mathbb{E}\left[\sum_{k=0}^{K-1} f_k - f_{k+1}\right] \\ &\geq \frac{1}{2L}\mathbb{E}\sum_{k=0}^{K-1}\left[\frac{\|g_k\|_2^2}{\sqrt{K}} - \frac{\sigma^2}{K}\right].\end{aligned}$$

We can rearrange this inequality to yield the rate:

$$\mathbb{E}\left[\frac{1}{K}\sum_{k=0}^{K-1}\|g_k\|_2^2\right] \leq \frac{1}{\sqrt{K}}\left[2L(f_0 - f_*) + \sigma^2\right]$$

It will take $N = O(K)$ gradient calls to reach step K. Substitute this in and we are done. □

D. Proving the convergence rate of distributed SIGNSGD with majority vote

Theorem 2 (Non-convex convergence rate of distributed SIGNSGD with majority vote)**.** *Run algorithm 3 for K iterations under Assumptions 1 to 3. Set the learning rate and mini-batch size for each worker (independently of step k) as*

$$\delta_k = \frac{1}{\sqrt{\|\vec{L}\|_1 K}} \qquad n_k = K$$

*Then **(a)** majority vote with M workers converges at least as fast as* SIGNSGD *in Theorem 1.*

*And **(b)** further assuming that the noise in each component of the stochastic gradient is unimodal and symmetric about the mean (e.g. Gaussian), majority vote converges at improved rate:*

$$\begin{aligned}&\mathbb{E}\left[\frac{1}{K}\sum_{k=0}^{K-1}\|g_k\|_1\right]^2 \\ &\quad\leq \frac{1}{\sqrt{N}}\left[\sqrt{\|\vec{L}\|_1}\left(f_0 - f_* + \frac{1}{2}\right) + \frac{2}{\sqrt{M}}\|\vec{\sigma}\|_1\right]^2\end{aligned}$$

where N is the cumulative number of stochastic gradient calls per worker up to step K.

Before we introduce the unimodal symmetric assumption, let's first address the claim that M-worker majority vote is at least as good as single-worker SIGNSGD as in Theorem 1 only using Assumptions 1 to 3.

Proof of (a). Recall that a crucial step in Theorem 1 is showing that

$$|g_i|\,\mathbb{P}[\text{sign}(\tilde{g}_i) \neq \text{sign}(g_i)] \leq \sigma_i$$

for component i of the stochastic gradient with variance bound σ_i.

The only difference in majority vote is that instead of using $\text{sign}(\tilde{g}_i)$ to approximate $\text{sign}(g_i)$, we are instead using $\text{sign}\left[\sum_{m=1}^{M} \text{sign}(\tilde{g}_{m,i})\right]$. If we can show that the same bound in terms of σ_i holds instead for

$$|g_i|\,\mathbb{P}\left[\text{sign}\left[\sum_{m=1}^{M} \text{sign}(\tilde{g}_{m,i})\right] \neq \text{sign}(g_i)\right] \qquad (\star)$$

then we are done, since the machinery of Theorem 1 can then be directly applied.

Define the signal-to-noise ratio of a component of the stochastic gradient as $S := |g_i|/\sigma_i$. Note that when $S \leq 1$ then $(\star)$ is trivially satisfied, so we need only consider the case that $S > 1$. S should really be labeled S_i but we abuse notation.

Without loss of generality, assume that g_i is negative, and thus using Assumption 3 and Cantelli's inequality (Cantelli, 1928) we get that for the failure probability q of a single worker

$$q := \mathbb{P}[\text{sign}(\tilde{g}_i) \neq \text{sign}(g_i)] = \mathbb{P}[\tilde{g}_i - g_i \geq |g_i|] \leq \frac{1}{1 + \frac{g_i^2}{\sigma_i^2}}$$

For $S > 1$ then we have failure probability $q < \frac{1}{2}$. If the failure probability of a single worker is smaller than $\frac{1}{2}$ then the server is essentially receiving a repetition code R_M of the true gradient sign. Majority vote is the maximum likelihood decoder of the repetition code, and of course decreases the probability of error—see e.g. (MacKay, 2002). Therefore in all regimes of S we have that

$$(\star) \leq |g_i|\,\mathbb{P}[\text{sign}(\tilde{g}_i) \neq \text{sign}(g_i)] \leq \sigma_i$$

and we are done. □

That's all well and good, but what we'd really like to show is that using M workers provides a speedup by reducing the variance. Is

$$(\star) \overset{?}{\leq} \frac{\sigma_i}{\sqrt{M}} \qquad (\dagger)$$

too much to hope for?

Well in the regime where $S \gg 1$ such a speedup is very reasonable since $q \ll \frac{1}{2}$ by Cantelli, and the repetition code actually supplies exponential reduction in failure rate. But we need to exclude very skewed or bimodal distributions where $q > \frac{1}{2}$ and adding more voting workers will not help. That brings us naturally to the following lemma:

Lemma D.1 (Failure probability of a sign bit under conditions of unimodal symmetric gradient noise)**.** *Let $\tilde{g}_i$ be an unbiased stochastic approximation to gradient component g_i, with variance bounded by σ_i^2. Further assume that the noise distribution is unimodal and symmetric. Define signal-to-noise ratio $S := \frac{|g_i|}{\sigma_i}$. Then we have that*

$$\mathbb{P}[\textit{sign}(\tilde{g}_i) \neq \textit{sign}(g_i)] \leq \begin{cases} \frac{2}{9}\frac{1}{S^2} & \textit{if } S > \frac{2}{\sqrt{3}}, \\ \frac{1}{2} - \frac{S}{2\sqrt{3}} & \textit{otherwise} \end{cases}$$

which is in all cases less than $\frac{1}{2}$.

Proof. Recall Gauss' inequality for unimodal random variable X with mode ν and expected squared deviation from the mode τ^2 (Gauss, 1823; Pukelsheim, 1994):

$$\mathbb{P}[|X-\nu|>k] \leq \begin{cases} \frac{4}{9}\frac{\tau^2}{k^2} & \text{if } \frac{k}{\tau} > \frac{2}{\sqrt{3}}, \\ 1-\frac{k}{\sqrt{3}\tau} & \text{otherwise} \end{cases}$$

By the symmetry assumption, the mode is equal to the mean, so we replace mean $\mu=\nu$ and variance $\sigma^2=\tau^2$.

$$\mathbb{P}[|X-\mu|>k] \leq \begin{cases} \frac{4}{9}\frac{\sigma^2}{k^2} & \text{if } \frac{k}{\sigma} > \frac{2}{\sqrt{3}}, \\ 1-\frac{k}{\sqrt{3}\sigma} & \text{otherwise} \end{cases}$$

Without loss of generality assume that g_i is negative. Then applying symmetry followed by Gauss, the failure probability for the sign bit satisfies:

$$\begin{aligned} \mathbb{P}[\text{sign}(\tilde{g}_i) \neq \text{sign}(g_i)] &= \mathbb{P}[\tilde{g}_i - g_i \geq |g_i|] \\ &= \frac{1}{2}\mathbb{P}[|\tilde{g}_i - g_i| \geq |g_i|] \\ &\leq \begin{cases} \frac{2}{9}\frac{\sigma_i^2}{g_i^2} & \text{if } \frac{|g_i|}{\sigma} > \frac{2}{\sqrt{3}}, \\ \frac{1}{2}-\frac{|g_i|}{2\sqrt{3}\sigma_i} & \text{otherwise} \end{cases} \\ &= \begin{cases} \frac{2}{9}\frac{1}{S^2} & \text{if } S > \frac{2}{\sqrt{3}}, \\ \frac{1}{2}-\frac{S}{2\sqrt{3}} & \text{otherwise} \end{cases} \end{aligned}$$

□

We now have everything we need to prove part (b) of Theorem 2.

Proof of (b). If we can show (†) we'll be done, since the machinery of Theorem 1 follows through with σ replaced everywhere by $\frac{\sigma}{\sqrt{M}}$. Note that the important quantity appearing in ($\star$) is

$$\sum_{m=1}^{M} \text{sign}(\tilde{g}_{m,i}).$$

Let Z count the number of workers with correct sign bit. To ensure that

$$\text{sign}\left[\sum_{m=1}^{M} \text{sign}(\tilde{g}_{m,i})\right] = \text{sign}(g_i)$$

Z must be larger than $\frac{M}{2}$. But Z is the sum of M independent Bernoulli trials, and is therefore binomial with success probability p and failure probability q to be determined. Therefore we have reduced proving (†) to showing that

$$\mathbb{P}\left[Z \leq \frac{M}{2}\right] \leq \frac{1}{\sqrt{M}S} \tag{§}$$

where Z is the number of successes of a binomial random variable $b(M,p)$ and S is our signal-to-noise ratio $S := \frac{|g_i|}{\sigma_i}$.

Let's start by getting a bound on the success probability p (or equivalently failure probability q) of a single Bernoulli trial.

By Lemma D.1, which critically relies on unimodal symmetric gradient noise, the failure probability for the sign bit of a single worker satisfies:

$$\begin{aligned} q &:= \mathbb{P}[\text{sign}(\tilde{g}_i) \neq \text{sign}(g_i)] \\ &\leq \begin{cases} \frac{2}{9}\frac{1}{S^2} & \text{if } S > \frac{2}{\sqrt{3}}, \\ \frac{1}{2}-\frac{S}{2\sqrt{3}} & \text{otherwise} \end{cases} \\ &:= \tilde{q}(S) \end{aligned}$$

Where we have defined $\tilde{q}(S)$ to be our S-dependent bound on q. Since $q \leq \tilde{q}(S) < \frac{1}{2}$, there is hope to show $(\dagger)$. Define ϵ to be the defect of q from one half, and let $\tilde{\epsilon}(S)$ be its S-dependent bound.

$$\epsilon := \frac{1}{2} - q = p - \frac{1}{2} \geq \frac{1}{2} - \tilde{q}(S) := \tilde{\epsilon}(S)$$

Now we have an analytical handle on random variable Z, we may proceed to show $(\S)$. There are a number of different inequalities that we can use to bound the tail of a binomial random variable, but Cantelli's inequality will be good enough for our purposes.

Let $\bar{Z} := M - Z$ denote the number of failures. $\bar{Z}$ is binomial with mean $\mu_{\bar{Z}} = Mq$ and variance $\sigma^2_{\bar{Z}} = Mpq$. Then using Cantelli we get

$$\begin{aligned}
\mathbb{P}\left[Z \leq \frac{M}{2}\right] &= \mathbb{P}\left[\bar{Z} \geq \frac{M}{2}\right] \\
&= \mathbb{P}\left[\bar{Z} - \mu_{\bar{Z}} \geq \frac{M}{2} - \mu_{\bar{Z}}\right] \\
&= \mathbb{P}\left[\bar{Z} - \mu_{\bar{Z}} \geq M\epsilon\right] \\
&\leq \frac{1}{1 + \frac{M^2\epsilon^2}{Mpq}} \\
&\leq \frac{1}{1 + \frac{M}{\frac{1}{4\epsilon^2} - 1}}
\end{aligned}$$

Now using the fact that $\frac{1}{1+x^2} \leq \frac{1}{2x}$ we get

$$\mathbb{P}\left[Z \leq \frac{M}{2}\right] \leq \frac{\sqrt{\frac{1}{4\epsilon^2} - 1}}{2\sqrt{M}}$$

To finish, we need only show that $\sqrt{\frac{1}{4\epsilon^2} - 1}$ is smaller than $\frac{2}{S}$, or equivalently that its square is smaller than $\frac{4}{S^2}$. Well plugging in our bound on ϵ we get that

$$\frac{1}{4\epsilon^2} - 1 \leq \frac{1}{4\tilde{\epsilon}(S)^2} - 1$$

where

$$\tilde{\epsilon}(S) = \begin{cases} \frac{1}{2} - \frac{2}{9}\frac{1}{S^2} & \text{if } S > \frac{2}{\sqrt{3}}, \\ \frac{S}{2\sqrt{3}} & \text{otherwise} \end{cases}$$

First take the case $S \leq \frac{2}{\sqrt{3}}$. Then $\tilde{\epsilon}^2 = \frac{S^2}{12}$ and $\frac{1}{4\tilde{\epsilon}^2} - 1 = \frac{3}{S^2} - 1 < \frac{4}{S^2}$. Now take the case $S > \frac{2}{\sqrt{3}}$. Then $\tilde{\epsilon} = \frac{1}{2} - \frac{2}{9}\frac{1}{S^2}$ and we have $\frac{1}{4\tilde{\epsilon}^2} - 1 = \frac{1}{S^2}\frac{\frac{8}{9} - \frac{16}{81}\frac{1}{S^2}}{1 - \frac{8}{9}\frac{1}{S^2} + \frac{16}{81}\frac{1}{S^4}} < \frac{1}{S^2}\frac{\frac{8}{9}}{1 - \frac{8}{9}\frac{1}{S^2}} < \frac{4}{S^2}$ by the condition on S.

So we have shown both cases, which proves $(\S)$ from which we get $(\dagger)$ and we are done. □

E. General recipes for the convergence of approximate sign gradient methods

Now we generalize the arguments in the proof of SIGNSGD and prove a master lemma that provides a general recipe for analyzing the approximate sign gradient method. This allows us to handle momentum and the majority voting schemes, hence proving Theorem 3 and Theorem 2.

Lemma E.1 (Convergence rate for a class of approximate sign gradient method)**.** *Let C and K be integers satisfying $0 < C \ll K$. Consider the algorithm given by $x_{k+1} = x_k - \delta_k sign(v_k)$, for a fixed positive sequence of δ_k and where $v_k \in \mathbb{R}^d$ is a measurable and square integrable function of the entire history up to time k, including $x_1, ..., x_k, v_1, ..., v_{k-1}$*

and all N_k stochastic gradient oracle calls up to time k. Let $g_k = \nabla f(x_k)$. If Assumption 1 and Assumption 2 are true and in addition for $k = C, C+1, C+2, ..., K$

$$\mathbb{E}\left[\sum_{i=1}^{d} |g_{k,i}| \mathbb{P}[sign(v_{k,i}) \neq sign(g_{k,i})|x_k]\right] \leq \xi(k) \tag{2}$$

where the expectation is taken over the all random variables, and the rate $\xi(k)$ obeys that $\xi(k) \to 0$ as $k \to \infty$ and then we have

$$\frac{1}{K-C}\sum_{k=C}^{K-1}\mathbb{E}\|g_k\|_1 \leq \frac{f_C - f_* + 2\sum_{k=C}^{K-1}\delta_k\xi(k) + \sum_{k=C}^{K-1}\frac{\delta_k^2\|\vec{L}\|_1}{2}}{(K-C)\min_{C\leq k\leq K-1}\delta_k}.$$

In particular, if $\delta_k = \delta/\sqrt{k}$ and $\xi(k) = \kappa/\sqrt{k}$, for some problem dependent constant κ, then we have

$$\frac{1}{K-C}\sum_{k=C}^{K-1}\mathbb{E}\|g_k\|_1 \leq \frac{\frac{f_C - f_*}{\delta} + (2\kappa + \|\vec{L}\|_1\delta/2)(\log K + 1)}{\sqrt{K} - \frac{C}{\sqrt{K}}}.$$

Proof. Our general strategy will be to show that the expected objective improvement at each step will be good enough to guarantee a convergence rate in expectation. First let's bound the improvement of the objective during a single step of the algorithm for $k \geq C$, and then take expectation. Note that $\mathbb{I}[.]$ is the indicator function, and $w_k[i]$ denotes the i^{th} component of the vector w_k.

By Assumption 2

$$\begin{aligned}
f_{k+1} - f_k &\leq g_k^T(x_{k+1} - x_k) + \sum_{i=1}^{d}\frac{L_i}{2}(x_{k+1,i} - x_{k,i})^2 && \text{Assumption 2}\\
&= -\delta_k g_k^T \text{sign}(v_k) + \delta_k^2\frac{\|\vec{L}\|_1}{2} && \text{by the update rule}\\
&= -\delta_k\|g_k\|_1 + 2\delta_k\sum_{i=1}^{d}|g_k[i]|\,\mathbb{I}[\text{sign}(v_k[i]) \neq \text{sign}(g_k[i])] + \delta_k^2\frac{\|\vec{L}\|_1}{2} && \text{by identity}
\end{aligned}$$

Now, for $k \geq C$ we need to find the expected improvement at time $k+1$ conditioned on x_k, where the expectation is over the randomness of the stochastic gradient oracle. Note that $\mathbb{P}[E]$ denotes the probability of event E.

$$\mathbb{E}[f_{k+1} - f_k|x_k] \leq -\delta_k\|g_k\|_1 + 2\delta_k\sum_{i=1}^{d}|g_k[i]|\,\mathbb{P}\Big[\text{sign}(v_k[i]) \neq \text{sign}(g_k[i])\Big|x_k\Big] + \delta_k^2\frac{\|\vec{L}\|_1}{2}.$$

Note that g_k becomes fixed when we condition on x_k. Further take expectation over x_k, and apply (2). We get:

$$\mathbb{E}[f_{k+1} - f_k] \leq -\delta_k\mathbb{E}[\|g_k\|_1] + 2\delta_k\xi(k) + \frac{\delta_k^2\|\vec{L}\|_1}{2}. \tag{3}$$

Rearrange the terms and sum over (3) for $k = C, C+1, ..., K-1$.

$$\sum_{k=C}^{K-1}\delta_k\mathbb{E}[\|g_k\|_1] \leq \sum_{k=C}^{K-1}(\mathbb{E}f_k - \mathbb{E}f_{k+1}) + 2\sum_{k=C}^{K-1}\delta_k\xi(k) + \sum_{k=C}^{K-1}\frac{\delta_k^2\|\vec{L}\|_1}{2}$$

Dividing both sides by $\left[(K-C)\min_{C\leq k\leq K-1}\delta_k\right]$, using a telescoping sum over $\mathbb{E}f_k$ and using that $f(x) \geq f_*$ for all x, we get

$$\frac{1}{K-C}\sum_{k=C}^{K-1}\mathbb{E}\|g_k\|_1 \leq \frac{f_C - f_* + 2\sum_{k=C}^{K-1}\delta_k\xi(k) + \sum_{k=C}^{K-1}\frac{\delta_k^2\|\vec{L}\|_1}{2}}{(K-C)\min_{C\leq k\leq K-1}\delta_k}$$

and the proof is complete by noting that the minimum is smaller than the average in the LHS. □

To use the above Lemma for analyzing SIGNUM and the Majority Voting scheme, it suffices to check condition (2) for each algorithm.

One possible way to establish (2) is show that v_k is a good approximation of the gradient g_k in expected absolute value.

Lemma E.2 (Estimation to testing reduction)**.** *Equation* (2) *is true, if for every* k

$$\sum_{i=1}^{d} \mathbb{E}|v_k[i] - g_k[i]| \leq \xi(k). \tag{4}$$

Proof. First note that for any two random variables $a, b \in \mathbb{R}$.

$$\mathbb{P}\Big[\text{sign}(a) \neq \text{sign}(b)\Big] \leq \mathbb{P}\Big[|a-b| > |b|\Big].$$

Condition on x_k and apply the above inequality to every $i = 1, ..., d$ to what is inside the expectation of (2), we have

$$\sum_{i=1}^{d} |g_k[i]| \mathbb{P}\Big[\text{sign}(v_k[i]) \neq \text{sign}(g_k[i])\Big| x_k\Big] \leq \sum_{i=1}^{d} |g_k[i]| \mathbb{P}\Big[|v_k[i] - g_k[i]| > |g_k[i]|\Big| x_k\Big] \leq \sum_{i=1}^{d} \mathbb{E}[|v_k[i] - g_k[i]||x_k].$$

Note that the final $\leq$ uses Markov's inequality and constant $|g_k[i]|$ cancels out.

The proof is complete by taking expectation on both sides and apply (4). □

Note that the proof of this lemma uses Markov's inequality in the same way information-theoretical lower bounds are often proved in statistics — reducing estimation to testing.

Another handy feature of the result is that we do not require the approximation to hold for every possible x_k. It is okay that for some x_k, the approximation is much worse as long as those x_k appears with small probability according to the algorithm. This feature enables us to analyze momentum and hence proving the convergence for SIGNUM.

F. Analysis for SIGNUM

Recall our definition of the key random variables used in SIGNUM.

$$\begin{aligned} g_k &:= \nabla f(x_k) \\ \tilde{g}_k &:= \frac{1}{n_k} \sum_{j=1}^{n_k} \tilde{g}^{(j)}(x_k) \\ m_k &:= \frac{1-\beta}{1-\beta^{k+1}} \sum_{t=0}^{k} \big[\beta^t g_{k-t}\big] \\ \tilde{m}_k &:= \frac{1-\beta}{1-\beta^{k+1}} \sum_{t=0}^{k} \big[\beta^t \tilde{g}_{k-t}\big] \end{aligned}$$

SIGNUM effectively uses $v_k = \tilde{m}_k$ and also $\delta_k = O(1/\sqrt{k})$.

Before we prove the convergence of SIGNUM, we first prove a utility lemma about the random variable $Z_k := \tilde{g}_k - g_k$. Note that in this lemma quantities like Z_k, Y_k, $|Z_k|$ and Z_k^2 are considered vectors—so this lemma is a statement about each component of the vectors separately and all operations, such as $(\cdot)^2$ are pointwise operations.

Lemma F.1 (Cumulative error of stochastic gradient)**.** *For any* $k < \infty$ *and fixed weight* $-\infty < \alpha_1, ..., \alpha_k < \infty$, $\sum_{l=1}^{k} \alpha_l Z_l$ *is a Martingale. In particular,*

$$\mathbb{E}\left[\left(\sum_{l=1}^{k} \alpha_l Z_l\right)^2\right] \leq \sum_{l=1}^{k} \alpha_l^2 \vec{\sigma}^2.$$

Proof. We simply check the definition of a Martingale. Denote $Y_k := \sum_{l=1}^{k} \alpha_l Z_l$. First, we have that

$$\begin{aligned}
\mathbb{E}[|Y_k|] &= \mathbb{E}\left[\left|\sum_{l=1}^{k} \alpha_l Z_l\right|\right] \\
&\leq \sum_l |\alpha_l| \mathbb{E}[|Z_l|] && \text{triangle inequality} \\
&= \sum_l |\alpha_l| \mathbb{E}\Big[\mathbb{E}[|Z_l||x_l]\Big] && \text{law of total probability} \\
&\leq \sum_l |\alpha_l| \mathbb{E}\left[\sqrt{\mathbb{E}[Z_l^2|x_l]}\right] && \text{Jensen's inequality} \\
&\leq \sum_l |\alpha_l| \vec{\sigma} < \infty
\end{aligned}$$

Second, again using the law of total probability,

$$\begin{aligned}
\mathbb{E}[Y_{k+1}|Y_1, ..., Y_k] &= \mathbb{E}\left[\sum_{l=1}^{k+1} \alpha_l Z_l \middle| \alpha_1 Z_1, ..., \alpha_k Z_k\right] \\
&= Y_k + \alpha_{k+1} \mathbb{E}\left[Z_{k+1} | \alpha_1 Z_1, ..., \alpha_k Z_k\right] \\
&= Y_k + \alpha_{k+1} \mathbb{E}\left[\mathbb{E}\left[Z_{k+1} | x_{k+1}, \alpha_1 Z_1, ..., \alpha_k Z_k\right] | \alpha_1 Z_1, ..., \alpha_k Z_k\right] \\
&= Y_k + \alpha_{k+1} \mathbb{E}\left[\mathbb{E}\left[Z_{k+1} | x_{k+1}\right] | \alpha_1 Z_1, ..., \alpha_k Z_k\right] \\
&= Y_k
\end{aligned}$$

This completes the proof that it is indeed a Martingale. We now make use of the properties of Martingale difference sequences to establish a variance bound on the Martingale.

$$\begin{aligned}
\mathbb{E}\left[\left(\sum_{l=1}^{k} \alpha_l Z_l\right)^2\right] &= \sum_{l=1}^{k} \mathbb{E}[\alpha_l^2 Z_l^2] + 2 \sum_{l<j} \mathbb{E}[\alpha_l \alpha_j Z_l Z_j] \\
&= \sum_{l=1}^{k} \alpha_l^2 \mathbb{E}[\mathbb{E}[Z_l^2 | Z_1, ..., Z_{l-1}]] + 2 \sum_{l<j} \alpha_l \alpha_j \mathbb{E}\Big[Z_l \mathbb{E}\big[\mathbb{E}[Z_j | Z_1, ..., Z_{j-1}] \big| Z_l\big]\Big] \\
&= \sum_{l=1}^{k} \alpha_l^2 \mathbb{E}[\mathbb{E}[\mathbb{E}[Z_l^2 | x_l, Z_1, ..., Z_{l-1}] | Z_1, ..., Z_{l-1}]] + 0 \\
&= \sum_{l=1}^{k} \alpha_l^2 \vec{\sigma}^2.
\end{aligned}$$

□

The consequence of this lemma is that we are able to treat $Z_1, ..., Z_k$ as if they are independent, even though they are not—clearly Z_l is dependent on $Z_1, ..., Z_{l-1}$ through x_l.

Lemma F.2 (Gradient approximation in SIGNUM)**.** *The version of the* SIGNUM *algorithm that takes $v_k = \tilde{m}_k$, and all parameters according to Theorem 3, obeys that for all integer $C \leq k \leq K$*

$$\|\mathbb{E}|\tilde{m}_k - g_k|\|_1 \leq \frac{2}{\sqrt{k+1}} \left(8\|\vec{L}\|_1 \delta \frac{\beta}{1-\beta} + \sqrt{3}\|\vec{\sigma}\|_1 \sqrt{1-\beta}\right).$$

Proof. For each $i \in [d]$ we will use the following non-standard "bias-variance" decomposition.

$$\mathbb{E}\left[|\tilde{m}_k[i] - g_k[i]|\right] \leq \underbrace{\mathbb{E}\left[|m_k[i] - g_k[i]|\right]}_{(*)} + \underbrace{\mathbb{E}\left[|\tilde{m}_k[i] - m_k[i]|\right]}_{(**)} \tag{5}$$

We will first bound $(**)$ and then deal with $(*)$.

Note that $(**) = \frac{1-\beta}{1-\beta^{k+1}}\mathbb{E}\left[|\sum_{t=0}^{k}\beta^{k-t}Z_t|\right]$. Using Jensen's inequality and applying Lemma F.1 with our choice of $\alpha_1, ..., \alpha_l$ (including the effect of the increasing batch size) we get that for $k \geq C$

$$(**) \leq \frac{1-\beta}{1-\beta^{k+1}}\sqrt{\mathbb{E}\left[\left|\sum_{t=0}^{k}\beta^t Z_{k-t}\right|^2\right]} \leq \frac{1-\beta}{1-\beta^{k+1}}\sqrt{\sum_{t=0}^{k}\left[\beta^{2t}\frac{\vec{\sigma}^2}{k-t+1}\right]},$$

where

$$\begin{aligned}
\sum_{t=0}^{k}\left[\beta^{2t}\frac{\vec{\sigma}^2}{k-t+1}\right] &= \sum_{t=0}^{\frac{k}{2}}\left[\beta^{2t}\frac{\vec{\sigma}^2}{k-t+1}\right] + \sum_{t=\frac{k}{2}+1}^{k}\left[\beta^{2t}\frac{\vec{\sigma}^2}{k-t+1}\right] && \text{break up sum}\\
&\leq \sum_{t=0}^{\frac{k}{2}}\left[\beta^{2t}\right]\frac{\vec{\sigma}^2}{\frac{k}{2}+1} + \sum_{t=\frac{k}{2}+1}^{k}\left[\beta^{k}\vec{\sigma}^2\right] && \text{bound summands}\\
&\leq \frac{1}{1-\beta^2}\frac{\vec{\sigma}^2}{\frac{k}{2}+1} + \frac{k}{2}\beta^k\vec{\sigma}^2 && \text{geometric series}\\
&\leq \frac{3}{1-\beta^2}\frac{\vec{\sigma}^2}{k+1} && \text{since } k \geq C
\end{aligned}$$

Combining, and again using our condition that $k \geq C$, we get

$$(**) \leq \frac{1-\beta}{1-\beta^{k+1}}\sqrt{\frac{3}{1-\beta^2}}\frac{\vec{\sigma}}{\sqrt{k+1}} \leq 2\sqrt{3}\sqrt{1-\beta}\frac{\vec{\sigma}}{\sqrt{k+1}} \tag{6}$$

We now turn to bounding $(*)$ — the "bias" term.

$$\begin{aligned}
\mathbb{E}[|m_k - g_k|] &= \mathbb{E}\left[\left|\frac{1-\beta}{1-\beta^{k+1}}\sum_{t=0}^{k}\left[\beta^t g_{k-t}\right] - \frac{1-\beta}{1-\beta^{k+1}}\sum_{t=0}^{k}\left[\beta^t g_k\right]\right|\right] && \text{since } \frac{1-\beta}{1-\beta^{k+1}}\sum_{t=0}^{k}\beta^t = 1\\
&\leq \frac{1-\beta}{1-\beta^{k+1}}\sum_{t=0}^{k}\left[\beta^t\mathbb{E}[|g_{k-t} - g_k|]\right]\\
&\leq 2(1-\beta)\sum_{t=1}^{k}\beta^t\mathbb{E}[|g_{k-t} - g_k|] && \text{since } k \geq C \qquad (7)
\end{aligned}$$

To proceed, we need the following lemma.

Lemma F.3. *Under Assumption 2, for any sign vector $s \in \{-1, 1\}^d$, any $x \in \mathbb{R}^d$ and any $\epsilon \leq \delta$*

$$\|g(x + \epsilon s) - g(x)\|_1 \leq 2\epsilon\|\vec{L}\|_1.$$

Proof. By Taylor's theorem,

$$g(x + \epsilon s) - g(x) = \left[\int_{t=0}^{1} H(x + t\epsilon s)dt\right]\epsilon s.$$

Let $v := \text{sign}(g(x + \epsilon s) - g(x))$, $H := \left[\int_{t=0}^{1} H(x + t\epsilon s)dt\right]$ and moreover, use H_+ to denote the psd part of H and H_- to denote the nsd part of H. Namely, $H = H_+ - H_-$.

We can write

$$\begin{aligned}
\|g(x + \epsilon s) - g(x)\|_1 &= v^T(g(x + \epsilon s) - g(x)) = v^T H(\epsilon s) = \epsilon v^T H_+ s - \epsilon v^T H_- s\\
&= \epsilon\langle H_+^{1/2}v, H_+^{1/2}s\rangle - \epsilon\langle H_-^{1/2}v, H_-^{1/2}s\rangle \leq \epsilon\|H_+^{1/2}v\|\|H_+^{1/2}s\| + \epsilon\|H_-^{1/2}v\|\|H_-^{1/2}s\|. \qquad (8)
\end{aligned}$$

Note that assumption 2 implies the semidefinite ordering

$$H_+ \prec \operatorname{diag}(\vec{L}) \text{ and } H_- \prec \operatorname{diag}(\vec{L})$$

and thus $\max\{s^T H_+ s, s^T H_- s\} \leq \sum_{i=1}^d L_i = \|\vec{L}\|_1$ for all $s \in \{-1,1\}^d$.

The proof is complete by observing that both v and s are sign vectors in (8). □

Using the above lemma and the fact that our update rules are always following some sign vectors with learning rate smaller than δ, we have

$$\begin{aligned}
\|g_{k-t} - g_k\|_1 &\leq \sum_{l=0}^{t-1} \|g_{k-l} - g_{k-l-1}\|_1 \\
&\leq 2\|\vec{L}\|_1 \sum_{l=0}^{t-1} \delta_{k-l-1} \leq \sum_{l=0}^{t-1} \frac{2\|\vec{L}\|_1 \delta}{\sqrt{k-l}} \\
&\leq 2\|\vec{L}\|_1 \delta \int_{k-t}^{k} \frac{dx}{\sqrt{x}} = 4\|\vec{L}\|_1 \delta \Big(\sqrt{k} - \sqrt{k-t}\Big) \\
&\leq 4\|\vec{L}\|_1 \delta \sqrt{k} \left(1 - \sqrt{1 - \frac{t}{k}}\right) \\
&\leq 4\|\vec{L}\|_1 \delta \frac{t}{\sqrt{k}} && \text{for } x \geq 0, 1 - x \leq \sqrt{1-x} \qquad (9)
\end{aligned}$$

It follows that

$$\begin{aligned}
\sum_i \mathbb{E}[|m_k[i] - g_k[i]|] &= \mathbb{E}\left[\|m_k - g_k\|_1\right] \\
&\leq 2(1-\beta) \sum_{t=1}^{k} \beta^t \mathbb{E}\|g_{k-t} - g_k\|_1 && \text{Apply (7)} \\
&\leq \frac{8(1-\beta)\|\vec{L}\|_1 \delta}{\sqrt{k}} \sum_{t=1}^{\infty} t\beta^t && \text{Apply (9) and extend sum to } \infty \\
&\leq \frac{8(1-\beta)\|\vec{L}\|_1 \delta}{\sqrt{k}} \frac{\beta}{(1-\beta)^2} && \text{derivative of geometric progression} \\
&\leq \frac{16\|\vec{L}\|_1 \delta}{\sqrt{k+1}} \frac{\beta}{1-\beta} && \text{for } k \geq 1, \sqrt{\frac{k+1}{k}} \leq 2 \qquad (10)
\end{aligned}$$

Substitute (6) into (5), sum both sides over i and then further plug in (10) we get the statement in the lemma. □

The proof of Theorem 3 now follows in a straightforward manner. Note that Lemma F.2 only kicks in after a warmup period of C iterations, with C as specified in Theorem 3. In theory it does not matter what you do during this warmup period, provided you accumulate the momentum as normal and take steps according to the prescribed learning rate and mini-batch schedules. One option is to just stay put and not update the parameter vector for the first C iterations. This is wasteful since no progress will be made on the objective. A better option in practice is to take steps using the sign of the stochastic gradient (i.e. do SIGNSGD) instead of SIGNUM during the warmup period.

Proof of Theorem 3. Substitute Lemma F.2 as $\xi(k)$ into Lemma E.1 and check that $\xi(k) = O(1/\sqrt{k}), \delta_k = O(1/\sqrt{k}), \min \delta_k = \delta/\sqrt{K}, C \ll K$, and in addition, we note that by the increasing minibatch size $N_K = O(K^2)$. Substitute $K = O(\sqrt{N})$ and take the square on both sides of the inequality. (We can take the $\min_k$ out of the square since all the arguments are nonnegative and $(\cdot)^2$ is monotonic on $\mathbb{R}_+$). □

Figure 9: Zero-shot image-text retrieval results on MSCOCO (**Top**) and Flickr30K (**Bottom**) for LiT-B/16-B. Recall@K is calculated based on if the ground truth label of the query appears in the top-K retrieved examples.

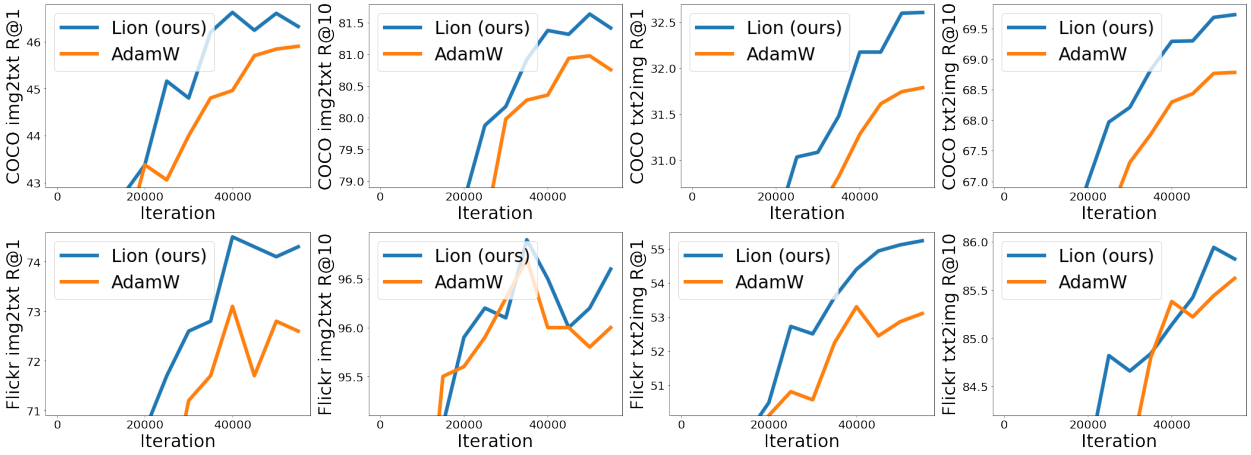

- NLG: TriviaQA (Joshi et al., 2017), Natural Questions (Kwiatkowski et al., 2019), Web Questions (Berant et al., 2013).
- NLU: HellaSwag (Zellers et al., 2019), StoryCloze (Mostafazadeh et al., 2016), Winograd (Levesque et al., 2012), Winogrande (Sakaguchi et al., 2020), RACE (Lai et al., 2017), PIQA (Bisk et al., 2020), ARC (Clark et al., 2018), OpenbookQA (Mihaylov et al., 2018), BoolQ (Clark et al., 2019), Copa (Gordon et al., 2012), RTE (Dagan et al., 2006), WiC (Pilehvar and Camacho-Collados, 2019), Multirc (Khashabi et al., 2018), WSC (Levesque et al., 2012), ReCoRD (Zhang et al., 2018), CB (de Marneffe et al., 2019), Adversarial NLI (Nie et al., 2020).

Program 5: Algorithm with a better regularization. It dynamically calculates the dot product between the weight and gradient, before computing the weight decay.

```
def train(w, g, m, v, lr):
  m = interp(m, g, 0.16)
  g2 = square(g)
  v = interpolate(v, g2, 0.001)
  v753 = dot(g, w)
  sqrt_v = sqrt(v)
  update = m / sqrt_v
  wd = v753 * w
  update = sin(update)
  update = update + wd
  lr = lr * 0.0216
  update = update * lr
  v = sin(v)
  return update, m, v
```

Program 6: Algorithm that tracks the second moment without EMA decay, which is the same as AdaGrad.

```
def train(w, g, m, v, lr):
  m = interp(m, g, 0.1)
  g2 = square(g)
  g2 = v + g2
  v = interp(v, g2, 0.0015)
  sqrt_v = sqrt(v)
  update = m / sqrt_v
  v70 = get_pi()
  v = min(v, v70)
  update = sinh(update)
  lr = lr * 0.0606
  update = update * lr
  return update, m, v
```

Program 7: Algorithm uses the difference between gradient and momentum to track the second moment, resembling AdaBelief.

```
def train(w, g, m, v, lr):
  m = interp(m, g, 0.1)
  g = g - m
  g2 = square(g)
  v = interp(v, g2, 0.001)
  sqrt_v = sqrt(v)
  update = m / sqrt_v
  wd = w * 0.0238
  update = update + wd
  lr = lr * 0.03721
  update = update * lr
  return update, m, v
```

Table 9: Architecture details for language modeling.

Model	#Params	n_{layers}	d_{model}	n_{heads}	d_{head}
Small-scale					
Small	110M	12	768	12	64
Medium	336M	24	1024	16	64
Large	731M	24	1536	16	96
Large-scale					
1.1B	1.07B	24	1536	16	96
2.1B	2.14B	32	2048	16	128
7.5B	7.49B	32	4096	32	128

Table 10: Training error L_{train} and landscape flatness $L^{\mathcal{N}}_{train}$ of ViT-B/16 trained from scratch on ImageNet.

Optimizer	AdamW	Lion
ImageNet	75.48	77.44
ReaL	80.64	82.57
V2	61.87	64.81
L_{train}	0.61	0.75
$L^{\mathcal{N}}_{train}$	3.74	1.37

Figure 10: Learning curve of ViT-S/16 (**Left**) and ViT-B/16 (**Right**) associated with Table 7. The curves of the five adaptive optimizers are similar to each other.

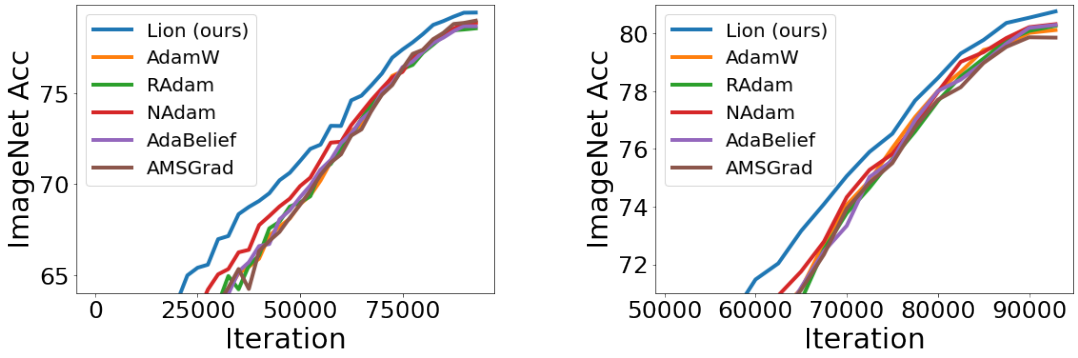

D Other Discovered Programs

By varying the task setting, different types of algorithms can be discovered. For example, if we reduce the amount of data in the proxy task, we are more likely to discover algorithms with better regularization (Program 5), and if we reduce the search progress, we are likely to find simple variants of AdamW (Program 6 and 7). Future work can explore this potential to discover optimizers specialized for different tasks.

E Architecture Details for Language Modeling

Table 9 shows the Transformer architecture details for language modeling (Section 4.4). The dimension of the feed-forward layer is $4 \times d_{model}$. We use vocabulary size 32K for small-scale and 256K for large-scale models.

F Details of Proxy Tasks

For vision tasks, we train a ViT with three layers, 96 hidden units and three heads, on 10% ImageNet for 30k steps with batch size 64. The image size is 64×64 and the patch size is 16. For language tasks, we train a Transformer with two layers, 128 hidden units and two heads on LM1B (Chelba et al., 2013) for 20K steps with batch size 64, sequence length 32 and vocabulary size 3K. The evaluation time may vary for different programs, but typically a evaluation can be done on one TPU V2 chip within 20min. The validation accuracy or perplexity is used as the fitness.

Figure 11: **Left**: Validation perplexity when we perform masked language modeling on the C4 dataset. **Right**: Training loss of ViT-B/16 on ImageNet.

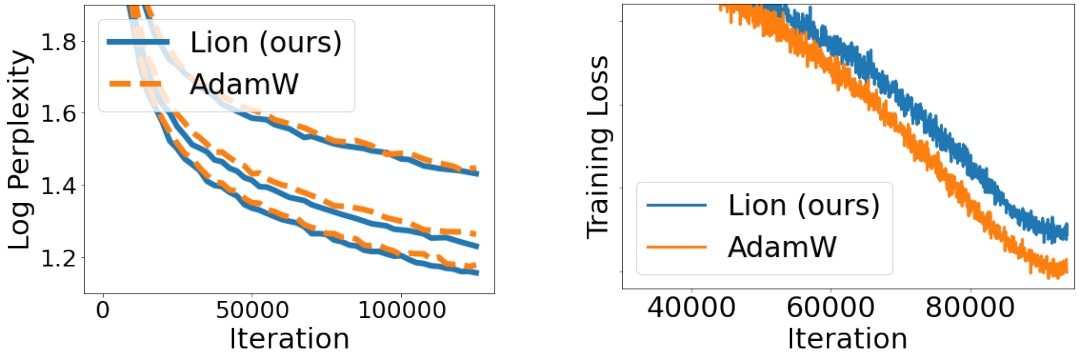

G Analysis of Loss Landscape

In this section, we try to understand why our Lion optimizer achieves better generalization than AdamW from the lens of loss geometry. The convergence to a smooth landscape has been shown to benefit the generalization of deep neural networks (Chen and Hsieh, 2020; Chen et al., 2022; Foret et al., 2021; Keskar et al., 2017). Following Chen et al. (2022), we measure the landscape flatness at convergence by $L_{train}^{\mathcal{N}} = \mathbb{E}_{\epsilon\sim\mathcal{N}}[L_{train}(w+\epsilon)]$ (average over 1K random noises) in Table 10. We observe that the ViT-B/16 trained by AdamW enjoys a smaller training error L_{train}. However, Lion can enable ViT to converge to flatter regions, as it helps the model retain comparably lower error against Gaussian perturbations.

H Available Functions

We include 43 available functions that can be used in the program during search. Note that the input of the functions can be one n-dimensional array, dictionaries or lists of arrays, similar to the *pytrees* in JAX.

Basic math functions from NumPy / JAX This includes unary functions like `abs`, `cos`, `sin`, `tan`, `arcsin`, `arccos`, `arctan`, `exp`, `log`, `sinh`, `cosh`, `tanh`, `arcsinh`, `arccosh`, `arctanh`, `sign`, `exp2`, `exp10`, `expm1`, `log10`, `log2`, `log1p`, `square`, `sqrt`, `cube`, `cbrt`, `sign`, `reciprocal` and binary functions like `+`, `-`, `*`, `/`, `power`, `maximum`, `minimum` with the same semantic as the corresponding function in NumPy / JAX.

Linear algebra functions commonly used in first-order optimization algorithms This includes: (1) unary function `norm` that computes the norm of each arrays in the input; (2) unary function `global_norm` that computes the global norm by treating all the numbers in the input as one vector; (3) binary function `dot` that treats the two inputs as two vectors and computes their dot product; (4) binary function `cosine_sim` that treats the two inputs as two vectors and computes their cosine similarity; (5) binary `clip_by_global_norm` (`clip`) that clips the global norm of the first input to the value of the second input that is required to be a scalar; (6) ternary function `interpolate` (`interp`) that uses the third argument `a`, required to be a scalar, to compute a linear inter-

Program 8: Raw program of Lion before removing redundent statements.

```
def train(w, g, m, v, lr):
  g = clip(g, lr)
  m = clip(m, lr)
  v845 = sqrt(0.6270633339881897)
  v968 = sign(v)
  v968 = v - v
  g = arcsin(g)
  m = interp(g, v, 0.8999999761581421)
  v1 = m * m
  v = interp(g, m, 1.109133005142212)
  v845 = tanh(v845)
  lr = lr * 0.0002171761734643951
  update = m * lr
  v1 = sqrt(v1)
  update = update / v1
  wd = lr * 0.4601978361606598
  v1 = square(v1)
  wd = wd * w
  m = cosh(update)
  lr = tan(1.4572199583053589)
  update = update + wd
  lr = cos(v845)
  return update, m, v
```

Figure 12: Log perplexity of the small (**Left**), medium (**Middle**), and large (**Right**) size Transformer on PG-19. Since $\beta_1 = 0.95, \beta_2 = 0.98$ in Lion when performing language modeling, we compare to Ablation$_{0.95}$ and Ablation$_{0.98}$ with $\beta = 0.95$ and $\beta = 0.98$, respectively (see Section 4.6 for the definition). Lion is still the best-performing one.

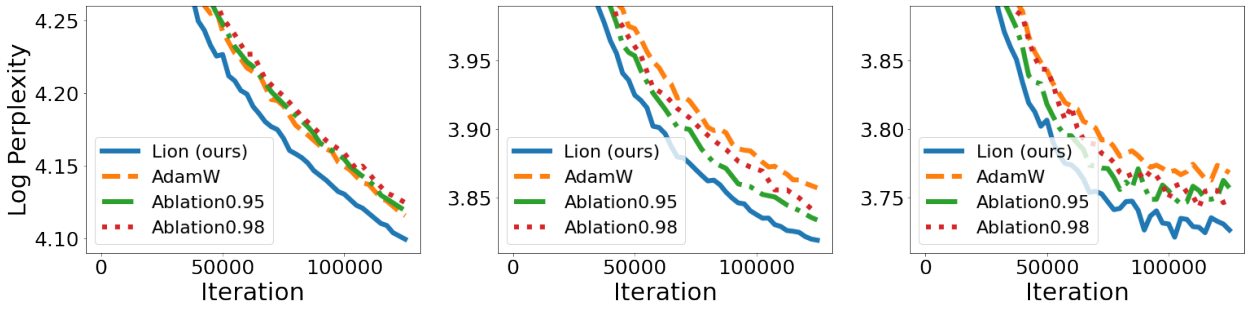

polation of the first two arguments `x` and `y` with `(1 - a) * x + a * y`.

Functions producing commonly used constants This includes `get_pi`, `get_e`, `get_eps` that generates π, e and $\epsilon = 10^{-8}$ respectively.

I Abstract Execution

We propose to prune the large search space with abstract execution. Our approach is motivated by the fact that a large number of programs are invalid, functionally equivalent, or contain redundant statements that waste compute during evaluation. To address this, we introduce an abstract execution step that checks the type and shape of each variable, and computes a hash for each unique computation from inputs to outputs to detect redundant statements. The abstract execution can be seen as a static analysis of the program, achieved by replacing functions and inputs with customized values. We outline the specifics of the customized values and abstract execution procedure for three use cases below. The cost of the abstract execution is usually negligible compared to the actual execution of the program.

Detecting errors with type / shape inference To detect programs containing errors, we infer the type and shape of each variable in the program through the following steps: (1) replace each input with an abstract object that only contains type and shape information, and replace each statement with a type and shape inference function; (2) iterate through all statements. Instead of executing the original statement, we validate a function call by checking the function signature and type and shape information of its arguments. If valid, we compute the type and shape information of the output and assign it to the new variable; (3) verify the validity of the derived type and shape of the output. This process essentially performs a static analysis of the program, exposing errors caused by type and shape mismatch. Note that there are still run-time errors, such as division by zero, that cannot be detected in this manner. Without such filtering of invalid programs, the search would be overwhelmed with invalid programs, making it difficult to achieve meaningful progress.

Deduplicating with functional hash Among the valid programs that execute without errors, there are still lots of duplicates due to functionally equivalent programs that have different surface forms but the same underlying functionality. To address this issue, we calculate a functional hash value for every unique computation from the inputs to the outputs as follows: (1) a unique hash value is assigned to each input and function; (2) iterate through all statements, calculating the hash value of the outputs by combining the hash values of the functions and arguments; (3) compute the hash value of program by combining the hash values of all outputs. We then build a hash table that maps each unique functional hash value to the fitness of the corresponding program. When a new program is generated, we first look up its hash value and only perform evaluation if it is not found or if we want to evaluate it multiple times to reduce measurement noise. In our experiments, this technique reduces the search cost by ~10x, as depicted in Figure 2 (Right).

Table 11: One-shot evaluation on English NLP tasks. TriviaQA, NQs, and WebQs are NLG tasks and the rest are NLU tasks. This corresponds to Table 5 in the main text.

Task	1.1B		2.1B		7.5B		6.7B	8B
	Adafactor	Lion	Adafactor	Lion	Adafactor	Lion	GPT-3	PaLM
#Tokens	300B						300B	780B
TriviaQA (EM)	21.5	**25.1**	32.0	**33.4**	47.9	**48.8**	44.4	48.5
NQs (EM)	4.3	**4.8**	6.3	**7.3**	**12.3**	12.1	9.8	10.6
WebQs (EM)	**7.5**	6.3	8.4	**8.7**	12.1	**13.3**	15.1	12.6
HellaSwag	**50.7**	50.3	**59.4**	59.3	68.2	**68.3**	66.5	68.2
StoryCloze	**74.8**	74.4	78.2	**78.3**	81.2	**81.5**	78.7	78.7
Winograd	75.1	**80.2**	81.3	**82.1**	**85.3**	84.2	84.6	85.3
Winogrande	59.7	**60.5**	64.8	**65.7**	**71.4**	71.0	65.8	68.3
RACE-m	**52.0**	50.8	**55.1**	53.8	59.1	**61.3**	54.7	57.7
RACE-h	**36.8**	35.4	40.3	**40.7**	**44.5**	43.9	44.3	41.6
PIQA	69.4	**69.9**	71.3	**72.1**	**75.5**	74.5	76.3	76.1
ARC-e	**64.3**	62.0	**69.5**	68.9	72.4	**72.7**	62.6	71.3
ARC-c	31.2	**32.9**	37.3	**38.0**	**43.3**	42.6	41.5	42.3
OpenbookQA	44.8	**48.0**	48.4	**49.0**	51.4	**52.4**	53.0	47.4
BoolQ	54.3	**56.7**	**64.1**	62.9	73.5	**73.9**	68.7	64.7
Copa	75.0	**78.0**	83.0	**84.0**	85.0	**87.0**	82.0	82.0
RTE	**55.6**	52.4	49.8	**59.2**	**63.9**	62.5	54.9	57.8
WiC	**47.6**	47.3	46.1	**48.1**	**50.9**	48.1	50.3	47.3
Multirc (F1a)	35.9	**44.3**	45.0	**48.8**	44.7	**59.2**	64.5	50.6
WSC	**76.5**	75.4	**79.6**	79.3	**86.7**	85.6	60.6	81.4
ReCoRD	73.4	**73.7**	**77.8**	77.7	81.0	**81.1**	88.0	87.8
CB	**46.4**	44.6	**48.2**	44.6	**51.8**	46.4	33.9	41.1
ANLI R1	**33.3**	30.1	**32.4**	31.2	31.5	**34.0**	31.6	32.4
ANLI R2	29.8	**31.8**	29.8	**30.6**	**32.4**	31.9	33.9	31.4
ANLI R3	29.8	**31.8**	31.4	**31.9**	33.6	**34.2**	33.1	34.5
Avg NLG	11.1	**12.1**	15.6	**16.5**	24.1	**24.7**	23.1	23.9
Avg NLU	53.2	**53.9**	56.8	**57.4**	61.3	**61.7**	58.5	59.4

Identifying redundant statements by tracking dependencies In program evolution, redundant statements are included to enable combining multiple mutations to make larger program changes. However, these redundant statements increase the evaluation cost and make program analysis more challenging. To identify redundant statements, we need to determine the set of statements that the outputs depend on, which can be computed in a recursive manner using the following steps: (1) replace the value of each input with an empty set, as they do not depend on any statement; (2) iterate through each statement. Note that each statement is an assignment that calls a function and assigns the result to a variable, which in turn depends on the current statement and all the depending statements of the function arguments. Therefore we replace the value of the variable with its dependency, i.e., a set of all depending statements; (3) compute the union of all statements that each output depends on, which contains all non-redundant statements. By filtering out redundant statements, we obtain a simplified version of the program that is cheaper to execute and easier to analyze. In our experiments, this reduces the program length by $\sim$3x on average, as shown in Figure 2 (Right).

Table 12: Hyperparameters for all the experiments.

Model	Dropout	Stoch Depth	Augmentations	Optimizer	β_1	β_2	lr	λ
Train from scratch on ImageNet								
ResNet-50	-	-	-	AdamW Lion	0.9 0.9	0.999 0.99	$3e-3$ $3e-4$	0.1 1.0
Mixer-S/16	-	0.1	-	AdamW Lion	0.9 0.9	0.999 0.99	$1e-2$ $3e-3$	0.3 1.0
Mixer-B/16	-	0.1	-	AdamW Lion	0.9 0.9	0.999 0.99	$1e-2$ $3e-3$	0.3 3.0
ViT-S/16	0.1	0.1	-	AdamW Lion	0.9 0.9	0.999 0.99	$1e-2$ $1e-3$	0.1 1.0
	-	-	RandAug: 2, 15 Mixup: 0.5	AdamW Lion	0.9 0.9	0.999 0.99	$3e-3$ $3e-4$	0.1 1.0
ViT-B/16	0.1	0.1	-	AdamW Lion	0.9 0.9	0.999 0.99	$3e-3$ $1e-3$	0.3 1.0
	-	-	RandAug: 2, 15 Mixup: 0.5	AdamW Lion	0.9 0.9	0.999 0.99	$1e-3$ $1e-4$	1.0 10.0
CoAtNet-1	-	0.3	RandAug: 2, 15 Mixup: 0.8	AdamW Lion	0.9 0.9	0.999 0.99	$1e-3$ $2e-4$	0.05 1.0
CoAtNet-3	-	0.7	RandAug: 2, 15 Mixup: 0.8	AdamW Lion	0.9 0.9	0.999 0.99	$1e-3$ $2e-4$	0.05 1.0
Pre-train on ImageNet-21K								
ViT-B/16	0.1	0.1	-	AdamW Lion	0.9 0.9	0.999 0.99	$1e-3$ $1e-4$	0.1 0.3
ViT-L/16	0.1	0.1	-	AdamW Lion	0.9 0.9	0.999 0.99	$1e-3$ $1e-4$	0.3 1.0
Pre-train on JFT								
ViT-B/16	-	-	-	AdamW Lion	0.9 0.9	0.999 0.99	$6e-4$ $1e-4$	0.1 0.3
ViT-L/16	-	-	-	AdamW Lion	0.9 0.9	0.999 0.99	$3e-4$ $1e-4$	0.1 0.3
ViT-H/14	-	-	-	AdamW Lion	0.9 0.9	0.999 0.99	$3e-4$ $3e-5$	0.1 0.3
ViT-g/14 & ViT-G/14	-	-	-	Adafactor Lion	0.9 0.9	0.999 0.99	$8e-4$ $3e-5$	0.03 0.3
Vision-language contrastive learning								
LiT-B/$*$-B	-	-	-	AdamW Lion	0.9 0.9	0.999 0.99	$1e-3$ $3e-4$	-
LiT-g/14-L	-	-	-	AdamW Lion	0.9 0.9	0.999 0.99	$1e-3$ $2e-4$	0.1 0.5
BASIC-L	-	-	-	Adafactor Lion	0.9 0.9	0.999 0.99	$5e-4$ $2e-4$	0.01 0.1
Diffusion model								
Imagen base & super-resolution	-	-	-	AdamW Lion	0.9 0.9	0.999 0.99	$1e-3$ $1e-4$	-
Image generation on ImageNet	64×64: 0.1 128×128 & 256×256: 0.2	-	-	AdamW Lion	0.9 0.9	0.999 0.99	$3e-4$ $3e-5$	0.01 0.1
Autoregressive & masked language modeling								
Small & Medium (PG-19, C4) & Large	-	-	-	AdamW Lion	0.9 0.95	0.99 0.98	$3e-3$ $3e-4$	-
Medium (Wiki-40B)	-	-	-	AdamW Lion	0.9 0.95	0.99 0.98	$3e-3$ $3e-4$	0.001 0.01
1.1B & 2.1B	-	-	-	Adafactor Lion	0.9 0.95	0.99 0.98	$2e-3$ $2e-4$	0.0005 0.005
7.5B	-	-	-	Adafactor Lion	0.9 0.95	0.99 0.98	$1e-3$ $1e-4$	0.001 0.01
Language model fine-tuning								
T5-Base & Large & 11B	0.1	-	-	AdamW Lion	0.9 0.95	0.99 0.98	$3e-5$ $3e-6$	-